Faculty of Science and Engineering
Department of Petroleum Engineering

Experimental and Numerical Study of Interaction of a Pre-Existing Natural Interface and an Induced Hydraulic Fracture

Mohammad Sarmadivaleh

This thesis is presented for the Degree of
Doctor of Philosophy
of
Curtin University

May 2012

Declaration

To the best of my knowledge and belief this thesis contains no material previously published by any other person except where due acknowledgment has been made. This thesis contains no material which has been accepted for the award of any other degree or diploma in any university.

Name: Mohammad Sarmadivaleh

Signature: *Date: 10/05/2012*

Abstract

The emergence of major world growth in the need for more energy may not be fulfilled without using the relatively new source of unconventional gas production that is locked away in rocks and is required to be stimulated hydraulically. However, such unconventional reservoirs are heterogeneous and contain various types of interfaces which make the fracture treatment difficult. Operation of hydraulic fracturing in a naturally fractured formation is very complicated as the existing natural interfaces may significantly influence the propagation of a hydraulic fracture. Therefore, a good understanding of how a hydraulic fracture behaves upon its arrival at a natural interface is very important for improved fracture stimulation, gas production and fracturing operation and design. Opening, off-setting, crossing or arresting the fracture are possible interaction mechanisms in the event that an induced fracture reaches a natural discontinuity plane.

In this study, these interactions were investigated for the simple case of two parallel interface planes. Analytical calculations, lab experiments and numerical simulations were applied interchangeably. A new interaction criterion was developed by extending the Renshaw and Polard (1995) analytical solution for the case of a non-orthogonal hydraulic fracture facing a cohesive interface. The predicted interaction mechanism using this criterion was in good agreement with published experimental results.

The hydraulic fracturing experiments in this work were carried out on cube-shaped mortar samples which were subjected to three independent stresses. Prior to these tests, the hydro-mechanical properties of the mortar samples were accurately measured using various standard tests (e.g. triaxial tests and porosity and permeability measurements) on a large number of cylindrical samples. The acquired information was later used to design the scaled hydraulic fracturing tests. Two parallel artificial fracture planes were created into the sample to represent the natural interface. The in-fill material and the angle of the fracture planes were changed in different samples to investigate the effect of interface cohesion and the angle of approach on the interaction mechanism.

The results indicated how the interaction mode is influenced due to changing these parameters: interestingly the effect of the fracture filling material on the interaction mode was more pronounced than what was anticipated. The analytical criterion

proposed by Warpinski and Teufel (1987) was shown to predict the laboratory results more closely. Also, it was observed that analytical interaction criteria give a better prediction of the interaction mode for the case of brittle interfaces. The results demonstrated the importance and sensitivity of using analytical criteria very carefully and strong consideration of the range of their applications.

In the last part of this thesis, the 2D particle flow code (PFC^{2D}), which is a discrete element method (DEM) based numerical code, was used for numerical simulation of the interaction mechanism. The simulation results corresponding to different angles of approach, interface friction coefficient and shear strength showed how the interaction mode changes as a result of changing these parameters. A high angle of approach and high friction coefficient values indicated an increase in the chance for crossing mode to occur. However, hydraulic fractures tend to become arrested when both the angle of approach and friction coefficients are low. From the simulation results it appeared that there is a threshold for the angle of approach below which a hydraulic fracture will tend to be arrested by the natural interface regardless of the value of other parameters. The results of this study were, in general, in good qualitative agreement with a large number of my laboratory experiments and other numerical and experimental work reported in the literature.

Acknowledgements

I would like to express my gratitude to all those who gave me the possibility to complete this thesis.

I owe my deepest gratitude to my research supervisors, Associate Professor Vamegh Rasouli and Dr. Robert Jeffery, for their supervision and support. Their precious guidelines aided me to comprehend and to develop this research topic.

It is also my pleasure to thank Professor Brian Evans, the head of Department of Petroleum Engineering, for his constant support during the course of my studies. I would like to express my thanks to the Department of Petroleum Engineering for providing me with a scholarship and also to MERIWA for the top-up scholarship paid towards my PhD studies.

I appreciate the help of many friends and colleagues, including Amin Nabipour, Ahmadreza Younessi Sinaki, Bahman Joodi, Dr. Ali Saeedi, and Dr. Mohammad Sadegh Asadi, Dr. Maxim Lebedev, Mr Bruce Maney in CSIRO Geomechanics group and many others who shared our knowledge.

To

My wife Zahra, and my parents, who inspired my life in all manners and for their continuous support which helped me to pursue my higher education.

Contents

Page

Chapter 3 Experimental studies

List of Figures

Page

List of Tables

Nomenclature

FIP	Fracture initiation pressure
FPP	Fracture propagation pressure
ISIP	Instantaneous shut-in pressure
σ_v	Vertical in-situ stress
σ_{HMax}	Maximum horizontal stress
σ_{hMin}	Minimum horizontal stress
TTSC	True triaxial stress cell
PFC^{2D}	Two dimensional particle flow code
UCS	Uniaxial compressive strength
DEM	Discrete element method
HR	Hydraulic ram
FJ	Flat jack
ST	Screw type
DDM	Displacement discontinuity method
CV-BEM	Hyper-singular boundary element method
BEM	Boundary element method
VMIB	Virtual multidimensional internal bond
FEM	Finite element method
FMM	Fracture mechanisms map
FDM	Finite difference method
FVM	Finite volume method
FDTD	Finite difference time domain
XFEM	Extended finite element method
FEBEM	Hybrid of finite and boundary element method
θ	Angle of approach
τ	Shear stress acting on the plane of the natural interface
σ_n	Normal stress acting on the plane of the natural interface as a result of in-situ stresses
T_o	Rock tensile strength
σ_T	Sum of stress acting parallel to the natural fracture as a result of in-situ stresses

b	Coefficient that can be calculated from equation 2.3
c	Length of slippage zone
l	Half-length of open section of the fracture
μ_f	Friction coefficient
x_0	Location of the point at which re-initiation will occur
$v(x_0)$	Coefficient that can be calculated from equation 2.5
P_n	Overpressure or net pressure
W&T	Warpinski and Teufel
τ_0	Shear strength of the natural fracture plane
R&P	Renshaw and Pollard
σ_τ'	Total shear stress applied on the plane of the natural interface
σ_H'	Total normal stress applied on the plane of the natural interface
μ_f'	Apparent friction coefficient
μ_f''	Total friction coefficient
K_{IC}	Mode I rock fracture toughness
$r_c(\pm\pi/2)$	Critical distance from the intersection point where the stresses on the orthogonal ($\theta = \pm \pi/2$) natural interface is maximized
α	A coefficient that was described in equation 2.26
P_{resis}	Re-initiation resistance pressure
P_{fluid}	Fracturing fluid pressure
t_f	Time required to fill the joint
P_t	Average pressure in the hydraulic fracture over the entire treatment time
P_r	Reservoir pressure
t	Total fracturing time
y_f	Location of the fluid front
Lj	Joint length
y	Distance orthogonal to the fracture surface
ϕ	Rock porosity
ϕ_h	Hydraulic (real) porosity in the numerical model
DMS	Poly dimethylsiloxanes fluids
D_{10}	Effective size

D_{60}/D_{10}	Coefficient of uniformity
SCB	Semi-circular bend
E	Young's modulus
υ	Poisson's ratio
Φ	Internal friction angle
C_c	Rock matrix cohesion
σ_c	Confining pressure
P_f	Pore pressure
r_f	Fracture radius
Q'_o	Fracturing flow rate
μ	Fracturing fluid viscosity
κ	Dimensionless toughness parameter
E'	Plane strain modulus
i_{corr}	Corrected injection rate
p'	Borehole pressurization rate
V_{sys}	Total fluid volume of the system
C_{sys}	System compressibility
μ_p	Corrected viscosity
K_f	Fluid bulk modulus
V_d	Domain volume
Σq	Sum of the total fluid flow into the domain in one time step
Δt	Time step
ΔV_d	Domain volume change due to particle movement in each time step
q	Volume of fluid that is transferred per unit of time for each conduit between two specific domains
k	Mobility value
P_1 and P_2	Pressure of domain 1 and 2
L	Length of conduit
a	Conduit aperture
a_o	Initial conduit aperture
C_a	Aperture multiplication coefficient
Δt_i	Fluid time step of each domain

$t_{critical\ fluid}$	Critical fluid time step
$N_{mech\ to\ fluid}$	Number of mechanical steps
$t_{critical}$	Critical mechanical time step
K_p	Piezometric conductivity
k_{ma}	Matrix permeability
P_D, X_D, T_D	Dimensionless form of pressure, position, and time respectively
T_{0D}	Tensile strength measured by direct tension test
T_{0B}	Tensile strength measured by Brazilian test
T_{0ro}	Tensile strength measured by hydraulic fracturing reopening test
K_{ICD}	Fracture toughness measured by middle-tension panel test
F_o	Value of the compressional force F, applied to the conduit resulting to its aperture reducing to half of a_o
F	Compressional force on the conduit
K_{shear}	Fracture shear stiffness
K_{normal}	Fracture normal stiffness

1 Hydraulic fracturing and interaction mechanisms

1.1 Introduction

Perhaps no one expected that hydraulic fracturing operations would become a major player in disclosing different resources in the energy sector after it was first introduced in 1947. Hydraulic fracturing was initially used to improve the productivity of oil and gas wells and currently known as the only method to economically produce from new sustainable source of energy in low-permeable formations, i.e. tight formations or gas shale (Valko and Economides, 1995). Production from unconventional reservoirs has become one of the main sources of future energy supply around the world and particularly in Australia, due to a decline in recovery from conventional reservoirs in the last two decades. Therefore, a good understanding of hydraulic fracturing process in such formations is essential. In addition to the applications of hydraulic fracturing in tight formations, this method has been used for the stimulation of a wide range of formation types including weakly consolidated, fractured, lenticular and coal bed methane reservoirs (Adachi et al., 2007) as well as in geothermal energy (Berumen et al., 2000) and waste disposal (Hainey et al., 1999) applications. Hydraulic fracturing is also a major technique for measurement of in-situ stresses in mining and geotechnics related projects (Raaen et al., 2001).

In a hydraulic fracturing operation it is important that the fracture is contained within the reservoir interval and does not cross the cap rock. On the other hand, the fracture propagation may be influenced by the presence of any imperfection such as change in formation type. Natural fractures in different scales are another typical reason for possible change in fracture propagation status from what originally it was expected. These examples indicate how, in general, an interface such as a natural fracture or an interbed could influence the propagation of an induced fracture: this is known as an interaction between a hydraulic fracture and an interface. Different interaction mechanisms are expected including crossing, arresting and offsetting.

In this thesis the interaction mechanism is studied for some simple cases with the objective to understand the parameters affecting this process. Lab experiments under true triaxial stress conditions were performed on both synthetically made samples and on some real rocks at different scales. Also, the lab tests were simulated numerically using a distinct element method. In the following sections, a brief introduction will be given about the hydraulic fracturing and then the importance of studying the interaction of a natural and an induced fracture is presented through reviewing the major literature. This will be followed by the detailed objectives of this research, the major significance of this study and finally the structure of this thesis.

1.2 Hydraulic fracturing

In a typical fracturing operation, a viscous fluid referred to as "pad" is pumped into the wellbore with a constant flow rate such that downhole pressure increases to the state at which a crack is just initiated: this is known as initiation pressure. After the initiation, it takes a bit of time that wellbore pressure reaches to its maximum value which is called the breakdown pressure. For this pressure increment in a particular section of the wellbore, the injection flow rate should be high enough to overcome the rate of fluid filtrate into porous media or losses into existing natural fractures around the wellbore (Wong et al., 1993). After breakdown, the fracture starts to propagate into the rock formation and wellbore pressure continuously drops by the time.

The pad works as a frontier fluid to break the rock and control the filtration. Following the injection of a designed volume of pad fluid with a specific rate, another fluid that is called "slurry" carries proppant into the generated fracture(s). While the fracture length and volume increase, more fracture area will be exposed and wetted with pad fluid: this limits the extension of the fracture plane into the formation as the pad volume is being consumed (wetting new area and filtrate into the formation). The slurry carries the proppants and places them in opened (fractured) volume. The proppants stop the fracture walls to close completely after the release of pressure and will maintain the fracture conductivity (Veatch et al., 1989). The slurry will be injected is several stages at which proppant concentration is different. The last stage of slurry injection generally has the highest proppant concentration.

Figure 1.1 shows an estimated 2D geometry of a vertical fracture at different time intervals after propagation started. Also this figure shows the approximate proppant concentration along the fracture length. The darker areas represent higher concentration of proppant placement. Finally the slurry molecular structure breaks and it loses its original viscosity which helps to leave proppant behind in fracture and flow back out of fracture plane into the well. At this stage the fracturing job is completed.

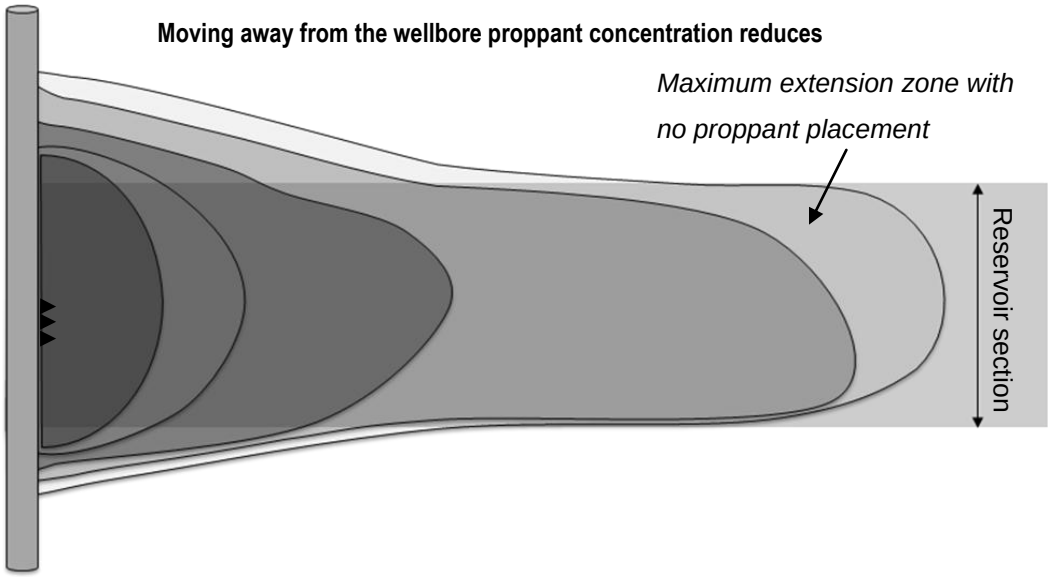

Figure 1.1 An estimated 2D geometry of a vertical fracture at different times after propagation.

A typical pressure-time curve corresponding to a hydraulic fracturing test is shown in Figure 1.2. As shown in this figure, after the wellbore pressure reaches the FIP the fracture pressure drops to propagation pressure (FPP). The steady portion of the pressure-time curve is the fracture propagation pressure. As depicted in Figure 1.2, FPP is larger than the minimum horizontal stress but is smaller than FIP. Fracture propagation stops once the maximum growth of fracture length under the current conditions is reached or, for example, fracturing fluid leak off occurs in permeable formations. Fracture initiation, propagation and containment pressures are the important data required for a hydraulic fracturing study. Here the containment capacity is defined as the ability of an interface to stop the fracture propagation. Estimation of these pressures is not straight forward, as they are influenced by a number of parameters including formation mechanical parameters, characteristics of discontinuities, friction, and the state of in-situ stresses (Sarmadivaleh and Rasouli, 2010).

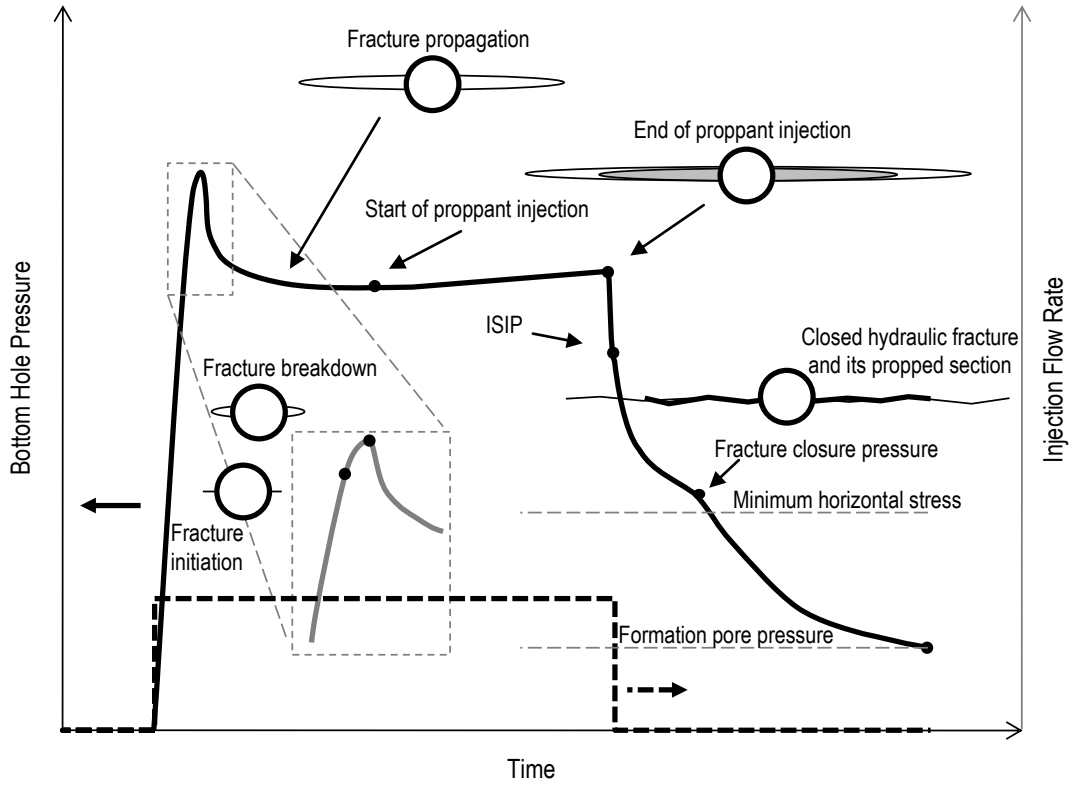

Figure 1.2 Typical pressure-time curve in a hydraulic fracturing test.

Several theories based on continuum or fracture mechanics have been developed to estimate the fracture breakdown pressure (Amadei and Stephansson, 1997). Rock strength, stress magnitude and anisotropy, and pore pressure are the parameters that are used in all of these methods (Sarmadivaleh and Rasouli, 2010). The initiation point depends on the magnitude of tangential or hoop stresses around the wellbore, which are functions of far-field stress states and any imperfection existing around the wellbore.

Fracture propagation is in the direction perpendicular to the least resistance stress (Daneshy, 2004). If the fracture, due to an imperfection around the borehole initiates at a different direction, it will eventually reorient towards the preferred direction (Dees, 1995). Depending on the operation depth, wellbore trajectory, and the state of stresses, horizontal or different types of vertical fracture planes may form (Economides et al., 1998): this is shown schematically in Figure 1.3.

It is important to note that fracture initiation and breakdown pressure terms are being exchangeably used in the literature, but here in this thesis we refer to these as the pressure at which the wellbore pressurization rate is maximised and the maximum borehole pressure is reached, respectively.

Ideally, after breakdown pressure, the fracture will propagate further away from the wellbore wall in the direction perpendicular to the minimum horizontal stress (considering a vertical fracture). However, if an imperfection or interface, such as a discontinuity plane is presented near or along the path of the induced fracture growth, it may affect the direction of fracture extension by changing the state of stresses. The discontinuities may be in different forms of bedding planes, natural fractures, joints or flaws, faults, and formation change which are widely observed in geological structures. In each of these cases, the hydraulic fracture will be affected by the presence of discontinuity planes. In the following section different interaction mechanisms when an induced fracture arrives at an interface will be explained.

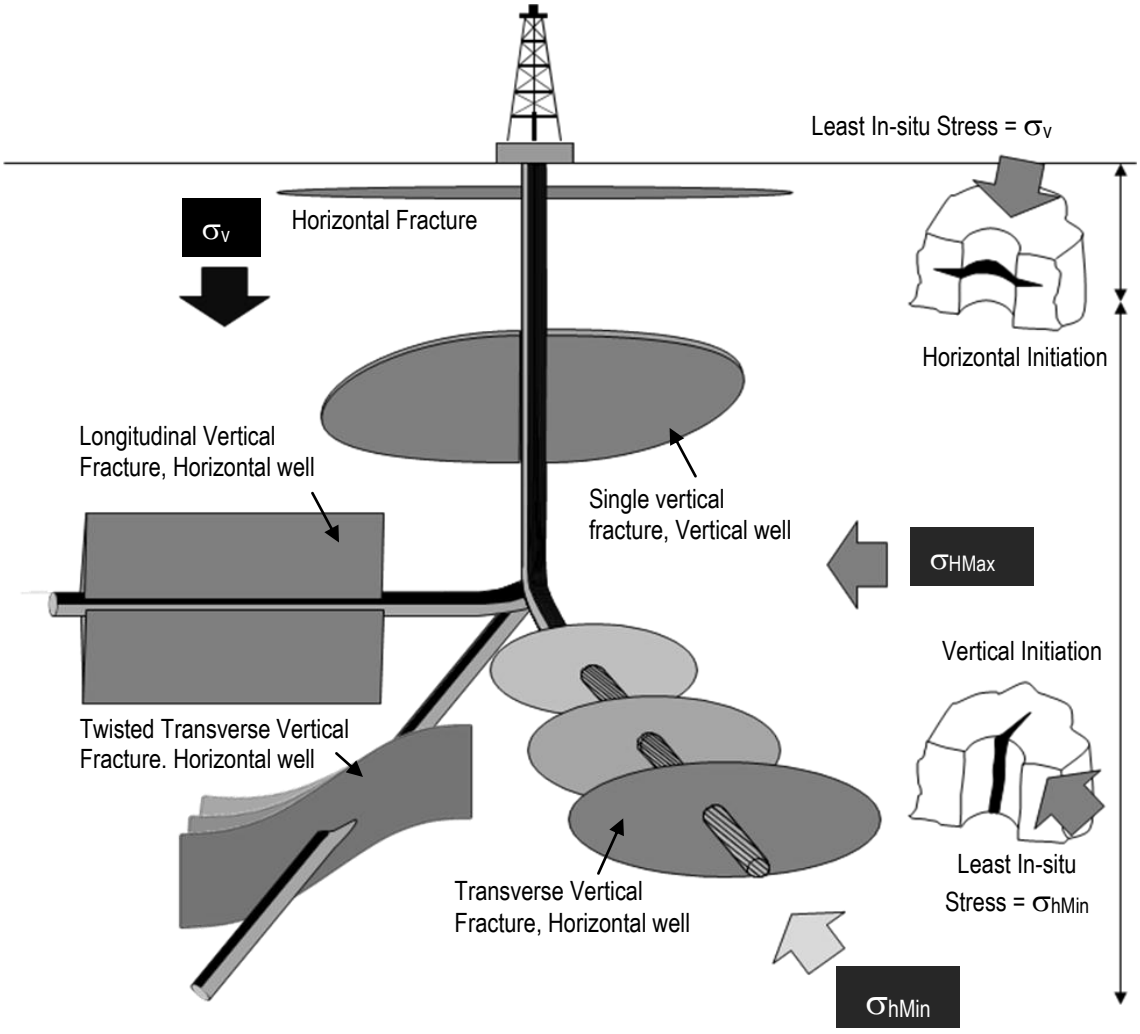

Figure 1.3 Horizontal or vertical fracture planes may initiate depending on the state of stresses (after Economides et al., 1998 and Valkó, 2005).

1.3 Interaction mechanisms

A natural interface in its general form can be considered as a boundary in which the physical or mechanical properties of the formation changes. A hydrocarbon-bearing sand lens in a thick shale layer or a single or network of natural fractures are examples where an interface exists. When a hydraulic fracture approaches a natural interface three modes of opening, crossing, and arresting are different interaction mechanisms that may occur depending on the orientation of induced fracture with respect to the natural interface, state of stresses, infilling material, and fluid properties. These interaction modes are illustrated in Figure 1.4. Offsetting, as shown in this figure, is sometimes considered as another interaction mode where the induced fracture firstly opens the natural interface and then reinitiates at some point different from the point of intersection.

In some practical cases it is desired that hydraulic fracture hits and crosses as many natural interfaces as possible such as sand lenses in order to connect them to a single borehole. However, containment of a hydraulic fracture within a reservoir section between two shale layers is another scenario which requires having an interface capable of arresting the induced fracture. In Figure 1.1 the fracture is almost contained in reservoir section except for about one third of its total length near the wellbore. Fracture containment occurs due to different mechanisms such as the stress contrast or different material properties of the two layers, formation permeability and pore pressure (Sarmadivaleh and Rasouli, 2010).

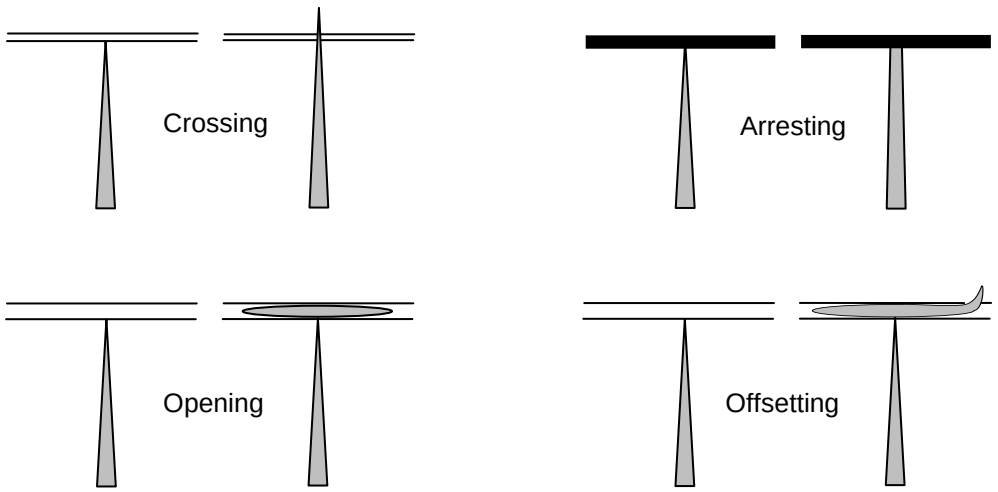

Figure 1.4 Different possible interaction scenarios when a hydraulic fracture meets a natural fracture.

The minimum horizontal stress contrast between the two overlaying layers is the dominant factor that controls the growth of hydraulic fractures (Warpinski and Teufel, 1987). When the stress contrast between adjacent zones is large enough, the growth of fracture height is expected to decline and ultimately stop (i.e. fracture is contained). If the minimum horizontal stress in the next layer is greater than the minimum horizontal stress in the former layer, the new layer can contain a hydraulic fracture with an overpressure equal to the minimum horizontal stress contrast. This overpressure is indeed the difference between the fracture propagation pressure and the minimum horizontal stress in the former layer.

The minimum horizontal stress contrast is the lower limit for fracture containment capacity of a layer. The upper limit for fracture containment can be calculated if no cohesive interbed contact is assumed. In this case, firstly, the hydraulic fracture will be arrested upon arriving at the interbed, then it will initiate on the other side of the interface. So, the pressure to propagate a fracture in the new layer needs not only to overcome the new layer's minimum horizontal stress, but also exceed the new layer's tensile strength. Theoretically, maximum containment capacity of any layer could be assumed as the sum of the least in-situ stress and the tensile strength of the rock at that depth. If the pressure of the hydraulic fracture exceeds the maximum containment capacity of a layer the interbed is not expected to contain the hydraulic fracture. However, hydraulic fracture may start to propagate along the interface before pressure exceeds the containment pressure.

A contrast in material properties in soft-hard interfaces is likely to govern the fracture containment (Wu et al., 2004). Interface slippage can result in immediate termination of fracture growth but usually this would only be considered in shallow depths where the overburden pressure is relatively low; however, at depths where shear strength is relatively small, such as high pore pressure zones with low normal stress at the interface, or at an interface with negligible friction coefficient (e.g. soft shale), a fracture may be contained (Teufel and Clark, 1984). However, depending on the condition interface slippage along with offsetting may occur at any depth (Zhang et al., 2008). In reality not all of the parameters contributing to an interaction mechanism are controllable, for example stress state and interface properties. Amongst different parameters, the natural interface properties including friction coefficient and shear strength play a great role in the interaction (Sarmadivaleh et al., 2011).

Both induced and natural (newly generated) fractures disturb the local stress field. The magnitude of stress perturbation is dictated by pressure, fluid properties of hydraulic fractures, in-situ stresses, permeability, elastic properties of the formation, orientations, opening, and roughness of natural fractures. As it mentioned earlier, if the overburden (vertical stress in normal stress regime) is assumed as the highest stress, a hydraulic fracture will propagate in the direction of local maximum horizontal stress. This is one probable reason for large branching and broad shear fractures reported in presence of discontinuity. Also, it may cause a random or off-balance fracture propagation growth pattern (Daneshy, 2005). This phenomenon has been extensively studied in previous laboratory works (Lamont and Jessen 1963; Daneshy 1974; Blanton 1982).

The above brief introduction indicates the complexity of the interaction of an induced and a natural interface. As it was discussed a number of parameters play a role in this interaction: considering all these parameters simultaneously complicates the problem. In order to understand the interaction mechanism and the importance of each parameter it is necessary to conduct a fundamental study on simple cases first. Hence, in this study we consider a single fracture plane with different orientations and investigate the interaction mechanism by changing the state of in-situ stresses, intact rock and interface mechanical properties and hydraulic fracturing fluid characteristics. The results of a number of lab experiments performed under true triaxial stress conditions will be presented. The lab experiments were simulated numerically, the results of which will be discussed and interpreted. The outcome of this study will indicate the complexity of the interaction mechanism and demonstrate the need for further investigations and study along this line of research.

1.4 Research objectives and methodology

As mentioned earlier the core objective of this research thesis is to investigate the interaction between an induced and a natural interface through lab experiments and numerical modeling. Here, the objectives of this study and the methodologies used to achieve these objectives are listed as follows:

- Perform hydraulic fracturing lab experiments a series of intact rocks to understand the application of scaling laws. The experiments will be performed on synthetically

made samples. The results will allow calibration of the true triaxial stress cell (TTSC) used for the future tests.

- In order to generalize the results of lab tests to field scale it is necessary to apply scaling laws through dimensionless parameters when fracturing experiments are planned in the lab. We applied simple elastic scaling laws proposed by de Pater (1994) and some others (see Chapters 2 and 3). These scaling laws then were used for designing all fracturing tests performed in this study.
- Numerical simulations were performed using particle flow code (PFC^{2D}) to simulate the experiments performed in the lab. The simulations were limited to 2D cases with the objective of understanding some aspects of interaction mechanisms in further details. The limited amount of time available and also the large volume of lab experiments involved in this study avoided extending the models into 3D. However, the results obtained from 2D simulations provided in-depth and valuable conclusions. These are discussed in Chapter 4 in detail.
- We considered a simple case of a single fracture plane to investigate the interaction mode with an induced fracture. This was studied by observation of hydraulic fracture plane which was influenced by small scale natural features within the intact rock. Also, synthetic samples with pre-existing fracture planes were built for this purpose. The geometry of the fracture plane was changed with respect to the expected direction of the induced fracture and also surface properties of the natural fracture were changed using different glues. This allowed investigation of various parameters which may affect the interaction mechanism. The results of these studies on various sample sizes will be presented. The results will indicate that a single fracture system is by itself a far complicated problem which is subjected to several unknowns and require further research before studying more complex fractured rocks.
- Analytical solutions were used to predict the mode of interaction mechanisms. The objective here was to compare the results with lab observations. A new analytical formula analogy to those introduced by Renshaw and Pollard (1995) interaction criterion will be presented in this study which includes the effect of interface cohesion and assumes a general angle for the interface plane.
- The interaction mechanism simulated numerically using PFC^{2D} in order to carried out sensitivity analysis of different parameters.

1.5 Research significance

This research study is unique in its different aspects and a number of new knowledge was developed during the course of this work. Followings are some of the major achievements of this study:

- New analytical formulae for predicting the interaction between hydraulic fracture and natural interface were developed in this thesis and compared with available literature experimental data as well as our experimental results.
- Calculation of dimensionless parameters for scaled hydraulic fracturing of samples with different sizes for designing field-like fracture tests in lab was performed in this study. This has not been done in the past by others to this extent due to the limited capability of testing samples with different sizes.
- Testing samples of different sizes from 10 cm to 20 cm in the lab provided an understanding on how the hydraulic fracture and natural interface interaction may behave differently as a function of sample size.
- The importance of natural interface properties on the interaction results were studied in depth in both laboratory experiments and numerical simulations.
- Numerical simulation of hydraulic fracturing and interaction mechanism using distinct element method is one of the very few attempts made in this work. The discussions about the ability of the PFC^{2D} code used in this study demonstrate how this is a useful approach for hydraulic fracturing simulations.
- In this study all samples used for lab experiments were firstly tested to obtain their mechanical and hydraulical properties in detail. Standard uniaxial compression strength (UCS), confined compressive strength, multi stage, Brazilian tensile, and fracture toughness tests as well as measurement of porosity and permeability at different confining pressures were performed on representative samples and this gives a high level of confidence in the final results obtained and interpretations made.

1.6 Thesis structure

In the previous sections, it was implied that studying the hydraulic fracturing parameters and the interaction mechanism when an induced fracture approaches a natural interface is the main objectives of this research. Lab experiments and numerical simulations are used for this purpose.

The thesis comprises five chapters. In Chapter 2 different interaction mechanisms are reviewed, and the parameters dominating each interaction mode are explained. This is where a new criterion developed for prediction of interaction of a cohesive natural interface with an arbitrary angle is presented.

In Chapter 3, the details of lab experiments carried out in this study will be discussed. A review of the true triaxial stress cell (TTSC) used for the lab tests and the applied modification for the purpose of this study will be given. This follows the details of different tests performed on both intact rocks and samples with a single fracture plane.

In Chapter 4 the results of numerical simulations using PFC^{2D} will be presented. This Chapter includes a brief discussion about different numerical methods and in particular distinct element method (DEM) which was used in this thesis. Then a short review of PFC code will be given and this is followed by the results of numerical simulations of lab experiments performed in Chapter 3.

Chapter 5 draws together the conclusions of this work, and also outlines proposals for further research in this subject.

Substantial references used in this study are given at the end of this thesis.

2 Review of literature and modified analytical criterion

A review of field studies, laboratory tests, numerical simulations and analytical solutions performed and proposed in the past to study the interaction modes when a hydraulic fracture arrives at a natural interface is given in this Chapter. Reviewing measurements made at field scale is valuable in the sense that it shows the geometry that is generated by the interaction, the complexity of the problem and motivates the need to analyze such interactions in detail so that the full effect can be understood and accounted for in designs. Numerical models are often tuned by adjusting input parameters until a match to experimental data is obtained. The calibrated model is then used for various analyses, for example, to study the effect of different parameters on interaction modes. Dimensional analysis and scaling laws are useful for determining which parameters or groups of parameters are dominant during the time of the experiment and for, on the other hand, designing an experiment so that the effect of varying certain parameters or groups of parameters can be studied systematically. Scaling also provides a method of establishing similitude between laboratory scale real field scale fracture behaviors.

A brief introduction to the scaling laws will be given in this Chapter. For simple cases, e.g. certain fracture geometries and elastic materials, analytical solutions may be derived to predict the interaction mechanism, but several simplified assumptions are considered to develop the solutions. However, these provide a good starting point and a comparative tool for undertaking sensitivity analysis on the effect of different parameters. In this chapter, a review of some of the important attempts which have been made to study the interaction mechanisms through field operations, lab experiments and numerical simulations are given. Also, the frequently used analytical solutions are presented and a modified criterion which is a general form of the well known Renshaw and Pollard (1995) interaction criteria will be presented. This chapter concludes with a proposed methodology for designing a laboratory experiments that are based on analytical formulae.

2.1 Field studies

The propagation of hydraulic fractures can be significantly affected when natural discontinuities are present in the formation. Complex fractures containing multi-branched geometries have been reported based on micro-seismic fracture mapping, mine-back studies (Warpinski and Teufel, 1987; Jeffrey et al., 1992; Steidl 1991), or coring the fractured zone (Warpinski et al, 1993; Fast et al., 1994). The discontinuities may be natural fracture, inclusions or flaws, faults, fissures, joints, bedding, or butt/face cleats. Warpinski and Teufel (1987) discuss how discontinuities influenced the geometry of the hydraulic fracture by arresting fracture propagation, reducing the total length of the fracture, and disturbing proppant transport and its placement. In addition, due to the increased net pressure promoting hydraulic fracture height growth. In this thesis, we consider the net pressure as the pressure difference between the wellbore pressure and minimum in-situ stress.

Also, zones of multiple fractures were found to form along the induced fracture (Warpinski et al., 1993). As an example to demonstrate the complexity of the problem, Figure 2.1 shows the results of a micro-seismic fracture mapping in a shale gas reservoir. The generated induced fractures appear to be in form of a very complex network: this is due to the presence of pre-existing natural fractures in the reservoir section which influenced significantly the growth of induced fractures. However, seismicity occurs wherever shear sliding occurs and therefore does not map precisely the location of the hydraulic fracture. Figure 2.2 shows the results of a field experiment performed in Central Colliery underground coal mine site (Jeffrey et al., 2009) where a hydraulic fracture has crossed an existing natural fracture plane, but initiated on the other side at a different point along the natural fracture plane –illustrating an offsetting mechanism– showed in Figure 1.4 in the previous chapter.

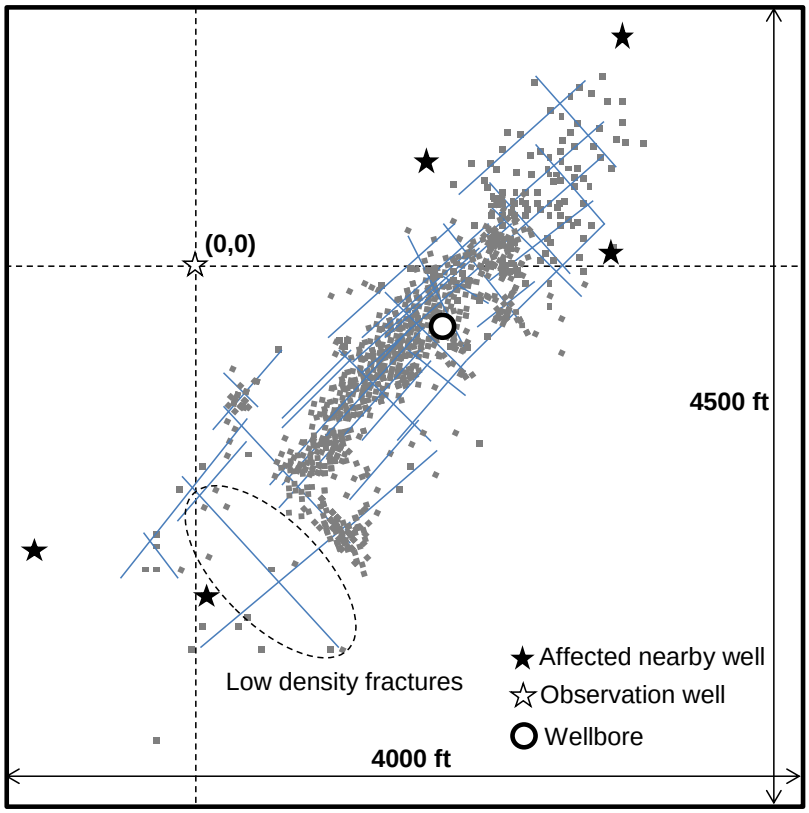

Figure 2.1 Interpreted micro-seismic events in gray rectangles for single fracturing treatment in a fractured shale reservoir (reproduced image, courtesy of Halliburton).

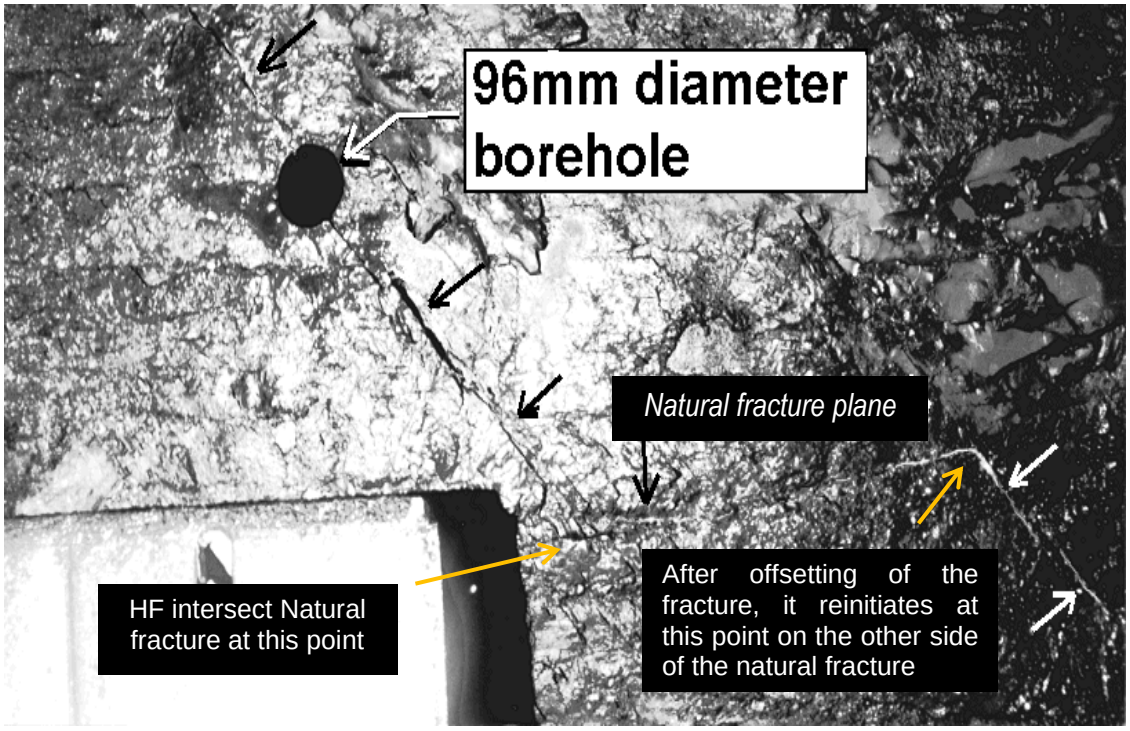

Figure 2.2 A clear offsetting case that was observed during mine backing of a fracturing test on Central Colliery underground coal mine site.(Jeffery et al., 2009)

From practical point of view, different problems may be encountered by a fracture treatment as a result of the hydraulic fracture interacting with natural fractures. Generation of multiple fractured zones, high propagation net pressures, extensive fluid leak-off, premature screen-out, thin aperture fracture, opening, offsetting, and/or arresting are some of the results of interaction widely reported in literature (Murphy and Fehler, 1986; Warpinski, 1991; Britt and Hager, 1994; Jeffrey et al., 1995; Branigan et al., 1996; Vinod et al., 1997; Rodgerson, 2000; Azeemuddin, 2002; Jeffrey et al., 2010). The high and strongly pressure dependent leak-off rate is caused by opening and enhancement of natural fracture permeability as the effective stress is reduced because of increased pore pressure caused by the fluid loss from the hydraulic fracturing.

From the results of field observations it can be concluded that in general, in contrast with formation permeability in hydraulic fracturing operation in a non-fractured reservoir, the dominant fluid loss is into the network of natural fractures and this loss has a strong effect on the propagation characteristics of an induced fracture (Britt and Hager, 1994; Barree and Mukherjee, 1996). Also, the generation of multi branched hydraulic fracture as a result of offsetting the hydraulic fracture and/or shear slippage of natural interface is possible in fractured formations (Murphy and Fehler, 1986). However, theoretically branching should be rare in homogeneous and isotropic formations (Freund, 1990; Valkó and Economides, 1995). From production point of view, forming multi branched fracture networks due to interaction of an induced fracture with natural fractures could be beneficial as it may increase the overall conductivity of formation (Cipolla et al., 2008).

2.2 Laboratory experiments

In this section a summary list of the specifications of the equipment used in the past to perform hydraulic fracturing lab experiments under true triaxial stress conditions will be given. This will be followed by a brief introduction to the scaling techniques and in particular those used in this study. Finally, a review of some of the experiments conducted to study fracturing interaction will be given.

2.2.1 Laboratory fracturing apparatus

Many reports exist on hydraulic fracturing experiments in the laboratory. These activities use different stress frames ranging from cylindrical biaxial (Haimson and

Fairhust, 1969) to cubical uni/bi-axial (Llanos et al., 2006) as well as true triaxial. Table 2.1 contains a summary of the specification of some of the true triaxial lab equipment that has been used for hydraulic fracturing experiments around the world. A good summary on some of hydraulic fracturing laboratory experiments can be found in Moreno, 2011. A newly built true triaxial stress cell used for our lab experiments in this study will be discussed in Chapter 3. It worth mentioning that conducting the fracturing test in conjunction with ultrasonic monitoring is going to be a standard method of fracture study. The equipment used in Delft University is perhaps one of the most versatile True Triaxial cells built for such test.

Table 2.1 Some of the past equipment used for hydraulic fracturing lab experiments

	Sample Dimension	**Vertical Stress** σ_v	**Min Horizontal Stress** σ_{hMin}	**Max Horizontal Stress** σ_{HMa}	**Cell Fluid Pressure** P_f	**Injection Pressure** P_{inj}
TerraTek (Behrmann and Elbel, 1991; Ahmed et al., 1983)	27×27×32 in (69×69×81cm)	FJ 8000psi (55MPa) or HR 1.7×106 lbf	FJ 8000 psi (55MPa)	FJ 8000 psi (55MPa)	Yes >2000psi (14MPa)	N/A
	11×11×15 in (28×28×38cm)	FJ 4500 psi (31 MPa)	FJ 4500 psi (31 MPa)	FJ 4500 psi (31MPa)	N/A	N/A
Delft University (Veeken et al., 1989)	12×12×12 in (30×30×30 cm)	HR 5700 psi (38.9 MPa)	HR 5700 psi (38.9 MPa)	HR 5700 psi (38.9 MPa)	No	7250psi (50MPa) 0.1-100 cc/min
Haliburton (Haimson and Fairhust, 1969; Rabaa, 1987)	5×5×5.5 in (12.7×12.7×14 cm)	HR 0.1×106 lbf	FJ 2500 psi (17 MPa)	FJ 2500 psi (17 MPa)	N/A	4-600 psi/s
	6×12×18 in (15×30.5×45.5 cm)	ST 0.12×106 lbf	HR 3000 psi (21 MPa)	HR 3000 psi (21 MPa)	N/A	10,000 psi (69MPa), 500 cc/min
Oklahoma University (Ong, 1994)	18.75×18.75×18 in (47×47×45.5 cm)	FJ 3000psi (21 MPa)	FJ 3000psi (21 MPa)	FJ 3000psi (21 MPa)	No	10,000 psi (69MPa), 1.4 cc/min
Eindhoven University of Technology (Van Mier, 1984).	7.8×4×4 in (20×10×10 cm)	HR 0.4 *106 lbf	HR 0.4×106 lbf	HR 0.4×106 lbf	No	N/A
CSIRO (personal communication with Dr. Rob Jeffery, Llanos et al., 2006)	16×16×16 in (40×40×40 cm)	FJ 3600 psi (25 MPa)	FJ 3600 psi (25 MPa)	FJ 3600 psi (25MPa)	No	10200 psi (70 MPa)
Petroleum University of China (Zhou et al., 2010)	12×12×12 in (30×30×30 cm)	FJ 5700 psi (39 MPa)	FJ 5700 psi (39 MPa)	FJ 5700 psi (39 MPa)	No	20,300 psi (140 MPa)

HR, Hydraulic Ram; FJ, Flat Jack; ST, Screw Type

Figure 2.3 shows a view of the true Triaxial cell available in Delft University. It uses 48 ultrasonic transducers it is possible to monitor fracture propagation geometry during the test. The transducers configuration is also shown on the left bottom side of figure 2.3. Except for the pore pressure which cannot be applied on the tests carried out using the Delft Triaxial frame, its other specifications are one of the best in the world. Another good example of such facility can be found in CSIRO Melbourne.

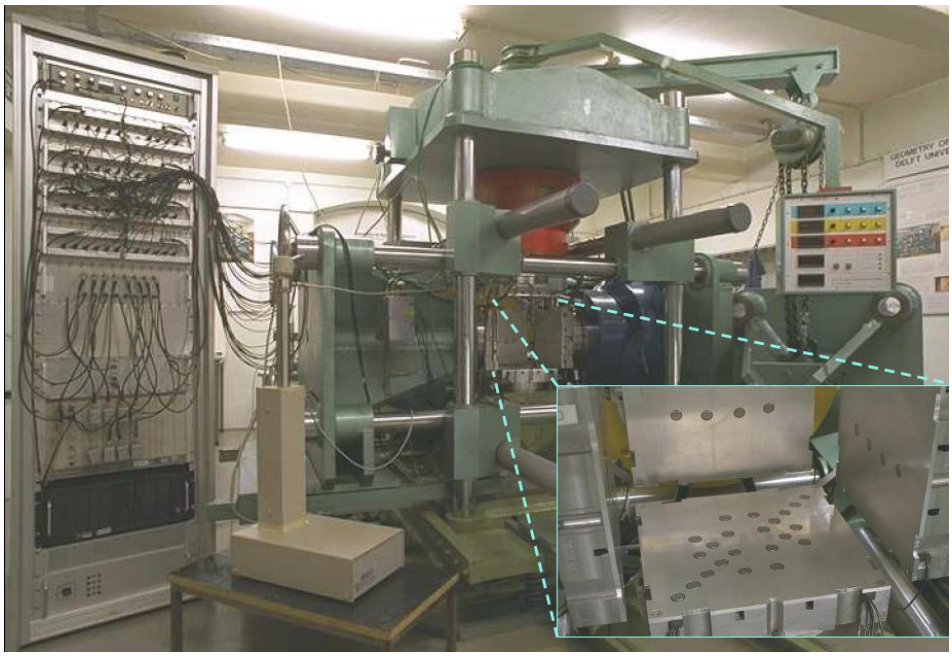

Figure 2.3 The true triaxial cell at Delft University (Taken from a, Smeulders (2007) presentation, Lower quality image is available in Weijers, 1995).

2.2.2 Scaling laws

In order to consider a hydraulic fracture field test being simulated in laboratory scale, scaling laws are to be applied to scale the fracturing parameters. This is briefly discussed below; however, many experiments have been carried out without using scaling as part of the experimental design. Most of the hydraulic fracturing tests performed in the laboratory represent a highly exaggerated injection rate and a very low fluid viscosity as they used a fracturing fluid very similar to what being used in a real fracturing job in the field (Weijers, 1995). However, in order to monitor fracture propagation in a reasonable time on a sample that can be handled in the laboratory, a fluid with much higher viscosity is typically required when using a low injection rate.

This ensures that the hydraulic fracture is contained within the sample boundaries and the propagation can be monitored without being affected by the boundary conditions. In fact, the scaling laws are applied to model field representative fracture growth in the lab by defining the fracturing parameters (e.g. viscosity) in such a way that the laboratory and field fracture propagation regimes are as similar as possible (dePater, 1994; Bunger et al., 2005a). For a driven hydraulic fracture, the dominant factor that governs the energy and mass balance processes depends on the propagation regime: the scaling design is dependent on this factor (Adachi, 2001; Detournay, 2004). In a small scale laboratory test considering the case of a penny shaped fracture, it is most likely that toughness controls the fracture propagation regime at the final stage of propagation after a period of specific time. However, almost all of the field scale hydraulic fractures over nearly all of their propagation history are viscose dominated (Cleary, 1980; Detournay, 2004; Mack and Warpinski, 2000; Adachi et al., 2007).

For this purpose, a set of dimensionless groups of physical parameters that describe a specific fracturing process are defined in the way that they become identical using lab and field parameters. These dimensionless variables are driven from the fluid flow (mass and momentum conservation laws) and rock behaviour (rock deformation, crack opening and extension) partial differential equations. As one simple approach, the results of such calculations could be represented in a parametric space with three extreme boundaries of viscosity, toughness, and leak-off dominated propagation regimes as depicted in Figure 2.4 (Bunger, 2005). It is worth mentioning that in general, a parametric space with infinite edges (rather than three) could be assumed; however one or few of these parameters will govern the overall process at any specific time (Bunger, 2005). In this thesis, this triangular parametric space will be used as a part of the scaling analysis (following figure).

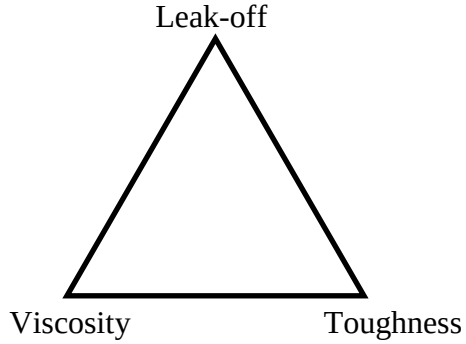

Figure 2.4 Triangular parametric space when only toughness, viscosity, and leak-off regimes are considered (Simplified and reproduced from Bunger, 2005).

The importance of using the term "specific time" should be highlighted here because the dominate propagation regime may change from one time to another during a single fracturing test. The fracture propagation mechanism, hydro-mechanical properties of the rock, fluid properties and flow rate at a specific time are those that determine the propagation regime, i.e. location of the fracture evolution in the parametric space. Proposed scaling scenarios have been considered in the literature that include cases with different combinations of zero, small, finite, and large toughness for permeable or impermeable rocks that are being fractured using viscous or inviscid fluid (Carbonell et al., 1999; Adachi and Detournay, 2002; Savitski and Detournay, 2002; Bunger, 2005; Bunger et al., 2005b; Garagash and Detournay, 2005; Lhomme, 2005; Garagash, 2006; Adachi and Detournay, 2007; Mitchell et al., 2007).

While the scaling laws can be applied, the non homogeneous nature of the rock samples at the small size considered means that the impact of micro heterogeneities on fracture propagation pattern (e.g. pore size distribution and pore shape and small beddings or facies) presents a difficulty for extrapolating the results to large scales. Scaling microstructral properties like ratio of the fracture length to grain size in lab or field operation is not practically a possible task (de Pater, 1994). Therefore the effect of grain size on fracture propagation is neglected in this thesis.

In real field fracturing operations, fracture extension is toughness dominated at the early stages of propagation, during initiation, but rapidly becomes viscous dominated (Mack and Warpinski, 2000). And finally, for a radial fracture, it become again toughness dominated (Detournay, 2004). We apply the scaling laws proposed by de Pater et al. (1994) in this work, which uses synthetic mortar samples for the laboratory testing. Also, the final laboratory conditions were checked against other more recent scaling studies (i.e. Detournay, 2004; Bunger, 2005; Lhomme, 2005). It is to be noted that a similar scaling approach has been employed for laboratory fracturing tests for a few other rock types but with different sample sizes (Casas et al., 2006a; 2006b; Athavale, 2008).

2.2.3 Laboratory interaction studies

Integrating inherent properties of natural interfaces (e.g. orientation, aperture, shear strength, filling material, spacing and conductivity) and mechanical properties of the rock matrix in conjunction with the state of far-field stresses and the coupled hydraulic fracture mechanics means the analysis of the interaction mechanism is a difficult problem. In order to simulate the problem in the laboratory, simplifications are implemented, which mean the results are not comparable with real field conditions. This would also add into the complication of the problem. In this section, existing results from past lab experiments done with and without applying the scaling laws are reviewed with the objective of highlighting the main conclusions from this previous work.

As an early attempt, Lamont and Jassen (1963) conducted a set of experiments on six rock types. They carried out experiments considering different states of stress and angle of approaches. They found that the initiation of the hydraulic fracture on the other side of a natural fracture occurred on a random basis. Consequently, they concluded that the natural fracture disturbs the existing stress field in the nearby area. They also observed that for a closed natural fracture plane the interaction does not depend on the angle of approach but crossing is the expected mode of interaction: this conclusion is not supported by further experiments conducted by others later (e.g. Warpinski and Teufel, 1987). Lamont and Jassen's result might have been affected by the fast fracture propagation speed that was used in their experiments.

Daneshy (1974), carried out experimental studies and reported that the strength of the weakness plane, its orientation and the magnitude of deviatoric stress (difference between the principal stress magnitudes), together with the natural fracture aperture are the main controlling factors that affect crossing behaviour when a hydraulic fracture intersects a natural interface. He found that natural fractures with sizes smaller than the induced hydraulic fracture will be unable to alter the orientation of the propagating fracture. On the other hand, open natural fractures extensively affected the propagation of an induced fracture and typically stopped its growth.

The importance of frictional strength of an unbounded interface on the resulting interaction was emphasised by Anderson (1981). He set up several experiments in such a way that the fracture propagation moved towards an interface at right angles under uniaxial stress conditions. He concluded that a hydraulic fracture will cross an interface if the normal load exceeds a threshold.

Blanton (1982; 1986) stated that hydraulic fractures will tend to cross pre-existing fracture planes only when the sample is subject to high deviatoric stresses and high angles of approach. His experimental results showed that in the case of low deviatoric stresses or low angles of approach the pre-existing fractures will be opened by extending the fracture plane and fracturing fluid will be diverted into the natural fracture. Also, Blanton reported that arresting of the hydraulic fracture may occur in this situation. However, the results of field studies by Hopkins et al. (1998) showed that the geometry of natural fractures is the controlling factor of the interaction. Figure 2.5 shows the results of two tests on one sample carried out by Blanton. Fractures were initiated from two different points in each test and propagated towards the same natural fracture. For low angle of approach of 30°, hydraulic fracture was arrested by natural fracture whereas it crossed the interface for an angle of 60°.

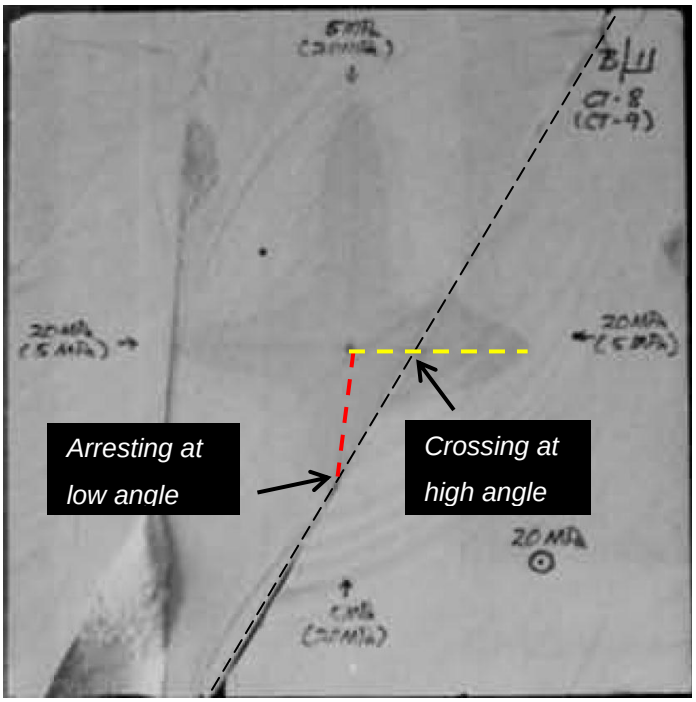

Figure 2.5 Crossing and arresting at high and low angles of approach (Blanton, 1982).

The effect of geological discontinuities on hydraulic fracture propagation was examined in mineback and laboratory experiments by Warpinski and Teufel (1987). By decomposing in-situ stresses on the surface of a natural fracture and considering pore pressure distribution along the joint plane, they derived an analytical criterion, which was confirmed through laboratory experiments, to determine the condition under which natural fracture dilates, experiences shear slippage, or crosses the hydraulic fracture

(Warpinski and Teufel, 1987). They showed that the combination of the interface friction coefficient, stresses, and fracture net pressure will determine the interaction result. This criterion will be discussed on section 2.4. The results of their laboratory work were later confirmed with the work done by Zhou et al. (2008). They investigated the effect of shear strength of natural fractures, tectonic and normal stress regimes, and aperture of natural fracture on the interaction mechanism.

Doe and Boyce (1989) found that propagation of straight non-branched fractures would be unlikely when the ratio of maximum and minimum stresses is below a certain value, i.e. less stress anisotropy. This was also found to be a function of the rock type. This demonstrates how the geometry of the induced fracture may be different depending on the magnitude of deviatoric stresses. As was stated earlier, the deviatoric stress will affect the interaction substantially.

Blair et al. (1990) published the results of a laboratory study where they considered the interaction mechanism of an orthogonal hydraulic fracture and a permeable interface. They embedded tungsten wires in a sample to track the fracture propagation path. Stepped pressure versus time was recorded and attributed to interaction of the hydraulic fracture with an embedded sandstone lens which showed that the hydraulic fracture extension would be temporarily prevented when it reaches such high permeability zones.

Renshaw and Pollard (1995) found that a fracture will cross a natural fracture if the normal stress applied on the natural fracture surface could provide enough frictional resistance so that the tensile stress sufficient to initiate a fracture was transferred to the other side of the interface. Their work was based on laboratory, analytical, and numerical work. They presented an analytical criterion called "Compressional Crossing". They considered the induced tip stress of a propagating tensile dry fracture (Mode I) on an orthogonal natural fracture. The natural fracture follows the Coloumb's frictional law. Their interaction criterion then was developed for two cases of crossing or arresting by slippage. Gu and Weng (2010) modified the analytical criterion proposed by Renshaw and Pollard (1995) using a simple for non-orthogonal cases and then they validated the new criterion through laboratory work (Gu et al., 2012). They also showed the application this criterion on propagation of hydraulic fracture in complex system of natural fracture (Wu et al., 2012). In Section 2.4 we present a generalized form of Renshaw and Pollard's criteria for a cohesive interface with an arbitrary angle of approach.

Researchers in Delft University (Beugelsdijk and de Pater, 2000; de Pater and Beugelsdijk, 2005) investigated the effects of angle of approach, deviatoric stress, influences of flow rate, viscosity, joint patterns, and normal and tectonic stress regimes on synthetic blocks to examine the scaled hydraulic fracture and natural fracture interactions. They found that high flow rate or viscosity results in the fluid-driven fractures crossing the natural fracture while low flow rate results in the hydraulic fracture entering and opening the natural fracture. The scaling technique makes their results much more valuable than the former studies.

Recently, Meng (2010) reported the results of another series of tests for the interaction problem. He showed that crossing is more likely when the normal stress on the natural fracture plane and the fluid viscosity are high. His fracturing tests were done using no scaling technique. Also, work similar to what has done in earlier in Delft University was conducted by Zhou et al. (2010) and Zhou and Xue (2011) at the Petroleum University of China that confirm the Delft researchers findings. They did not mentioned whether they applied the scaling laws in their work.

Llanos et al. (2006) reported a retarded fracture growth as a result of the propagation through natural fractures based on their study in CSIRO. The angle of approach of 90 degree was chosen for the tests. She stated that an increase of the normal load on the plane of the natural fracture will facilitate crossing. Some of her laboratory test results are shown in Figure 2.6 which used a fracturing fluid consisting of honey with blue food dye. She used a scaling method that distinguishes between toughness and viscous propagation regimes.

Two examples of scaled interaction tests were reported by researchers at the Colorado School of Mines (CSM) who applied dePater's scaling laws (Casas et al., 2006a; 2006b) in their experiments. They studied the interaction between the fracture and interfaces filled with an epoxy and a grout. Later Athavale and Miskimins (2008) used the same scaling method for studying the interaction for different bonded/unbonded orthogonal interfaces. They showed how interface properties (filling material and cohesion (bounded/unbounded) state) affected the interaction. The fractures opened the unbonded interfaces and crossed the bonded one (Athavale and Miskimins, 2008). Also, it is shown that brittle interfaces are easier to cross than plastic interfaces (Casas et al., 2006a).

Figure 2.7 shows the interaction test result of a scaled hydraulic fracture performed by Casas et al. (2006a) in the TerraTek laboratory. The properties of the interface will be further investigated in the next experimental part of this thesis as the number of test conducted in CSM were not more than three.

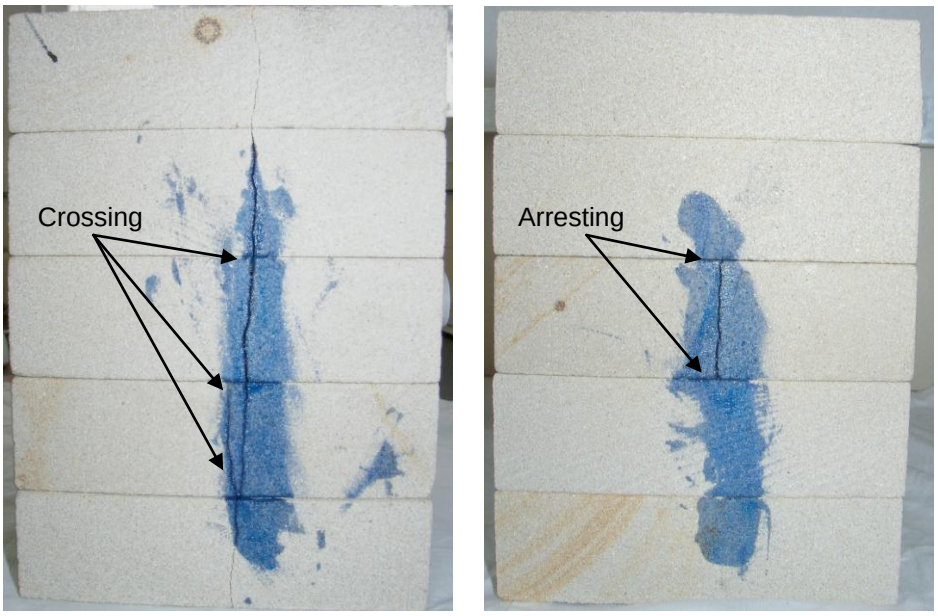

Figure 2.6 Lab experiments showing the crossing and arresting of the hydraulic fracture when it faces series of orthogonal natural fracture planes (figure: courtesy of Llanos).

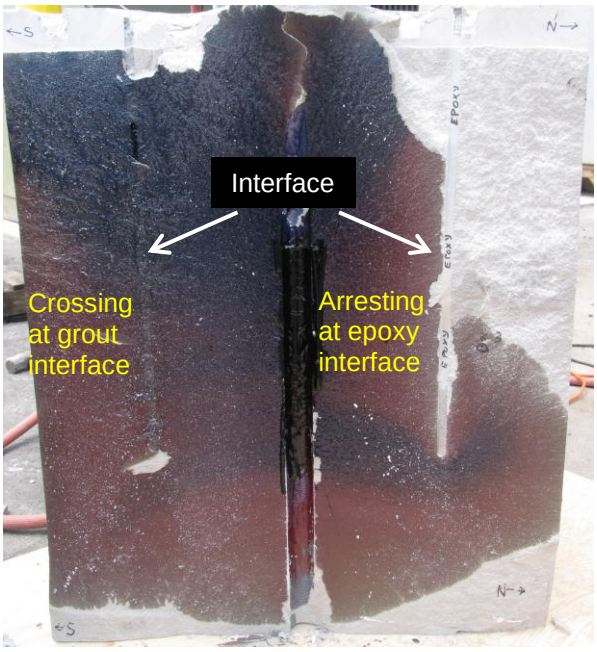

Figure 2.7 Arresting and crossing as a result of test on large sample size (30”×30”×36”) scaled fracturing test (Casas et al., 2006a).

2.3 Numerical simulations

The results of several numerical simulations have been reported by researchers on various aspects of the interaction between a hydraulic and a natural discontinuity. Cooke and Underwood (2001) studied the interaction of a stress driven crack and bedding using the Displacement Discontinuity method (DDM). They studied the interaction of sliding (arresting), opening, step over (offsetting), and crossing. Koshelev and Ghassemi (2003) investigated the propagation of a hydraulically driven flaw in the vicinity of a natural interface using the complex variable hyper-singular boundary element technique (CV-BEM). Zhang and Ghassemi (2010) studied the interaction based on virtual multidimensional internal bond (VMIB) and finite element method (FEM). They showed that orientation, geometry of a natural discontinuity, together with the in situ stress conditions will affect the propagation of a uniformly pressurised fracture substantially. A similar work was done by Xue (2010) to study the mechanical response of a natural fracture which is intersected by a propagating fracture at different angles of approach.

Wu et al. (2004) studied fracture behavior when facing a stiff/soft (or soft/stiff) interface using a Griffith-type global fracture criterion. The model assumptions include uniform fluid pressure along the hydraulic fracture and no slippage on the interface. They showed that the crack may be arrested while it is propagating in a softer layer toward a stiffer one. Also, in order to enhance the fracturing design, they proposed a fracture mechanisms map (FMM) for interface problems.

Potluri (2004; 2005) provided a simple numerical study of a 1D non-planar interaction based on the PKN fracture model. Later, Rahman et al. (2009) published a very similar work assuming elastic and poro-elastic media. They also developed a 2D poro-elastic model and studied the effect of angle of approach and deviatoric stress on the interaction (Rahman et al., 2010).

Zhang et al. (2004, 2005, and 2006) applied a Displacement Discontinuity (DDM) and finite difference methods (FDM) to model the coupled fracture propagation. For this purpose, rock medium was considered to be homogeneous impermeable elastic and fracturing fluid to be Newtonian and incompressible. The natural fracture was assumed to behave based on Coulomb's friction law. A detailed study of deformation and stresses was possible for different interaction scenarios using Zhang's model (Llanos et al., 2006). This study included viscous fluid flow in the hydraulic fracture in contrast to

the uniform pressure assumption which is equivalent to assuming a zero fluid viscosity. Zhang et al. (2004; 2005; 2006) demonstrated that many of the responses found are sensitive to including viscous fluid flow in the coupled fracture model.

Thiercelin and Makkhyu (2007) applied a semi-analytical model based on the dislocation theory to predict the behavior of a natural discontinuity facing a propagating hydraulic fracture. They showed that the most probable position of re-initiation can be found by analysing stresses along the natural fracture.

The interaction of hydraulic and natural fracture was studied in plane strain conditions on an impermeable infinite elastic medium by Akulich and Zvyagin (2008). They showed that fracturing fluid viscosity will affect the interaction. Later, Chuprakov and Zhubayev (2010) studied the interaction assuming a simple analytical model based on the strain energy density criterion. Chuprakov et al. (2010) published the results of a numerical model based on DDM. They studied the problem in three stages, which were described as the approach, contact, and infiltration in each interaction scenario.

Dahi-Taghavi and Olson (2009; 2011) presented a complex propagation pattern of fractures based on the extended finite element method (XFEM). They showed that propagating fractures may exert enough load on an interface to cross or unbound it before it reaches the intersection point. They also proposed a Pseudo-3D numerical simulation for this purpose (Olson and Dahi-Taleghani, 2009). In their work they showed that even in sub-parallel system of natural fracture, induced fracture may be deviated from predicted direction of propagation based on the magnitude of in-situ stresses and the treating net pressure (see Figure 2.8).

Recently, a discrete element method (DEM) has been used to study the interaction problem (Zhao and Young, 2009; Damjanac et al., 2010). These researchers showed that the angle of approach, cohesion of natural fracture and the compressibility of fracturing fluid are important parameters in an interaction problem. Also they observed that the fracture propagates in shear as well as tensile mode.

The above brief discussion indicates the large volume of numerical models used in this area of research. FEM and DDM are perhaps mostly used numerical methods for this purpose. However, the complexity of the problem resulted in several simplifications for modelling purposes: this may deviate the results from reality. The DEM, although rarely used for interaction studies appears to be a useful tool which can consider some aspects of fracture propagation and its interaction with a natural fracture plane more realistically. As a result the DEM is the numerical method which was used in this study

to simulate the cases tested in the laboratory. Particle flow code (PFC^{2D}) is the numerical code which was used for this purpose. A brief review of PFC^{2D} and its functionalities will be given in Chapter 4.

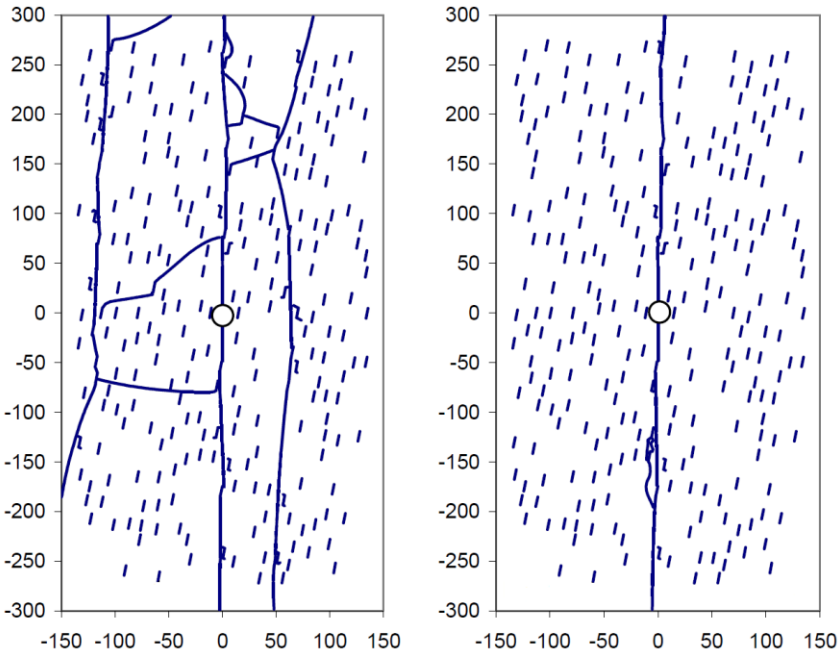

Figure 2.8 Multi-branched fracture propagation (left). Reduction in net pressure or an increase in the magnitude of deviatoric stresses will result in propagation of one fracture plane (Olson and Dahi-Taghavi, 2009).

2.4 Analytical solutions

Figure 2.9 is an illustration of a hydraulic fracture intersecting a natural interface. In this figure, θ is the angle of approach, $\sigma_{H\ Max}$ and $\sigma_{h\ Min}$ are the maximum and minimum horizontal stresses, and τ and σ_n are the shear and normal stresses acting on the plane of the natural interface, respectively.

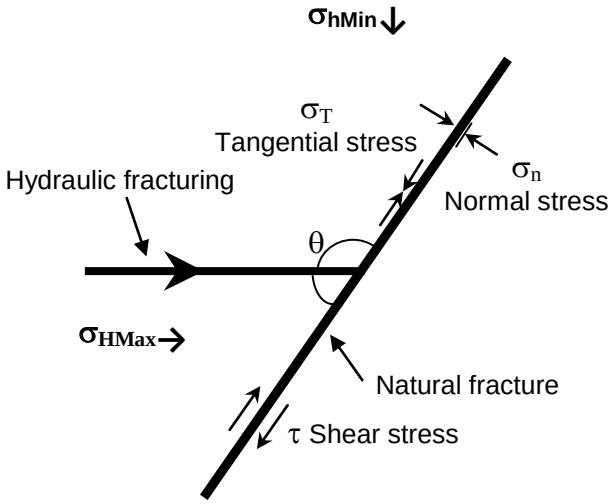

Figure 2.9 A schematic of a hydraulic fracture approaching a natural interface

Several analytical solutions have been proposed in the past to predict the mode of interaction when a hydraulic fracture intersects a pre-existing natural interface. The criteria proposed by Blanton (1982; 1986) and Warpinski and Teufel (1987) are based on the differential stress and angle of approach. Renshaw and Pollard's (1995) criterion considers crossing across an unbounded frictional interface with an orthogonal angle with respect to the induced fracture. This was later modified by Gu and Weng (2010) who expanded the model to be applicable for non-orthogonal angle of approaches. None of these criteria, however, consider the cohesion and adhesion of the interface plane. In the following subsections a short review of these criteria are given which is followed by a new criteria developed by the author based on Renshaw and Pollard's criteria where a cohesive interface with a non-orthogonal angle of approach are allowed.

2.4.1 Blanton's criterion (Blanton, 1986)

Blanton considered a momentary arresting of the hydraulic fracture when it reaches a natural fracture plane. While injection into wellbore continues, the pressure at the interface starts to rise until either the natural fracture opens or re-initiation occurs on the other side of the interface: the possibility of each case to happen is a function of the angle of approach and differential in-situ stresses. The crossing will take place if required fracture pressure for re-initiation is less than the opening pressure. A simple crossing condition will happen if treating pressure exceeds the sum of stress acting parallel to the natural fracture σ_T and rock tensile strength, T_o, i.e.:

$$P > \sigma_T + T_0 . \tag{2.1}$$

In this equation σ_T depends on the far-field stresses, fracture treating pressure, geometry of the interaction zone, friction coefficient, angle of approach, and opening along the natural fracture. Accordingly, Blanton derived the following crossing criterion with respect to the parameters that affect σ_T:

$$\frac{(\sigma_{HMax} - \sigma_{hMin})}{T_o} > \frac{-1}{Cos2\theta - bSin2\theta}. \tag{2.2}$$

Here, b is calculated as:

$$b = \frac{1}{2c}\left[v(x_0) - \frac{(x_0 - l)}{\mu_f} \right], \tag{2.3}$$

where c is the length of slippage zone, l is the half length of open section (from $-l$ to $+l$) of the natural fracture (see Figure 2.10), μ_f is the friction coefficient and x_0 is the location of the point at which re-initiation will occur. Terms x_0 and $v(x_0)$ can be calculated as:

$$x_0 = \left[\frac{(1+c)^2 + e^{\frac{\pi}{2\mu_f}}}{1 + e^{\frac{\pi}{2\mu_f}}} \right]^{0.5}, \tag{2.4}$$

and

$$v(x_0) = \frac{1}{\pi}\left[(x_0 + l)\ln\left(\frac{x_0 + l + c}{x_0 + l} \right)^2 + (x_0 - l)\ln\left(\frac{x_0 - l - c}{x_0 - l} \right)^2 + c\ln\left(\frac{x_0 + l + c}{x_0 - l - c} \right)^2 \right]. \tag{2.5}$$

No shear stress exists along the open section of the fracture, i.e. over ±*l*: the shear stress appears the ends of the open portion at these points and gets larger moving away from these points over the distance of plus or minus c along the natural fracture plane until it becomes equal to the far-field shear stresses.

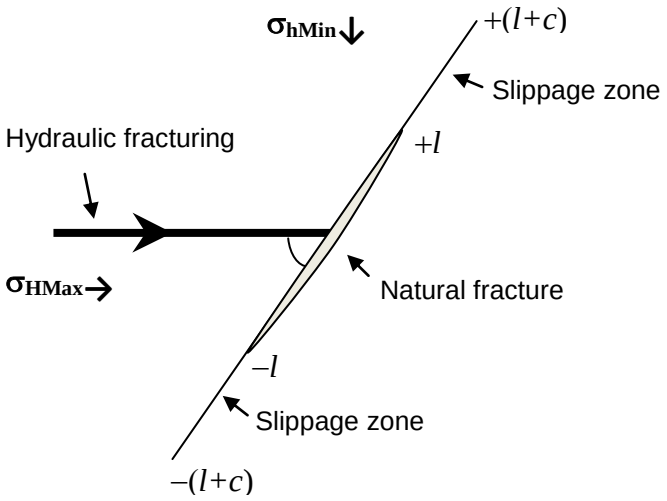

Figure 2.10 Zone of slippage for natural fracture

From Equation 2.3 it is seen that when *c* tends to zero (no slippage zone or no slip), *b* approaches infinity which results a zero value for the right hand side of equation 2.5. This means that equation 2.5 will state that crossing occurs. By increasing the value of *c*, the value of b drops very quickly. On the other hand, when *c* tends to infinity, term *b* tends to

$$b = \frac{1}{2\pi} \ln \left[\frac{1 + \left(1 + e^{\frac{\pi}{2\mu_f}} \right)^{0.5}}{1 - \left(1 + e^{\frac{\pi}{2\mu_f}} \right)^{0.5}} \right]^2 , \tag{2.6}$$

and b becomes a function of the natural fracture friction coefficient. Blanton used this value for comparison of his analytical and experimental results. In Figure 2.11, the results of Equation 2.2 are plotted for three different values of *b*=0.2, 0.4, and 0.6 (from Equation 2.6). In this figure the regions of opening and crossing are shown, which are to the left and right of the curves, respectively.

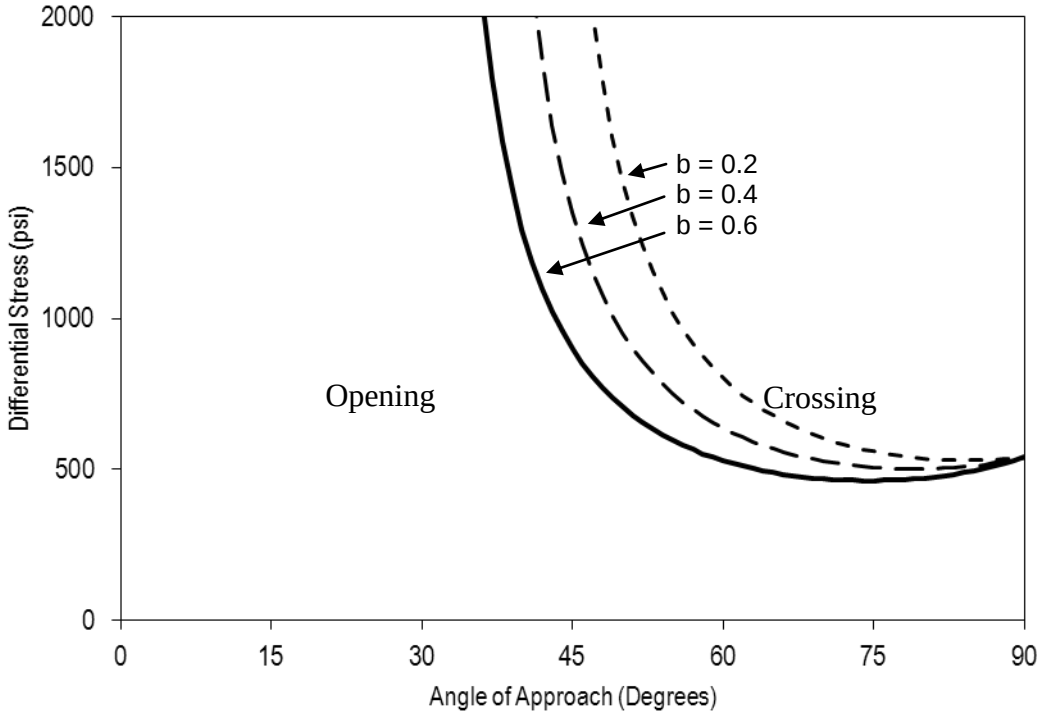

Figure 2.11 Crossing and opening interactions as predicted by the Blanton criterion for three different values of b=0.2, 0.4, and 0.6. A rock tensile strength of 510 psi (see table 3.2) is assumed for this plot.

Comparing to lab results reported by Lianos (2006), higher normal stresses are needed in Blanton's criterion for crossing to happen. This is because Blanton's criterion neglects the effect of stresses induced by the propagating hydraulic fracture on the interface and assumes a simplified shear stress distribution along the interface.

2.4.2 Warpinski and Teufel's criteria (1987)

Warpinski and Teufel, W&T (1987) considered four models to predict the pore pressure distribution inside the joint plane. This pressure is used to calculate fracture overpressure or net pressure, P_n, which is defined as fracture pressure minus minimum horizontal stress. They consider the Coulomb failure criterion for shear failure along the natural fracture. Superposition of in-situ stresses on the plane of the natural fracture gives the state of stresses, i.e. σ_n, normal stress and τ, shear stress. Based on these stresses, opening will occur when fracture pressure exceeds the far-field normal stress acting normal to the plane of fracture. The opening condition, in terms of deviatoric stress (i.e. left hand side of Equation 2.7) can be expressed as:

$$\sigma_{HMax} - \sigma_{hMin} < \frac{2p_n}{(1 - Cos2\theta)}. \tag{2.7}$$

Equation 2.7 is plotted in Figure 2.12 for three net pressures of 0.1, 0.7, and 1.0 MPa shown by dashed lines. The area below the dashed lines shown in this figure corresponds to the opening mode.

W&T proposed a relationship that governs arresting mode based on deviatoric stresses as:

$$\sigma_{HMax} - \sigma_{hMin} \geq \frac{2\tau_0 - 2p_n\mu_f}{Sin2\theta + \mu_f Cos2\theta - \mu_f}. \tag{2.8}$$

In this equation τ_0 is the shear strength of the natural fracture plane. Equation 2.8 has been plotted in Figure 2.12 as three solid lines corresponding to net pressures of 0.1, 0.7, and 1.0 MPa, respectively to distinguish between the regions of opening and arresting interaction modes. Below these solid lines the crossing interaction is more prone to happen whereas the area above these lines represents the region with high chance of arresting. For the angles greater the one that makes the denominator of right hand side of equation 2.8 zero, shear slippage will not occur as normal stress on the plane of natural interface is big enough that stops the slippage. This angle for the condition at which figure 2.12 was plotted is 55 degree.

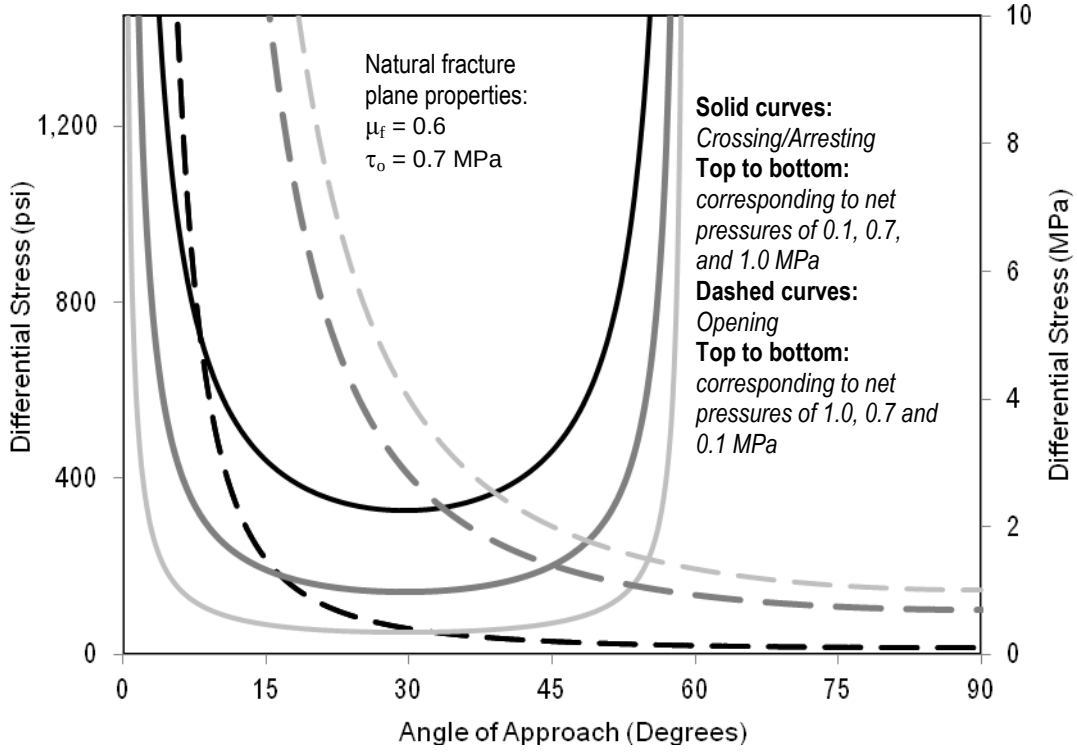

Figure 2.12 Regions of different interaction modes based on W&T's criterion for three different net pressures of P_n = 0.1, 0.7, 1.0 MPa.

2.4.3 Renshaw and Pollard criteria (1995)

The concept of "compressional crossing" was developed by Renshaw and Pollard, R&P (1995) who studied the interaction of a frictional interface with a dry fracture. If the interface does not slip, a crossing type interaction is assumed to occur which is as a result of tensile stress being transferred from one side of the natural fracture, where the induced fracture is propagating, to the other. For this case, no slip or opening must occur along the interface. When the frictional strength (shear strength) of the interface is less than the induced tensile stress, the interface will slip and the fracture will be arrested upon its arrival at the intersection point. This criterion considers an induced fracture intersecting an interface orthogonally.

R&P's criterion assumes elastic fracture theory and that for continuous propagation of the fracture across an interface is favoured by higher compressive stress. Only crossing, essentially without any interaction or blunting when slip occurs, are considered. Also, a homogenous and isotropic rock with a constant elastic modulus for the material on the second side of the natural interface is assumed. The criterion is still valid for bi-material interfaces under specific conditions. R&P's interaction criterion is expressed as:

$$\frac{-\sigma_{HMax}}{(T_o - \sigma_{hMin})} > \frac{1+\mu_f}{3\mu_f}. \tag{2.9}$$

R&P assume that crossing will not occur if slip occurs: this is in contrast with some experimental results showing that crossing may happen after slip and fluid penetration into the natural fracture plane. This indicates that R&P criterion underestimates the discontinuity strength required to allow an induced fracture to cross it. Thus, crossing may occur at lower crossing stress ratios than that predicted by R&P (Llanos, 2006). The term appearing at the left hand side of Equation 2.9 is known as the "crossing stress ratio".

2.4.4 Modified Renshaw and Pollard's criteria

Here we attempt to expand R&P's criteria to a more general case for a non-cohesive interface with a non-orthogonal angle of approach.

Interface with shear strength

If the interface has cohesion, it will be less susceptible to slippage. Mathematically, this changes the interface shear condition from

$$\left|\sigma_{\tau}^{'}\right| < -\mu_f \sigma_H^{'}, \tag{2.10}$$

which was proposed by Renshaw and Pollard (1995) to:

$$\left|\sigma_{\tau}^{'}\right| < \tau_0 - \mu_f \sigma_H^{'}, \tag{2.11}$$

where $\sigma_{\tau}^{'}$ and $\sigma_H^{'}$ are shear and normal stresses applied on the plane of the natural interface. In the case of an orthogonal angle of approach, the applied shear stress is just a function of the shear stress induced by the stress around the tip of the hydraulic fracture. In general, for non-orthogonal interfaces, these stresses are the results of both in-situ stresses and induced stress from the tip of the fracture. If, in the case of compressional crossing, for any normal stress on the plane of natural fracture and any interface cohesion, an imaginary coefficient of friction can be assumed at which

$$\tau_0 = -\mu^{'}_f \sigma_H^{'}, \tag{2.12}$$

then equation 2.11 can be rewritten as

$$\left|\sigma_{\tau}^{'}\right| < -\mu_f{}^{'} \sigma_H^{'} - \mu_f \sigma_H^{'} = -\left(\mu^{'}_f + \mu_f\right)\sigma_H^{'} = -\mu^{''}_f \sigma_H^{'}. \tag{2.13}$$

Equation 2.13 can be rewritten in a similar form as Equation 2.9 proposed initially by Renshaw and Pollard (1995). This is:

$$\frac{-\sigma_{HMax}}{\left(T_o - \sigma_{hMin}\right)} > \frac{1+\mu_f^{''}}{3\mu_f^{''}}, \tag{2.14}$$

where $\mu_f'' = \mu_f' + \mu_f$.

To calculate $\mu_f^{''}$ we need to calculate $\mu_f^{'}$ first. Form Equation 2.12:

$$\mu_f^{'} = -\frac{\tau_0}{\sigma_H^{'}}. \tag{2.15}$$

In this equation, the value of the denominator from R&P's criterion is:

$$\sigma_H^{'} = \sigma_{HMax} + \frac{K_{IC}}{\sqrt{r_c\left(\pm\frac{\pi}{2}\right)}} \times \left(Cos\frac{\pi}{4}\left(1 - Sin\frac{\pi}{4}Sin\frac{3\pi}{4}\right)\right), \tag{2.16}$$

in which K_{IC} is the mode I rock fracture toughness and $r_c(\pm\pi/2)$ is the critical distance from the intersection point where the stresses on the orthogonal ($\theta = \pm \pi/2$) natural interface is maximized. Thus $\mu_f^{'}$ can be stated as:

$$\mu_f^{'} = -\frac{\tau_0}{\sigma_{HMax} + \frac{K_{IC}}{\sqrt{r_c\left(\pm\frac{\pi}{2}\right)}} \times \left(Cos\frac{\pi}{4}\left(1 - Sin\frac{\pi}{4}Sin\frac{3\pi}{4}\right)\right)}. \tag{2.17}$$

The value of $\sqrt{r_c}(\pm \pi/2)$ can be calculated using the same approach that was taken by Renshaw and Pollard (1995) considering the boundary conditions. This will result in:

$$\sqrt{r_c\left(\pm\frac{\pi}{2}\right)} = \frac{K_{IC}}{T_o - \sigma_{hMin}} \times \left(Cos\frac{\pi}{4}\left(1 + Sin\frac{\pi}{4}Sin\frac{3\pi}{4}\right)\right). \tag{2.18}$$

Substituting Equation 2.18 into Equation 2.17 leads to:

$$\mu_f^{'} = -\frac{\tau_0}{\sigma_{HMax} + \frac{\left(T_o - \sigma_{hMin}\right)\left(1 + Sin\frac{\pi}{4}Sin\frac{3\pi}{4}\right)}{\left(1 - Sin\frac{\pi}{4}Sin\frac{3\pi}{4}\right)}} = -\frac{\frac{\tau_0}{\sigma_{HMax}}}{1 + \frac{\left(T_o - \sigma_{hMin}\right)}{3\sigma_{HMax}}}. \tag{2.19}$$

From Equation 2.9, Equation 2.19 can be rewritten as:

$$\mu_f^{'} = \frac{\frac{\tau_0}{\sigma_{HMax}}}{\frac{-1}{1 + \mu_f}}. \tag{2.20}$$

This equation depends on the friction coefficient and the ratio of τ_0/σ_{HMax}. Figure 2.13 is a graphical representation of Equation 2.14 for various ratios of shear strength to maximum horizontal stress. When this ratio is zero, it corresponds to R&P's criterion represented by Equation 2.9. It is to be noted that the vertical axis in Figure 2.13 is a logarithmic scale. The area above the curves corresponds to the region where crossing is the dominant interaction mode.

As is seen from this figure the larger the ratio of shear strength over maximum horizontal stress, the more likely the crossing mechanism would be. The crossing criterion also becomes less dependent on the friction coefficient as the ratio increases.

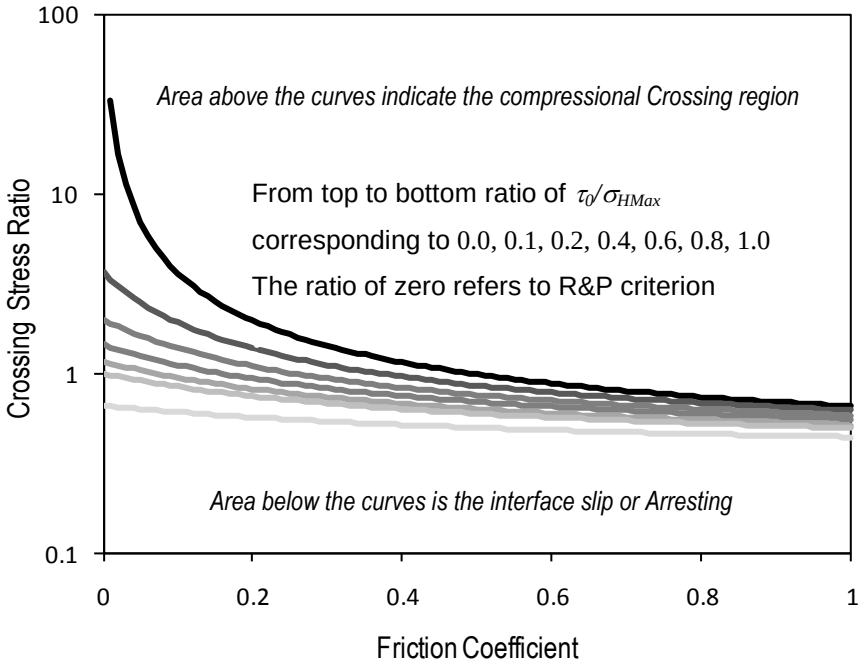

Figure 2.13 Interaction regions based on Renshaw and Pollard criterion and its modification for cohesive interface.

Non-orthogonal angle of approach

A more general form of the R&P criterion would be the case of interaction between the hydraulic fracture and a non-orthogonal cohesionless interface. For this purpose, transformation of in-situ stresses on the plane of natural fracture should be considered, as illustrated in Figure 2.9. Shear stress applied along the interface can be calculated from (Jaeger et al., 2007):

$$\tau = -\frac{\sigma_{HMax} - \sigma_{hMin}}{2} Sin(\pi - 2\theta) \tag{2.21}$$

The value of shear stress induced by far field stresses on the natural fracture should be added to shear stress actuated by tip stresses created by the hydraulic fracture in order to find the left hand side of Equation 2.10. If we assume that there is one α which satisfies the condition of

$$\tau = \alpha \frac{K_{IC}}{\sqrt{r_c(\theta)}}, \tag{2.22}$$

then Equation 2.9 can be rewritten in the following form where σ_n and σ_T are normal and tangential stresses applied on the natural fracture surface as a result of transformation of far-field in-situ stresses, σ_{HMax} and σ_{hMin} (see Figure 2.9):

$$\frac{-\sigma_n}{(T_o-\sigma_T)} > \frac{\left(1-Sin\frac{\theta}{2}Sin\frac{3\theta}{2}\right)+\frac{1}{\mu_f Cos\frac{\theta}{2}}\left(\left|Sin\frac{\theta}{2}Cos\frac{\theta}{2}Cos\frac{3\theta}{2}+\alpha\right|\right)}{\left(1+Sin\frac{\theta}{2}Sin\frac{3\theta}{2}\right)} \tag{2.23}$$

σ_n and σ_T can be calculated as (Jaeger et al., 2007):

$$\sigma_n = \frac{\sigma_{HMax}+\sigma_{hMin}}{2}+\frac{\sigma_{HMax}-\sigma_{hMin}}{2}Cos(\pi-2\theta) \tag{2.24}$$

$$\sigma_T = \frac{\sigma_{HMax}+\sigma_{hMin}}{2}-\frac{\sigma_{HMax}-\sigma_{hMin}}{2}Cos(\pi-2\theta) \tag{2.25}$$

From Equation 2.22, α can be calculated from

$$\alpha = \frac{\tau}{\frac{K_{IC}}{\sqrt{r_c(\theta)}}}. \tag{2.26}$$

Applying the same approach that was implemented to obtain Equation 2.18:

$$\sqrt{r_c(\theta)} = \frac{K_{IC}}{T_o-\sigma_T}\times\left(Cos\frac{\theta}{2}\left(1+Sin\frac{\theta}{2}Sin\frac{3\theta}{2}\right)\right). \tag{2.27}$$

Substituting Equation 2.27 into 2.26:

$$\alpha = \frac{\tau}{\frac{T_o-\sigma_T}{\left(Cos\frac{\theta}{2}\left(1+Sin\frac{\theta}{2}Sin\frac{3\theta}{2}\right)\right)}} \tag{2.28}$$

It is important that, as is seen from Figure 2.9, if θ is the angle of approach, Equation 2.23 is checked for both angles of θ and π-θ. When θ approaches $\pm\ \pi/2$ Equation 2.23 will reduce to Equation 2.9 (i.e. $\sigma_n = \sigma_{HMax}$, $\sigma_T = \sigma_{hMin}$, and $\tau = 0$), which is a special case identical to R&P's criteria. It should be noted that the graphs resulting from Equation 2.23 should be only compared for *one specific angle of approach* as the left hand side of the equation is changing as a function of angle θ.

General case of non-orthogonal cohesive natural interface

Now, it would be simple to drive a general form. Using similar approach that was used to derive Equations 2.14 and 2.20, a general form of interaction criterion corresponding to a cohesive natural fracture intersecting a non-orthogonal propagating fracture can be written as:

$$\frac{-\sigma_n}{(T_o-\sigma_T)} > \frac{\left(1-Sin\frac{\theta}{2}Sin\frac{3\theta}{2}\right)+\frac{1}{\mu_f{}''Cos\frac{\theta}{2}}\left(\left|Sin\frac{\theta}{2}Cos\frac{\theta}{2}Cos\frac{3\theta}{2}+\alpha\right|\right)}{\left(1+Sin\frac{\theta}{2}Sin\frac{3\theta}{2}\right)}. \quad (2.29)$$

In this equation $\mu_f''=\mu_f+\mu_f'$, and μ_f' can be calculated using:

$$\mu_f{}' = \frac{\frac{\tau_0}{\sigma_n}}{\left(\frac{1-Sin\frac{\theta}{2}Sin\frac{3\theta}{2}}{\left(1-Sin\frac{\theta}{2}Sin\frac{3\theta}{2}\right)+\frac{1}{\mu_f Cos\frac{\theta}{2}}\left|Sin\frac{\theta}{2}Cos\frac{\theta}{2}Cos\frac{3\theta}{2}+\alpha\right|}-1\right)} \quad (2.30)$$

Similar to Equation 2.23, if the angle of approach is θ, Equations 2.27 and 2.28 should be checked for both angles of θ and (π-θ). To check the applicability of this criterion, we compared the results obtain from this equation against the laboratory work published by Zhou et al. (2008). Table 2.2 shows the summary of the results, which indicates a very good agreement except in a few cases. The shaded cells of the following table show the cases at which the model did not satisfy the laboratory work.

Further modification of R&P criterion

Another recent modification on R&P proposed by Gu and Weng (2010) that is difficult to compared with the original criterion because it has an unrealistic assumption and is in a different mathematical form. The criterion is applicable for cohesive non-orthogonal interfaces. However, the criterion does not have an analytical form in the general case and it needs to be calculated numerically. For orthogonal cohesive natural interfaces they proposed the following criterion:

$$\frac{\frac{\tau_0}{\mu}-\sigma_{HMax}}{(T_o-\sigma_{hMin})} > \frac{0.35+\frac{0.35}{\mu}}{1.06} \quad (2.31)$$

Table 2.2 Comparing Zhou et al. (2008) and our developed analytical models

θ (Degree)	σ_v (MPa)	σ_{HMax} (MPa)	σ_{hMin} (MPa)	σ_n (MPa) Eq. 2.24	σ_T (MPa) Eq. 2.25	τ (MPa) Eq. 2.21	τ_0 (MPa)	μ_f	Eq. 2.29	Experiment results Zhou (2008)
90	-20	-10	-5	-10	-5.00	0.00	0	0.89	Crossing	Crossing
90	-20	-10	-3	-10	-3.00	0.00	0	0.89	Crossing	Crossing
60	-20	-10	-3	-8.25	-4.75	-1.52	0	0.89	Crossing	Crossing
60	-20	-13	-3	-10.50	-5.50	-2.17	0	0.89	Crossing	Crossing
60	-20	-8	-5	-7.25	-5.75	-0.65	0	0.89	Crossing	Dilated
30	-20	-10	-5	-6.25	-8.75	1.08	0	0.89	No Crossing	Dilated
30	-20	-8	-5	-5.75	-7.25	0.65	0	0.89	No Crossing	Dilated
30	-20	-13	-3	-5.50	-10.50	2.17	0	0.89	No Crossing	Arrested
90	-20	-8	-3	-8.00	-3.00	0.00	0	0.38	Crossing	Crossing
90	-20	-8	-5	-8.00	-5.00	0.00	0	0.38	No Crossing	Crossing
60	-20	-10	-3	-8.25	-4.75	-1.52	0	0.38	Crossing	Crossing
60	-20	-8	-3	-6.75	-4.25	-1.08	0	0.38	Crossing	Dilated
30	-20	-10	-3	-4.75	-8.25	1.52	0	0.38	No Crossing	Arrested
30	-20	-8	-3	-4.25	-6.75	1.08	0	0.38	No Crossing	Dilated
90	-20	-8	-3	-8.00	-3.00	0.00	0	1.21	Crossing	Dilated
90	-20	-13	-3	-13.00	-3.00	0.00	0	1.21	Crossing	Crossing
60	-20	-13	-3	-10.50	-5.50	-2.17	0	1.21	Crossing	Dilated
60	-20	-10	-3	-8.25	-4.75	-1.52	0	1.21	Crossing	Dilated
30	-20	-13	-3	-5.50	-10.50	2.17	0	1.21	No Crossing	Dilated
30	-20	-8	-3	-4.25	-6.75	1.08	0	1.21	No Crossing	Dilated

2.4.5 Analytical approach for prediction of interaction in laboratory work

All interaction modes should be checked when a study is undertaken as one criterion may be insufficient to cover different possible scenarios at different time of propagation. For example, Renshaw and Pollard (1995) suggested that if there is a re-initiation on other side of the interface, it probably has occurred before fracture tip intersected the natural interface. So interaction might happen at such early times.

Considering all of the cases discussed above, the following guidelines on how and when to use a particular analytical model to predict the interaction mode is presented. First of all, three important concepts should be explained.

1. If shear strength of an interface because of its cohesion, angle of approach, friction, and/or normal induced stress is high enough around the intersection point, slippage will not occur. In this case, the symmetry of crack-tip stress field will be maintained and the propagating fracture will cross the interface. The statement of "high enough shear strength" refers to any case for which the shear strength of the natural interface is higher that the value of the applied shear stress acting on it.
2. If a low shear strength natural interface is subjected to stresses arising from the interaction with an extending hydraulic fracture, it will be slipped and an asymmetric crack-tip stress field will be generated (Lash and Engelder, 2009). Similar to the first case, the shear strength of the interface depends on its cohesion, the angle of approach, the interface friction coefficient, and/or the normal induced stress.
3. As was mentioned earlier, the fracture corrects its path based on the direction that minimises the energy required for growth. So as a result of natural interface slippage, the fracture may deviate from its originally propagating direction and intersect the interface with an angle different from the expected angle of approach: this is shown schematically in Figure 2.14. In this figure, if the shear strength of the natural interface is high, the propagating fracture will cross it (left side), otherwise the extending fracture may deviated and become arrested by the natural interface (right side). These potential scenarios give rise to complexity in the interaction mechanism. The fracture behaviour that results will be shown and discussed in the next chapter (laboratory work) of this thesis.

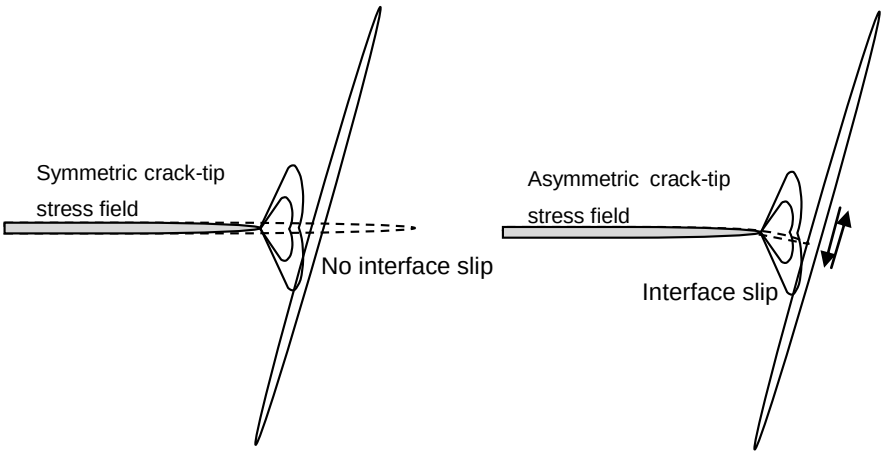

Figure 2.14 The tip induced tangential stress may result in change of angle of approach and cause crossing (left) or arresting interaction mode (After Lash and Engelder, 2009).

Knowing these facts, the interaction prediction may be conducted in the following steps

1. The possibility of crossing is first checked against Modified R&P criterion (Equation 2.27). If the resultant interaction is crossing, there will be no need to check for other cases. If no crossing occurs, the stress at the tip will be reduced by slip or opening and the fracture will be arrested at least for a moment (Dollar and Steif, 1989). So further pressurization of the fracture at the intersection point is necessary.
2. Putting aside the possible deviation of the propagating fracture shown in Figure 2.14, the likely interaction mode of opening (say arresting by opening) or shear slippage (arresting by shear slippage) can be checked from Equations 2.7 and 2.8, respectively (see figure 2.10).
3. If Equation 2.8 is not satisfied, the arrested hydraulic fracture may re-initiate at the intersection point and propagate from the other side of the natural interface. In laboratory tests, this is likely to be the end of the experiment as at this stage the fracture plane will possibly reach the sample boundaries, ending the test.
4. For field cases or lab experiments on samples that include very small natural interfaces like randomly generated natural fractures (e.g. see Beugelsdijk and de Pater, 200; Zhou and Xue, 2011), the natural fractures are unlikely to take significant flow but they are either crossed or first opened and then crossed by the hydraulic fracture.
5. If Equation 2.8 is satisfied and the fracture is arrested because of shear slippage, nothing will happen until the pressure in the propagating fracture increases. While pressurizing the intersection point, fracturing fluid may leak into the natural

interface or open the interface and increase the fluid pressure. The result of opening or leaking will be the same as if the final interaction is crossing. At any location, i.e. the fracture tip, intersection, or any points in between, if fluid pressure exceeds the re-initiation resistance, i.e.:

$$P_{fluid} > P_{resis}, \tag{2.32}$$

fracture starts its propagation on the other side of the natural interface.

The re-initiation resistance (P_{resis}) at any point can be defined as:

$$P_{resis} = \sigma_{hMin} + T_0 , \tag{2.33}$$

where T_0 is the tensile strength. However, the re-initiation will most likely happen at the intersection point as it carry the highest fluid pressure. Otherwise, it will happen at a point between the tip and the intersection at which there is a flaw or surface imperfection. At such points the tensile strength is reduced significantly. Finally crossing may happen at the tip of the natural interface where the local tensile strength may be assumed to be zero. Prediction of pore pressure along the natural interface will be crucial for this step. Table 2.3 shows the formulation of four different cases of fluid pressure along a natural fracture developed by Warpinski and Teufel (1987).

Table 2.3 Natural fracture fluid pressure for four different cases (Warpinski and Teufal, 1987)

Case 1

Linear flow, Infinite joint, No leak off out of the joint, Joint is filled with the same fluid used in the hydraulic fracture treatment

$$p = p_t + (p_t - p_R)\,erfc\left(\frac{\phi\mu c y^2}{4kt}\right) \tag{2.34}$$

Case 2

Evacuated joint
Infinite joint

$$p = p_t + (p_t - p_R)\left(\frac{y}{y_f}\right) \tag{2.35}$$

where

$$y_f = \sqrt{\frac{2k(p_t - p_R)t}{\phi\mu}} \tag{2.36}$$

Case 3

Finite joint, Joints is filled with the same fluid used in the hydraulic fracture treatment

$$p = p_t - \frac{4(p_t - p_R)}{\pi}\sum_{n=0}^{\infty}\frac{1}{(2n+1)}\exp\left[-\frac{(2n+1)^2 k\pi^2 t}{4\phi\mu c L_j^2}\right]Sin\left[\frac{(2n+1)\pi y}{2L_j}\right] \tag{2.37}$$

Case 4

Evacuated joint, Finite joint

$$p = p_t - \frac{4(p_t - p_R)}{\pi}\sum_{n=0}^{\infty}\frac{1}{(2n+1)}\exp\left[-\frac{(2n+1)^2 k\pi^2 t}{4\phi\mu c L_j^2}\right]Sin\left[\frac{(2n+1)\pi y}{2L_j}\right] \tag{2.38}$$

where

$$t \prec \frac{\phi\mu L_j^2}{2k(p_t - p_R)} = t_f \tag{2.39}$$

$$p = p_t + \frac{8(p_t - p_R)}{\pi^2}\sum_{n=0}^{\infty}\frac{(-1)^n}{(2n+1)^2}\exp\left[-\frac{(2n+1)^2 k\pi^2 (t - t_f)}{4\phi\mu c L_j^2}\right]Sin\left[\frac{(2n+1)\pi y}{2L_j}\right] \tag{2.40}$$

where

$$t \succ \frac{\phi\mu L_j^2}{2k(p_t - p_R)} = t_f \tag{2.41}$$

where;
P_t = average pressure in the hydraulic fracture over the entire treatment time
P_r = reservoir pressure
y_f = location of the fluid front
Lj = joint length
y = distance orthogonal to the fracture surface.
t *and* t_f = total fracturing time and time required to fill the joint respectively

2.5 Summary

In this chapter a review has been presented of previous studies on the interaction of a hydraulic fracture intersecting a natural interface. It was explained that for lab experiments to be representative of field operations scaling laws are to be applied. Numerical simulations have been used for this purpose but few attempts have been reported on the use of discrete element method: the DEM will be used in this study for numerical simulations and the results will be presented in Chapter 4. In that chapter, a discussion will be presented on how DEM is advantageous in some aspects for simulations of hydraulic fracturing and interactions.

In real situations the reaction of a hydraulically induced fracture phenomenon itself and/or when it is approaching a discontinuity plane (i.e. an inhomogeneous medium) or arriving at different formations with different rock properties in an anisotropic stress field, is complicated. Many researchers have addressed this phenomenon either by laboratory or numerical simulation work. From these studies, the important aspects regarding fracturing treatment and its interaction with natural fractures can be summarized as follow:

- In addition to tensile failure, shear failure also needs to be considered in a hydraulic fracturing study (Solberg et al., 1977).
- A symmetrical double-wing planar straight fracture does not always initiate or propagate from the wellbore (Scott et al., 2000).
- Hydraulic fracture direction will change with respect to the least local resistance path. (Daneshy 2004). This path is where require propagation energy minimizes. The energy required includes elastic energy to overcome stress and to open the fracture and viscous dissipation resulting from flow of fluid inside the fracture channel. The path can be along natural fractures for some segments and these segments form offsets along the path. So the fracture does not always grow only orthogonal to the minimum stress when the rock contains natural fractures.
- Natural fracture will change the main propagation path of a hydraulic fracture by changing the local stresses (Daneshy, 1974), the viscous flow resistance and the rock fracture toughness. The viscous dissipation in the fracture also plays a role in determining the path (see Zhang et al., 2011 for an example of this).
- The presence of natural fractures may result in a high net pressure, extensive fluid leak-off, premature screenout, multiple stranding fracture growth,

segmented propagation pattern, and fracture arrestment problems during fracturing treatments (Jeffrey et al, 2010; Azeemuddin et al., 2002).

- Hydraulic fracture will tend to cleanly cross pre-existing fractures only under high differential principal stresses and high angles of approach (Blanton, 1986).
- Hydraulic fracture extension may be at least temporarily prevented when it reaches a high permeability layers (Blair, 1989).
- Depending on the rock type, a straight non-branched fracture would not be created if the ratio of maximum to minimum stress is below a certain value (Doe and Boyce, 1989).
- A hydraulic fracture will cross a natural fracture if the normal stress applied on the natural fracture surface provides enough frictional resistance along the natural fracture to allow transfer of tensile stress to the other side of natural fracture sufficiently to initiate a new crack on the opposite side (Renshaw and Polard, 1995).
- The higher the product of fracturing fluid viscosity and flow rate, the higher the chance of crossing (Beugelsdijk and de Pater, 2005).
- Use of a higher viscosity of injection fluid may induce slip on the discontinuity before the fracture reaches the discontinuity (Lecampion and Zhang, 2005).
- The properties of the filing material in an interface filing will affect the interaction (Casas et al., 2006a).

Also, a new analytical were developed based on the study of Renshaw and Pollard (1995). This expands the capability of the interaction criterion to a general case for the cohesive and non-orthogonal interfaces. This criterion was examined based on published interaction study and good agreement were observed.

3 Experimental studies

A large amount of literature is available on hydraulic fracturing laboratory experiments (Daneshy, 1971; 1973a; 1973b; 1974; Ahmed et al., 1983; Rabaa, 1989; Veeken et al., 1989; Hallam and Last, 1990; Behrmann and Elbel, 1991; Bunger, 2005; Lhomme, 2005; Llanos, 2006; Athavale and Miskimins, 2008; Gu et al., 2011). As was discussed in the previous chapter, scaling laws are to be applied to ensure that field fracturing is represented by the laboratory scale experiments. A series of scaled lab experiments were performed in this study to understand the parameters affecting hydraulic fracturing and interaction modes when the fracture intersects an impermeable cohesive natural interface. In addition, the results of standard tests conducted to estimate the samples' hydro-mechanical behavior are given. Details of sample preparation and a brief review of the equipment used for hydraulic fracturing tests are presented first.

3.1 Equipment

A True Triaxial Stress Cell (TTSC) was used to conduct the fracturing experiments in this study (Rasouli and Evans, 2010). Figure 3.1 (top) shows a view of the TTSC. The maximum block size that can be accommodated by the TTSC is 30 cm. By using a series of shims, samples with smaller sizes can be tested too. In this study we tested samples with sizes of 10, 15 and 20 cm. Figure 3.1 (bottom) shows a 10 cm sample placed in the TTSC with the horizontal rams for applying the two sets of stresses. The vertical stress is applied when the top cap is installed.

The friction which is generated between the ram or shim and the sample face may cause a change in stress distribution on the sample (Vonk, 1993). This effect may be reduced by inserting a very thin Teflon sheet and applying grease as a lubricant. The shims are made of Aluminium or steel material with their size being 2.5% smaller than the sample sizes in order to prevent them coming into contact with each other in case of relatively large displacements. This arrangement applies stress free zones around the edges corners of the sample but during our experiments we found this not to be a major

problem affecting the results. TTSC is able to apply 3000 psi of independently controlled pore pressure in the cell using a reciprocating pump.

The injection of fracturing fluid is applied using four syringe pumps, each capable of providing a constant flow rate of 1-300 cc/hr (0.017-5 cc/min). For larger flow rates the pumps are used in parallel. The injection capacity of each pump is about 300 cc which gives a total fluid injection ability of 1200 cc for all pumps. The maximum injection pressure for these pumps is 15,000 psi. To obtain a wider flow rate range, another pump with an injection rate of 0.001-10 cc/min but maximum working pressure of 6000 psi was used. The fracturing fluid is isolated from hydraulic oil with a piston located in a displacement chamber. Pressurising the hydraulic oil pushes the piston and hence the high viscosity fracturing fluid into the injection line (see Figure 3.2).

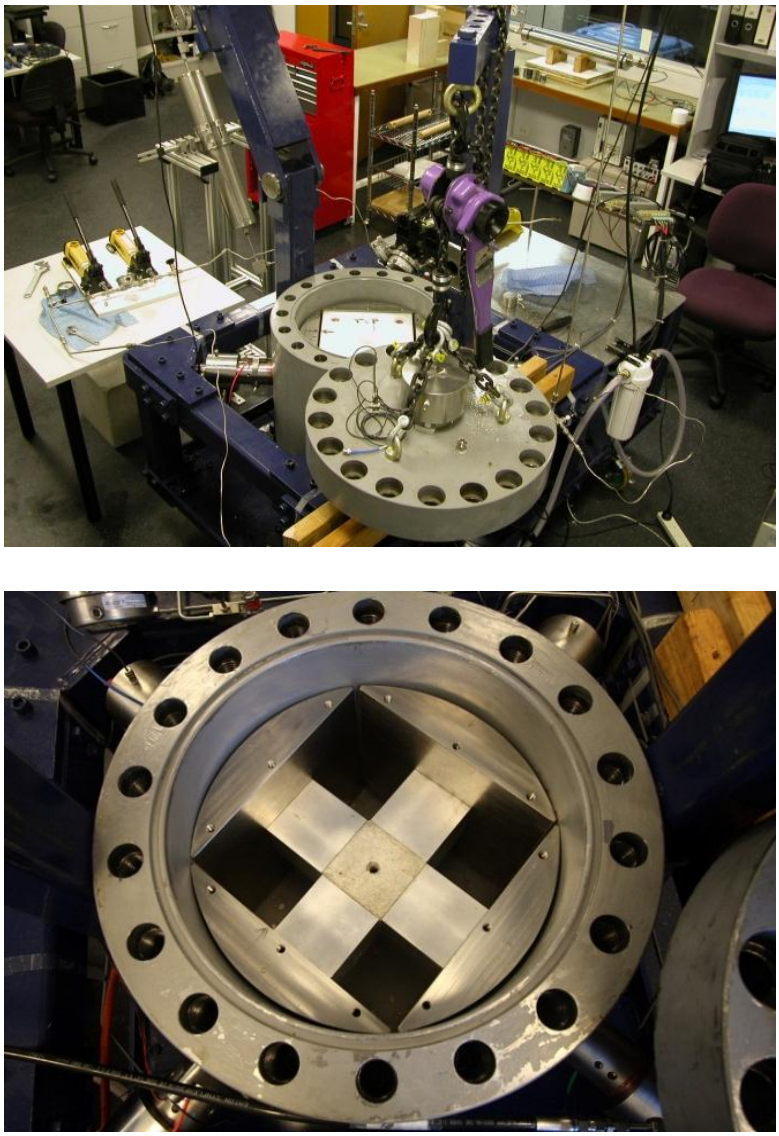

Figure 3.1 A view of TTSC (top) and the arrangement used for testing a 10 cm sample.

Three different displacement chambers with maximum working pressure of 15,000 psi and different volumes of 20, 120, 750 cc were designed for testing different sample sizes. However, in order to minimize the system dead volume, the smaller chambers was used for fracturing tests. Filling the small diameter displacement tube with extremely high viscosity fracturing fluid is cumbersome and heating of the fluid may be needed in order to remove the air bubble more easily, but this may change fluid properties. A better approach is to fill the largest diameter cylinder and vacuum the fluid for few days to ensure all air bubbles have been removed from the fluid. This de-aired fluid is then displaced into the smaller size chambers.

The fracturing fluid is injected into a hole drilled at the centre of the sample from beneath the cell and the injection pressure is recorded at the nearest possible point to the sample using two digital pressure gauges (inj1 and inj2). The position of these transducers is shown in Figure 3.2 for a 20 cm sample placed in the cell. The use of a flow restriction device before the last transducer would immensely help to gradually regulate the flow of a large volume of fracturing fluid into a newly initiated fracture plane. This large flow rate is driven by the compressibility of fracturing fluid plus hydraulic oil in the displacement chamber and, to a lesser extent, the expansion of the metal pressure vessels. The flow restriction device will reduce unstable fracture growth especially during the fracture initiation. As shown in Figure 3.2, the chock (a slightly opened needle valve) located between transducers restricts the flow (Bunger, 2005). In this figure a dial pressure gauge is shown along the injection line which is used as a backup pressure reading for transducer inj2. The dial pressure gauge is approximately 20cm away from the initiation point of the hydraulic fracture. The chock generates a considerable pressure reduction and transducers inj1 and inj2 record different values but with the same trend.

Using the TTSC three independent stresses can be applied to the sample. In current configuration the maximum forces that can be practically applied to the sample is s are 70,650 lb_f in horizontal directions and 125,600 lb_f in vertical direction. Also, using Enerpac hydraulic ram, the vertical load can be increased up to 250,000 lb_f. A constant stress can be maintained on the sample during the course of experiment using three syringe pumps in the same approach explained for the injection system (see figure 3.2). The stresses and injection pressures are acquired using cDAQ9174 National Instrument chassis having two modules of NI9303 and NI9206 and visualised by LabView software.

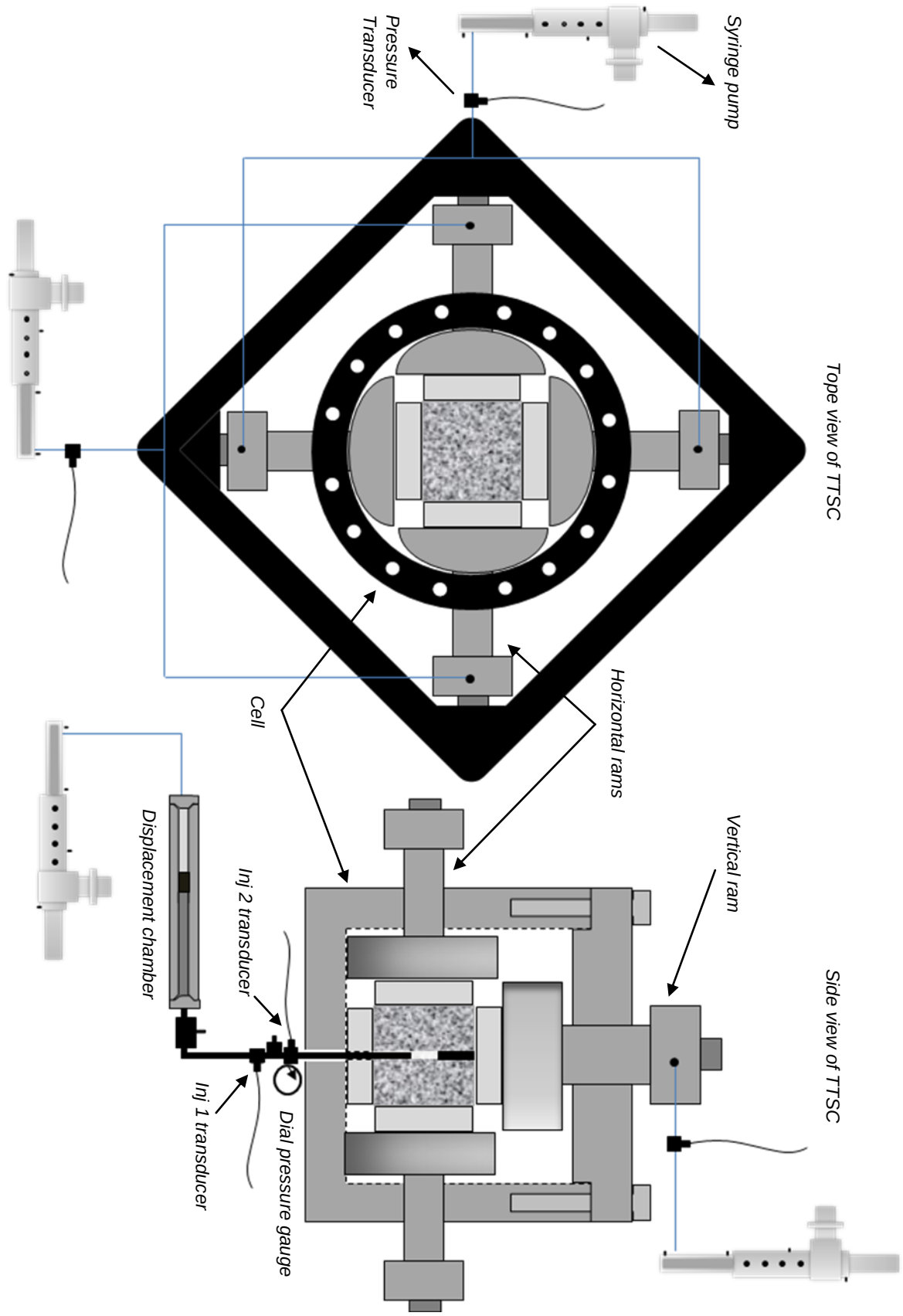

Figure 3.2 A schematic view of TTSC.

Silicon oils with different viscosities were examined for fracturing fluid. Table 3.1 lists different properties of fracturing fluids. From this Table it is noted that the viscosity of these fluids is very high: this is due to the fact that for small size samples tested in the lab large fluid viscosity is to be used to satisfy scaling laws as discussed previously.

Table 3.1 Physical properties of different fracturing fluids.

Fracturing fluids	Viscosity* (cSt)	Specific Density	Viscosity (cp)	**Compressibility (1/psi)	Flow rate range for Newtonian Behavior	Water Solubility	Molecular Weight
Honey	27,200	***1.36	~20,000	***0.69×10-6	~Always	Soluble	-
Poly DMS-T51	*100,000	0.977	97,700	<6.5×10-6	****Up to 234.5 cc/min	insoluble 100-200 ppm	139k
Poly DMS-T56	*600,000	0.978	586,800	<6.5×10-6	****Up to 4.750 cc/min	insoluble 100-200 ppm	204k
Poly DMS-T61	*1,000,000	0.978	978,000	<6.5×10-6	****Up to 1.901 cc/min	insoluble 100-200 ppm	308k
Poly DMS-T63	*2,500,000	0.978	2,445,000	<6.5×10-6	****Up to 0.9501 cc/min	insoluble 100-200 ppm	423k
Poly DMS-T72	*20,000,000	0.979	19,580,000	<6.5×10-6	****Up to 0.048 cc/min	insoluble 100-200 ppm	>500k

*Viscosity specifications for poly dimethylsiloxanes (DMS) fluids
**at 5,000psi
***From Min et al., 2010.
****This values were calculated for a quarter inch tube that usually was used for our test and based on critical Newtonian velocity that was provided by silicon oil manufacturer.

3.2 Sample preparation

In this study, hydraulic fracturing tests were performed on cubical samples with sides 10, 15 and 20 cm. Before conducting the experiments, it was necessary to obtain an estimation of hydro-mechanical behavior and properties of the samples. This is important in terms of interpreting the results and these properties will be used as input to the DEM numerical simulations, which will be discussed in detail in Chapter 4.

Cement mortar and sample casting

The cement to sand mass ratio of one and water to cement weight percentage of 40% was used for all mortar samples. This was to study the fracturing properties consistently. The grain size distribution of the sand is shown in Figure 3.3. Based on this figure, the effective size (D_{10}) of the grains is 0.25mm and the coefficient of uniformity (D_{60}/D_{10}) is 1.76. Figure 3.4 shows the size distribution of sand grains.

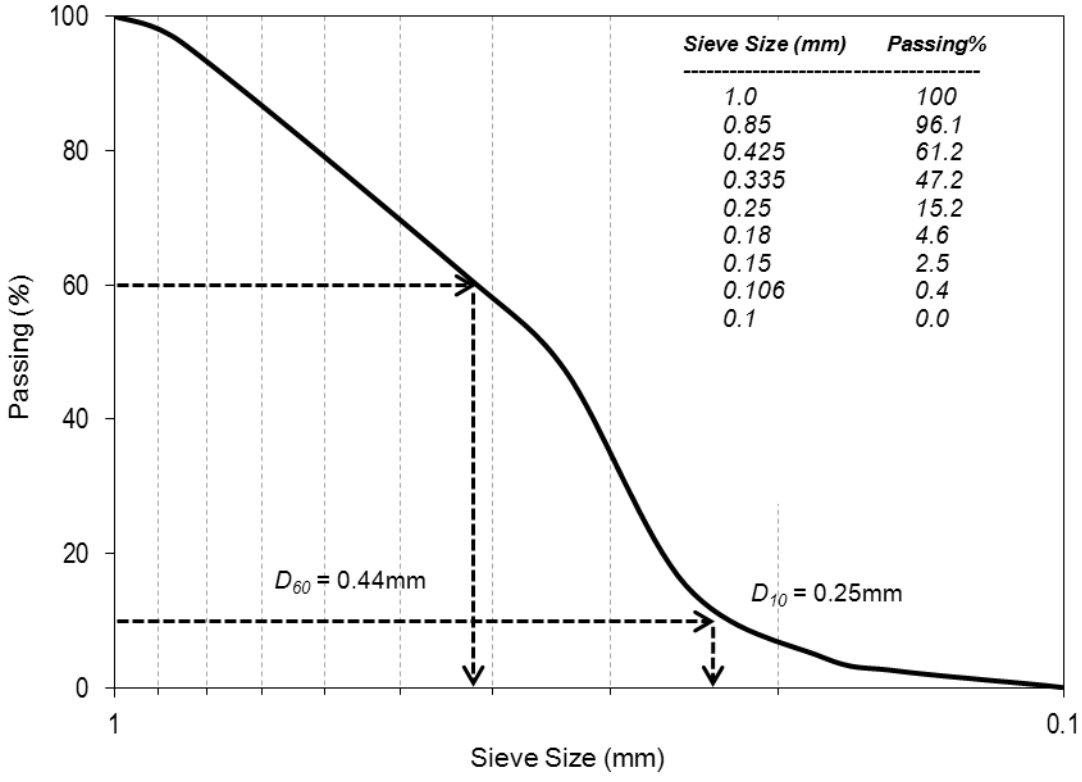

Figure 3.3 Grain size distribution of the sand particles used for preparing the mortar.

Water, sand, and cement were mixed for 15 min. This time was found adequate to ensure that sand grain distribution was uniform in the mortar. The mix was poured into different mould sizes gradually while a vibration table was used to remove the air bubbles trapped in the mix. The vibration time period was chosen in such a way that sand particles were not precipitating as mixture viscosity was relatively large to suspend them during the course of vibration. The top side of the sample was flattened using a finishing trowel one hour after casting. This is due to the fact that the mix will release some bleed water and consequently shrinks slightly.

To create artificial fracture surfaces (i.e. natural interfaces) oil coated galvanized steel sheets (2 sheets for each sample) with different sizes were placed into the mix before it sets in such a way that the sample is divided into three pieces. Artificial fractures with angles of 30, 60, and 90 degrees were made on 10 and 15 cm mortar cube samples. Figure 3.4 shows the top view of two 10cm samples with 90°and 60° natural interface together with 3D view of the latter sample. Sample was removed carefully from the mould after 12 hours and cured for 28 days in 25 ˚C water bath. It is expected that the cement cubes obtain their final strength (i.e. more than 90%) after 28 days (Mindess et al, 2003).

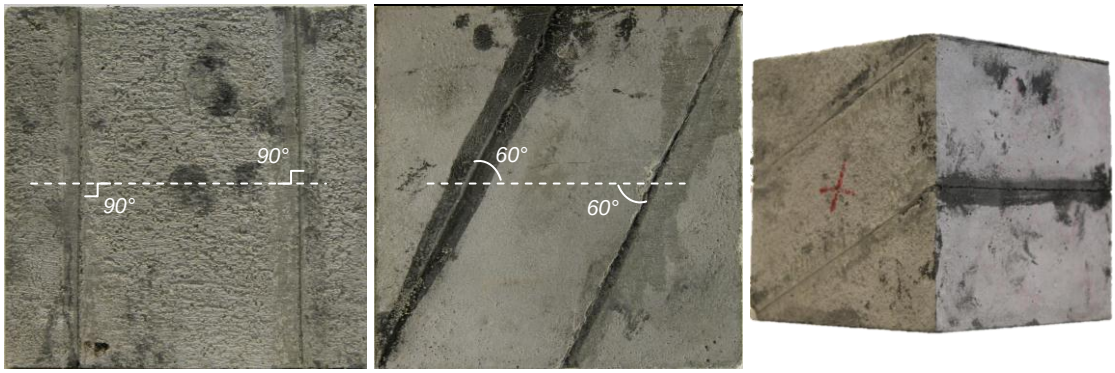

Figure 3.4 Two 10cm sample with interface of 90°(right) and 60°(middle and right).

At micro scale these blocks may have small pore spaces of 1 μm which enclosed with grains of 1-1000 μm size (deKetterij, 2001). The low fracture toughness, low permeability and low to moderate porosity are the key features that make the cement a good candidate for fracturing tests. A minimum of three cylindrical samples of 2×4 or 1.5×3 inches (diameter × length) were made to conduct standard hydro-mechanical tests. Also, two large diameter cylindrical samples were used for Brazilian and fracture toughness tests. The tensile strength and fracture toughness values came from the

Brazilian tests and mode I Semi-Circular Bend (SCB) test specimen (Chong and Kuruppu, 1984; Chong et al., 1987). All permeability and porosity tests were performed on 1.5×3 inches core plugs that were taken from large diameter cylindrical samples.

Natural interface preparation

The natural interface was introduced into the sample through the procedure explained in first part of the previous subsection. These interfaces were made by placing a thin steel sheet into the casted mortar before it sets. These interfaces were then glued using four different adhesives. Shear strength of these glues are listed in Table 3.2. Two plastic glues (Brown and Black) and two brittle ones (cement and white glue) were chosen to study the effect of interface filing material. The thickness and curing time period were kept identical for all adhesives except for the cement which needed to be cured in water. Figure 3.4 shows two samples one with white glue (left) and the other with black glue (middle and right).

Uniaxial compressive test

The average uniaxial compressive strength of the mortar samples was estimated to be 11,530 psi (79.5 MPa) as the result of 15 tests. The following figure shows the stress-strain curves corresponding to the UCS test of three samples. The axial and lateral strains were measured during the test. An average Young's modulus (E) and Poisson's ratio (υ) of 4.0×10^6 psi (27.7 GPa) and 0.2 were obtained for the aforementioned samples, respectively.

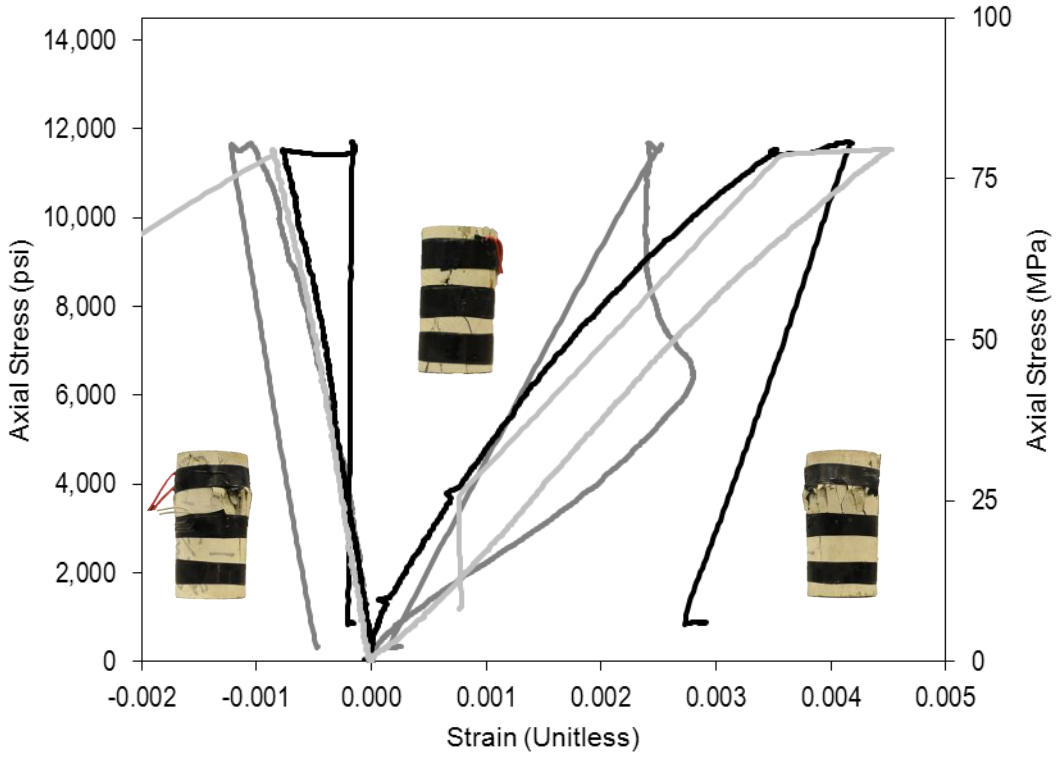

Figure 3.5 Stress-strain curve of UCS test for three mortar samples.

Confined compressive test

Internal friction angles and cohesion values of the mortar samples were measured using a Hoek Cell to apply confining stress during testing. 40 cylindrical samples of 2 and 1.5 inches in diameter with the length to diameter ratio of 2-2.5 were used for this purpose. Average internal friction angle of °44.3 (Φ) and cohesion (C_c) of 2524 psi (17.3 MPa) were determined (see figure 3.6). Figure 3.7 shows the plot of some of these confined compressive strength results for confining stresses that varied from 400-1400 psi (2.76-9.65MPa). The linear trendline of data reflects a value of 12,050 psi (83.1 MPa) for sample's UCS. This value is very similar to the average measured value of UCS (79.5MPa) using uniaxial compressive tests.

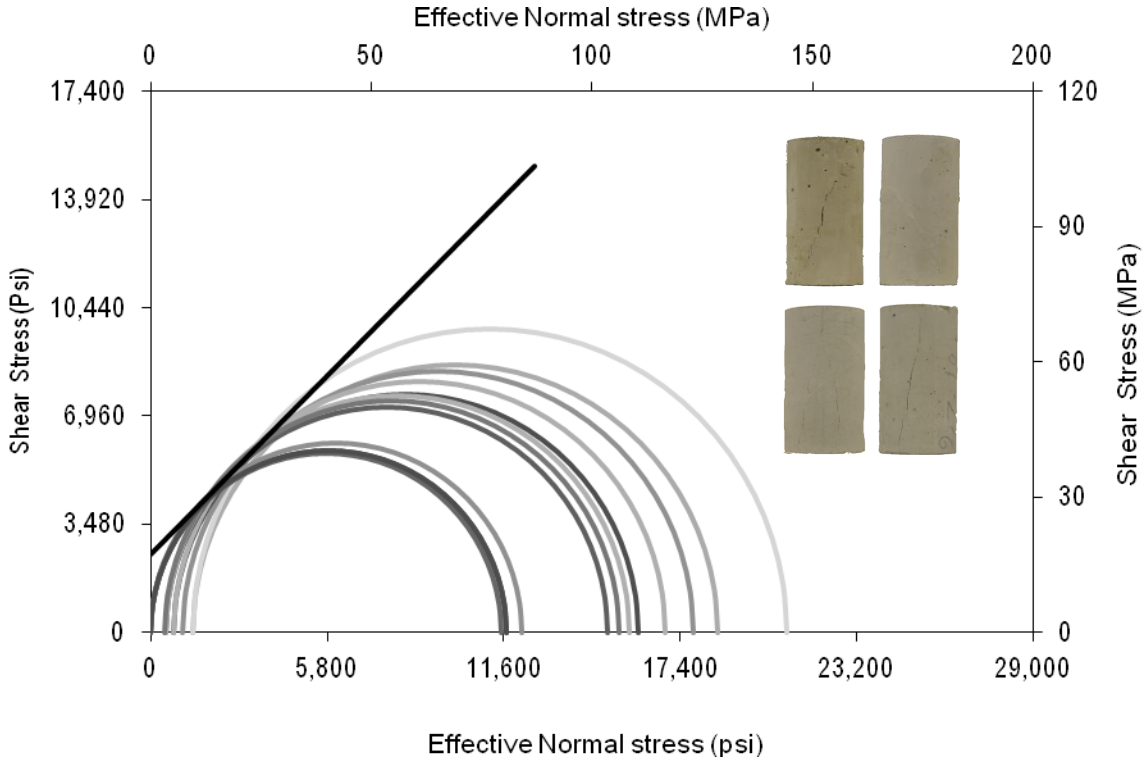

Figure 3.6 Mohr Circles corresponding to confined compressive tests of mortar samples.

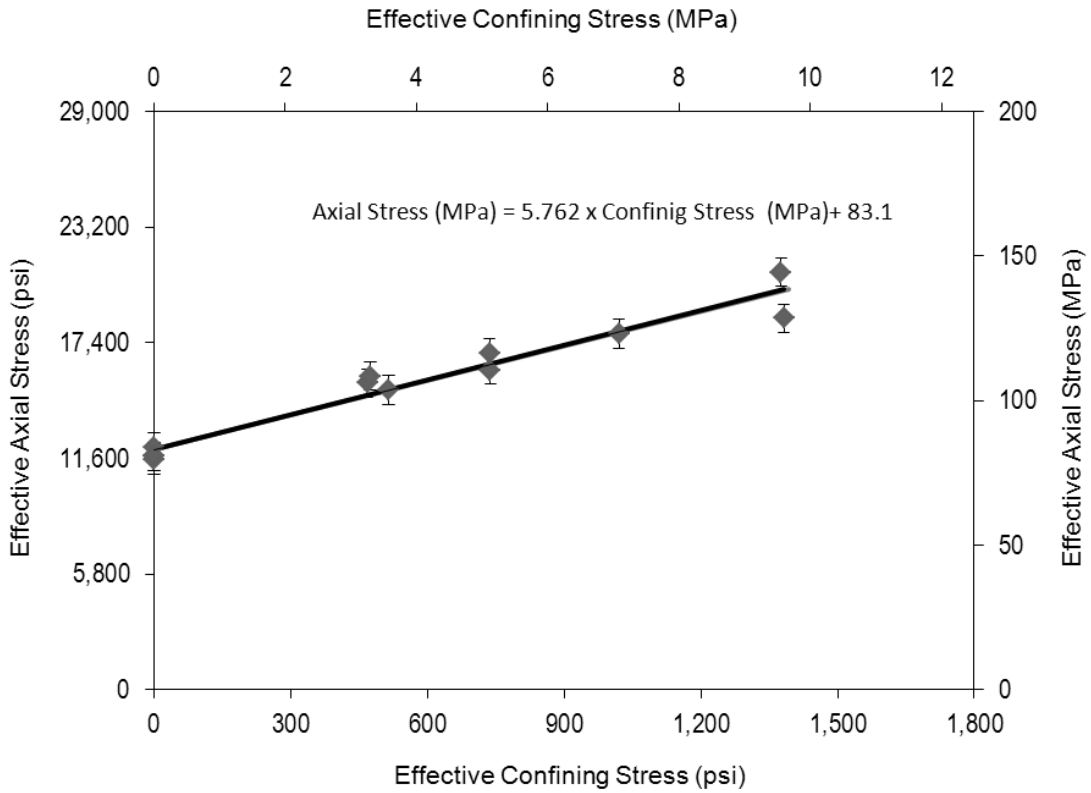

Figure 3.7 Axial versus confining failure envelope corresponding to mortar samples.

Multi-stage test

A multi-stage triaxial test was performed on a 1.5 in diameter plug taken from a larger size sample to compare the results with the series of single stage tests reported in the previous subsection. The samples all come from the same material. Figure 3.8 shows the results of the test. Using the multi-stage test, an internal friction angle of 44.63° and a cohesion of 2230 psi (15.4 MPa) were obtained: these are in close agreement with the results obtained from confined compressive tests. The calculated UCS from multi-stage test was 10,670 psi (73.6 MPa) which is 1380 psi (9.5 MPa) less in the latter test, which could be due to sample being weakened in its strength during coring.

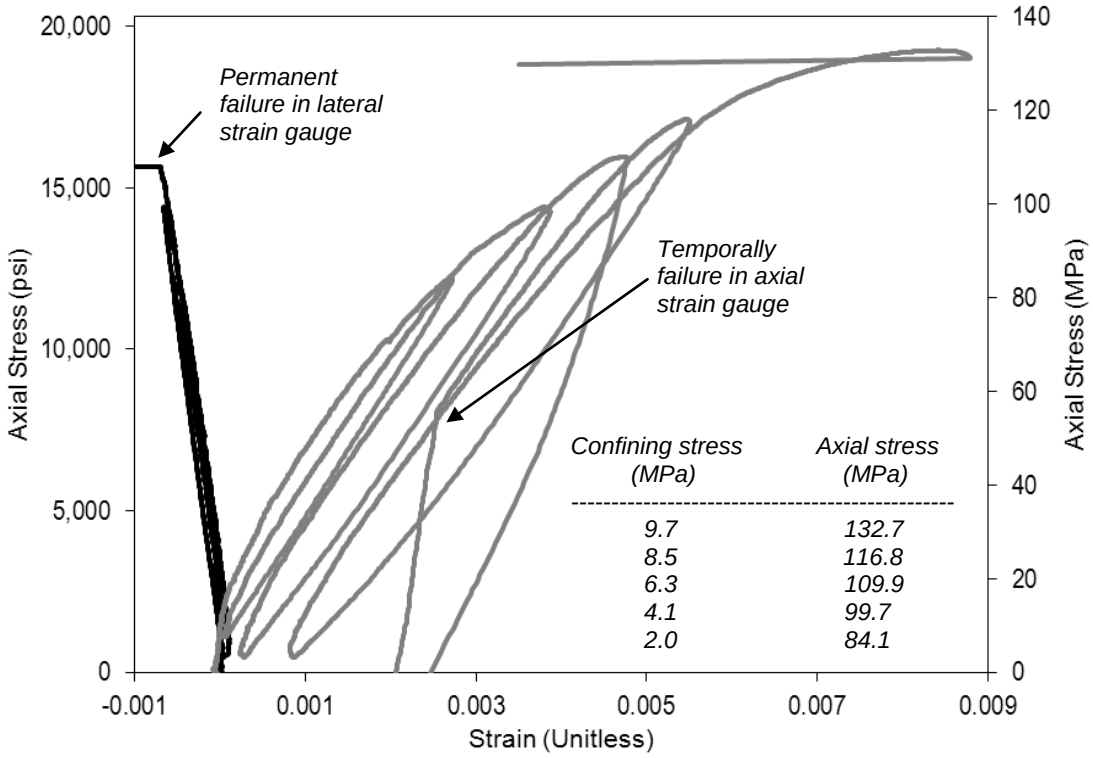

Figure 3.8 Plot of axial stress versus strain for multi-stage compressive test on a 1.5 inches cylindrical sample.

Brazilian test

To estimate the tensile strength (T_0) of the samples, Brazilian test were conducted on 12 cylindrical samples with three different sizes of 6×3.7, 3.8×3.5, 2×1.9 in (diameter× thickness). The measured tensile strength varied from 400-740 psi (2.8-5.1 MPa) with an average value of 510 psi (3.5 MPa). Figure 3.9 shows the load-time plot of Brazilian test for these three sample sizes.

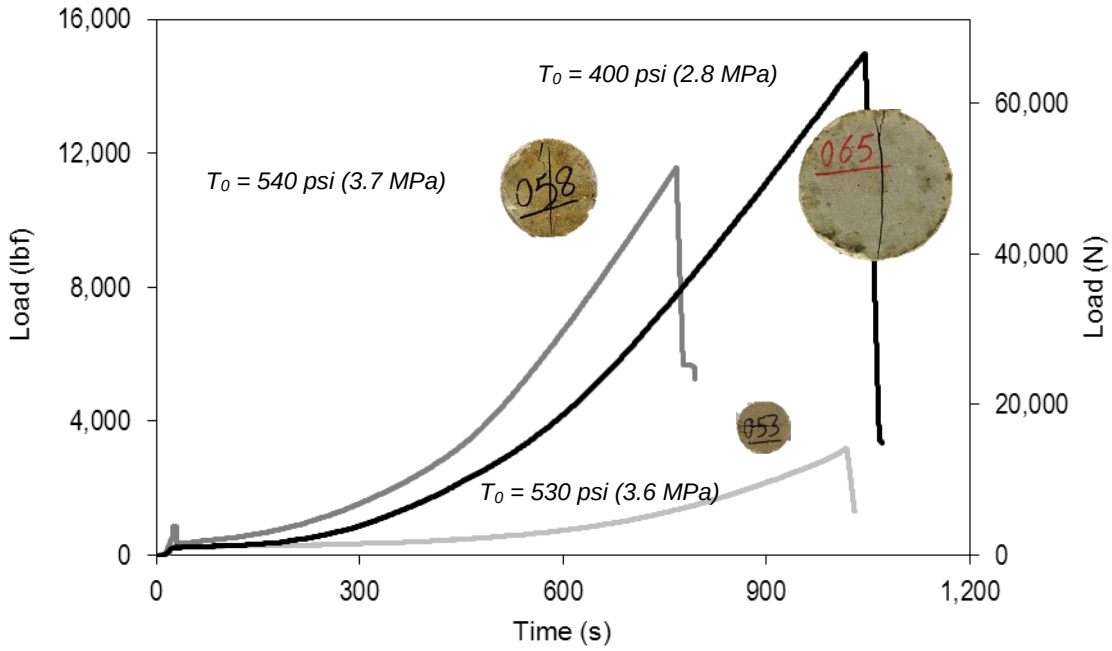

Figure 3.9 Plot of force versus time in Brazilian tests of three different sample sizes.

Semi-Circular Bend (SCB) test

Fracture toughness of the samples was estimated from semi-circular bend (SCB) test procedure based on the formula developed by Chong et al. (1987) for mode I fracture toughness. An average toughness value of 710 psi.in$^{1/2}$ (0.78 MPa.m$^{1/2}$) was obtained for the tested samples. Figure 3.10 shows the load-time plot for three tests carried out.

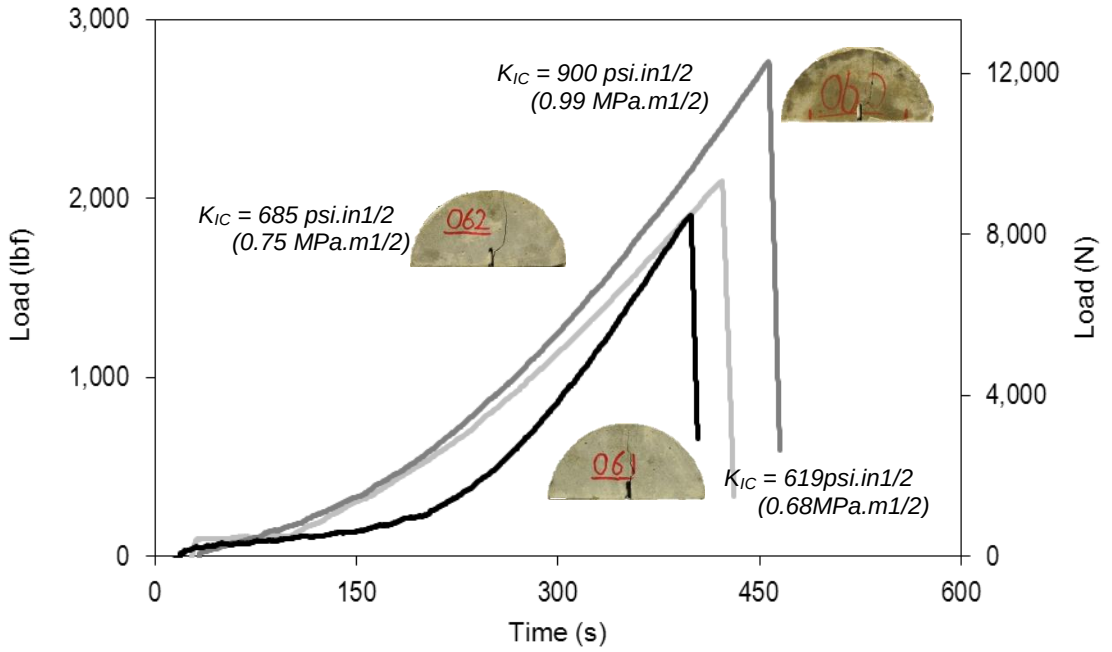

Figure 3.10 Plot of load versus time in toughness tests of three different samples.

Concrete-concrete friction coefficient

The set up shown in Figure 3.11 was used for measuring the friction coefficient of concrete-concrete interfaces. The normal stress was firstly applied to the samples (in this figure a 10 cm sample) and then axial stress was increased until the middle sample slides. This was repeated after increasing the normal stress to a larger value.

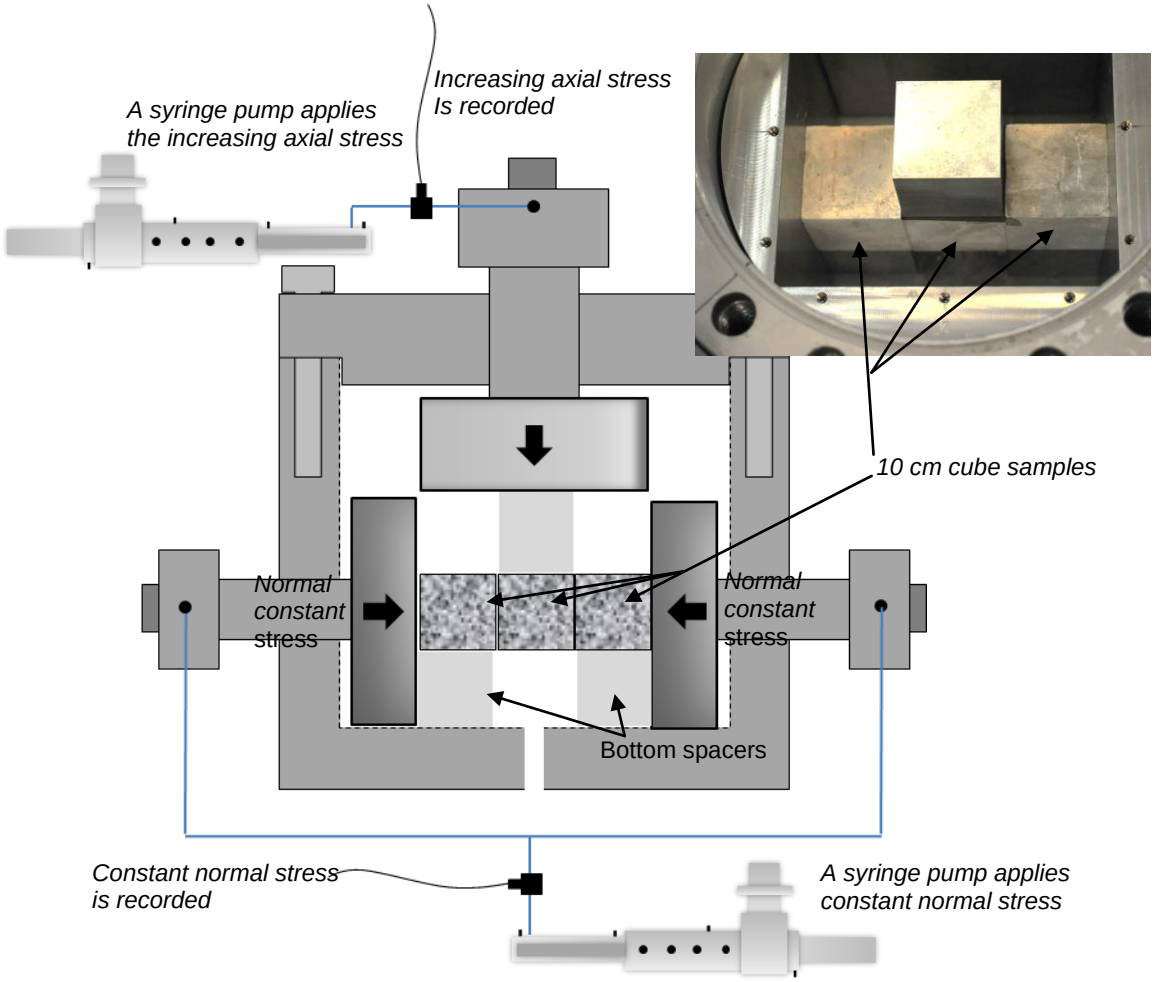

Figure 3.11 Arrangement used for concrete-concrete interface friction coefficient. The top right side figure shows three 10cm samples that were used for this test.

Figure 3.12 shows the plot of both axial and normal stresses and the value of friction coefficient that were calculated at each load step. The average friction coefficient of 0.698 was measured during this practice. It should be noted that the calculation of friction coefficient using this set up is different from conventional approach in that frictional force is present on two surfaces.

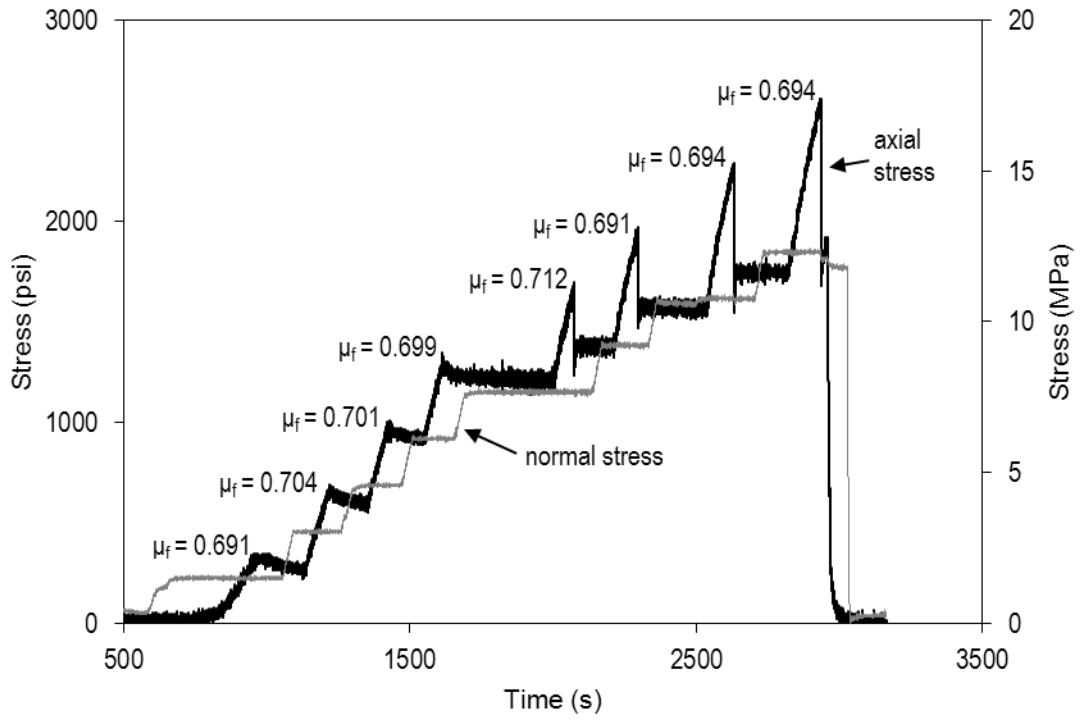

Figure 3.12 Plot of loads applied to the sample for measurement of concrete-concrete interface friction coefficient.

Permeability and porosity

It is well known that permeability and porosity of a sample are stress dependent. The samples used for this study were tight which made it almost impossible to measure their porosity and permeability using brine. The transient gas permeability measurement and two Boyle's law porosity tests were carried out at different net confining stresses on different samples. The samples were prepared, dried, and cured through an identical procedure. Figure 3.13 shows how porosity and permeability of the samples varied when confining stress changes.

The permeability of the samples drops down very fast as the net confining stress increases. Figure 3.14 shows the percentage change in permeability and porosity of sample with reference to corresponding values at 500 psi confining pressure. From this figure, it is seen that when stress increases to 3000 psi, the air permeability of the sample reduces to 20-40% of its original value. The figure also shows that although the porosity reduces as the net confining stress increases, it is not a strong function of the stress comparing to that of permeability.

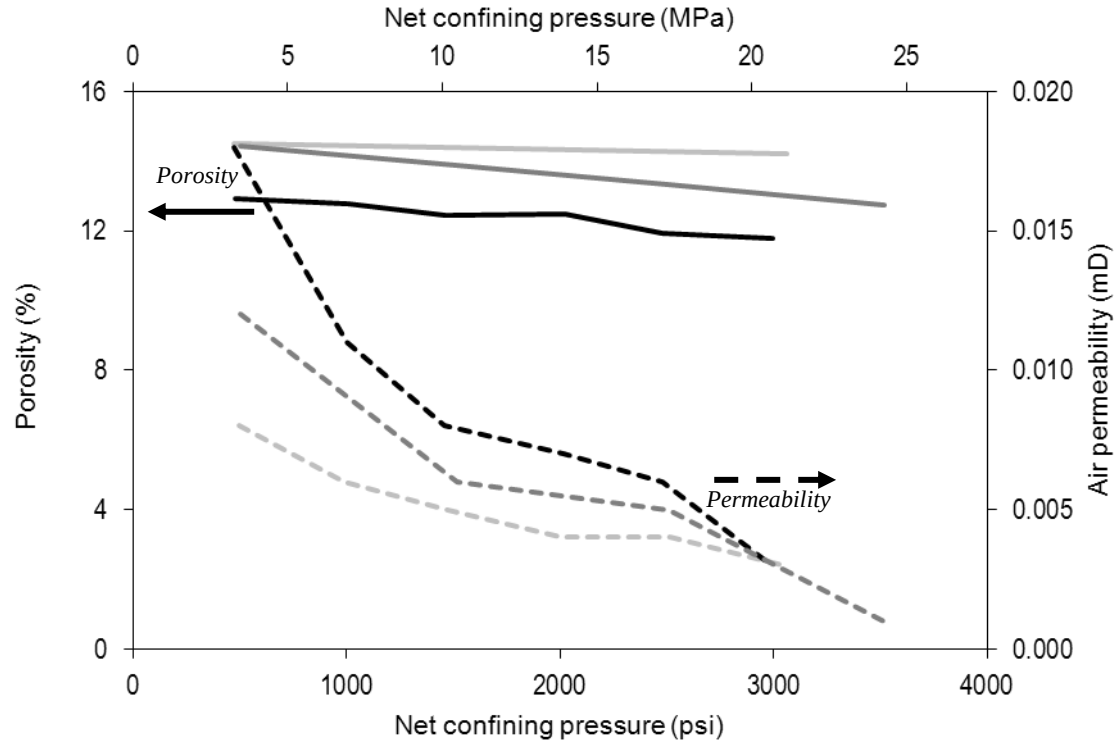

Figure 3.13 The change of porosity and permeability on three 1.5 inches cylindrical samples on different net confining stresses.

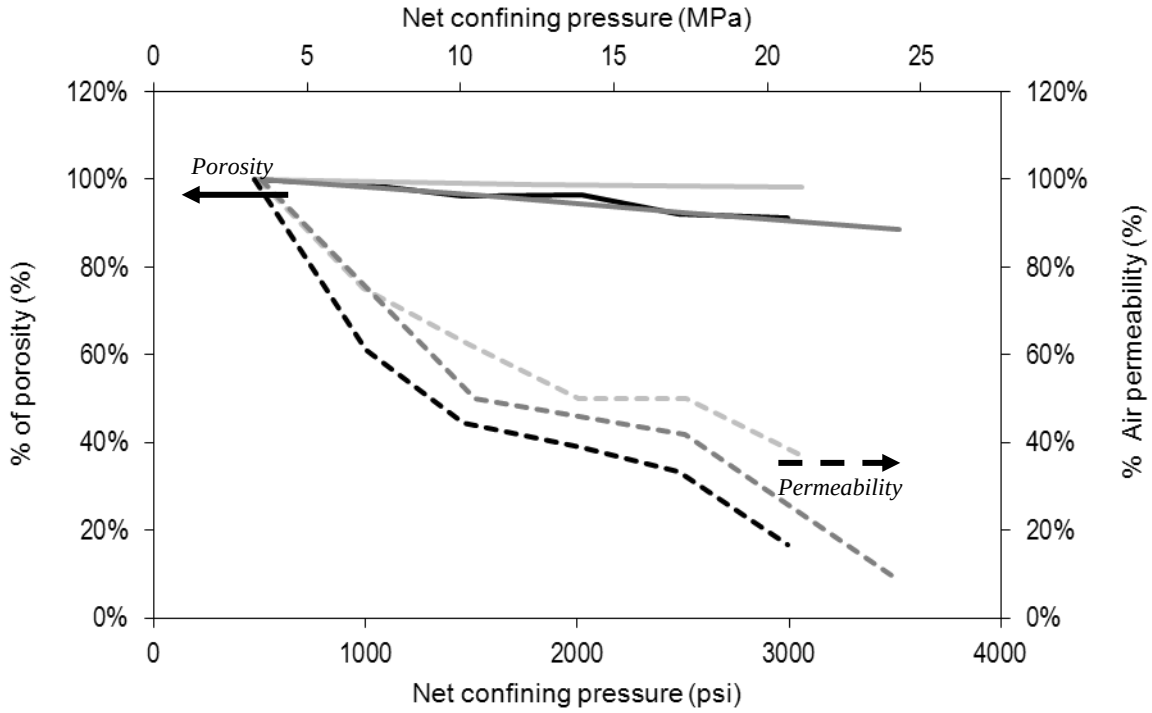

Figure 3.14 Percent of porosity and air permeability reduction of three different samples as results of different net confining stresses. These values were normalized using the permeability and porosity measurements at 500 psi confining net stress.

The following correlation was obtained for the permeability and porosity of the samples and the net pressure, i.e. confining pressure (σ_c) minus pore pressure (P_f):

$$k_{air} = -0.005\ln(\sigma_c - p_f) + 0.0186 \tag{3.1}$$

$$\varphi = -0.0006(\sigma_c - P_f) + 14.7\,. \tag{3.2}$$

As there is no pore pressure in these laboratory tests, the term (σ_c - P_f) in equations 3.1 and 3.2 reduce to σ_c. Table 3.2 summarises the hydro-mechanical properties of the samples and the method used to measure each property.

Table 3.2 The hydro-mechanical properties of the cement sample and the measurement method at which the measurements were arranged.

Hydro-mechanical property	**Value**		**Test method**
Uni-axial compressive Strength, UCS psi (MPa)		11,530 ±750 (79.5)	Unconfined compression test
Uni-axial poison's ratio, ν		0.197± 0.02	Unconfined compression test
Young's modulus, E, psi (GPa)		$4.018\times10^6 \pm 2\times10^5$ (27.74)	Unconfined compression test
Internal friction coefficient, Φ (degree)		44.3	Mohr circle, confined test
Cohesion, C_c psi (MPa)		2524 (17.3)	Mohr circle, confined test
Tensile strength, T_0, psi (MPa)		510±200 (3.5)	Brazilian tensile test
Fracture toughness, K_{IC}, psi √in (MPa√m)		710±200 (0.78)	CSB
Natural interface shear Strength, τ_0, psi (MPa)	cement	290 (2)	*sandblasted aluminum lap shear test, Provided by manufacturer
	Brown glue	*70(0.5)	
	Black glue	*145(1)	
	White glue	*3370 (26)	
Natural interface friction, μ_f		0.698±0.006	Direct Shear Test
Porosity, ϕ %		14.7±1	Two Boyle's cells
Permeability, K mD		0.018±0.005	Transient gas flood

3.3 Hydraulic fracturing test procedure

As drilling on dried sample may create small cracks around the wellbore, the samples were drilled through immediately after they were removed from the water bath. A very slow drilling speed was used and different drill bits with different lengths were attempted to ensure the hole is drilled appropriately with minimum damage to the sample. We found that the hole is best drilled with slightly smaller diameter than the targeted diameter and then enlarged using a reamer.

The hole was drilled through the entire sample length to ensure no new stress disturbance introduced to the rock due to partial penetration. A quarter inch tubing size, was used as the injection line for fracturing fluid. A couple of axial notches (in case of vertical fracture) or a round circumferential groove (in case of horizontal fracture) was made along the mid length of the inside wall of the wellbore to promote the fracture initiation. It is understood that the best practice is to apply the maximum stress during the test perpendicular to the direction of notches for easy fracture initiation. If this is not the case, the fracture may initiate in a direction different than the maximum stress direction but then reorient to align to this direction after propagating some distance away from the wellbore. The fracture initiation would be very difficult without having the notches on a homogeneous and smooth borehole wall.

There is a threshold for notch depth in order to provide a flow for a horizontal fracture to initiate correctly (Lhomme, 2005). To explain the importance of having a proper notch for fracture initiation, an example of a fracture test is explained here. Figure 3.15 shows the sample view after a fracturing test on a 20 cm block. The test was designed for horizontal fracture propagation and the sample was equipped with six pressure monitoring probes aiming to detect fracture arrival at different distances away from the wellbore wall. However, in absence of a proper horizontal notch, the fracture initiated in a vertical plane, and some distance away from the wellbore it changed its orientation into a horizontal plane. The results of some other experiments we performed indicated that without using notches, fracture initiation may occur at multiple points. In the example explained here a twisted fracture plane is produced which is not favourable.

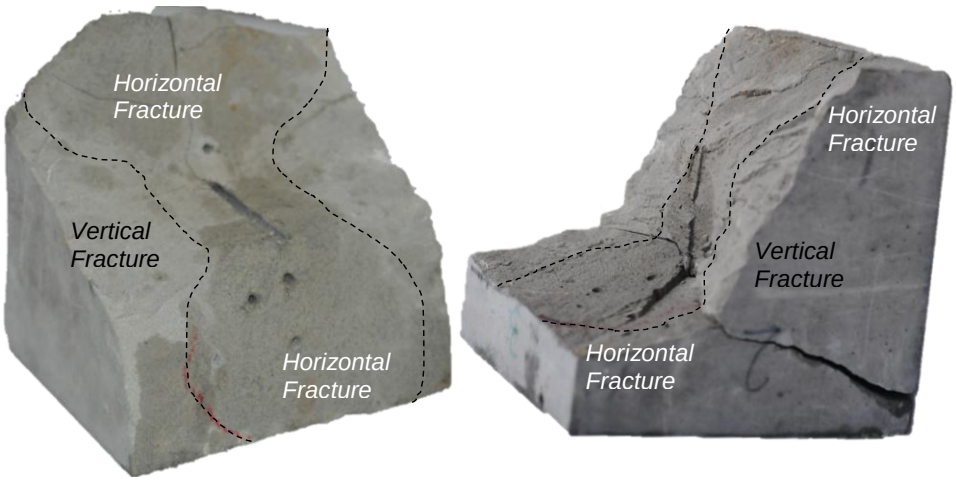

Figure 3.15 An example of a twisted fracture plane caused by improper notch placement.

The open hole section is isolated between the metal bar inserted to act as casing on top and the injection tube at the bottom. Both casing and the tube must be nicely glued to make a proper isolation of the open hole section for hydraulic fracturing purposes. Also, special care should be taken for drying the wellbore wall in order to ensure a good bond between the rock and metals using glue. The hole can be of any size between 2 and 0.125 inches and is placed at the centre of the sample. For hole sizes different than a quarter inches (i.e. the size of injection line), an adapter should be placed underneath the sample or alternatively a hollow Teflon cylinder rod can be used. Figure 3.16 shows the schematic of the sample with a drilled hole in the centre. This figure also shows the glued top casing and bottom injection tube as well as the vertical notches in the middle of the drilled hole.

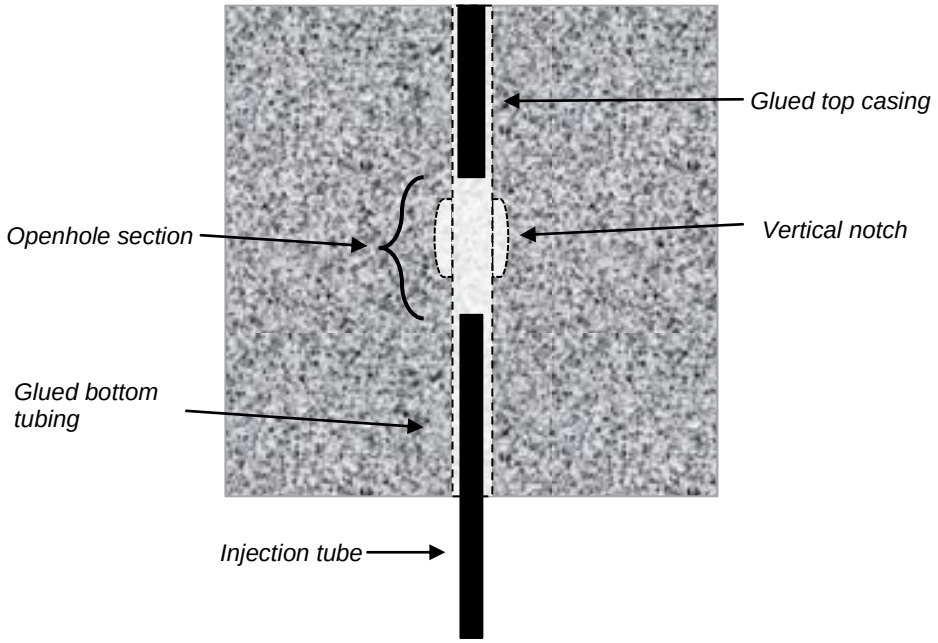

Figure 3.16 A schematic of a drilled hole with casing on top and injection tube at the bottom. A notch is made in the open hole section to ease fracture initiation.

The sample is placed inside the TTSC and metal shims are used to fill the gap between the sample and surrounding rams. The stresses are applied in steps. First we increase simultaneously all three stresses to the minimum in-situ stress magnitude. One stress is kept constant along the chosen direction for minimum stress: this is done using a constant pressure schedule of a syringe pump and then the other two stresses are increased to the magnitude of the intermediate stress.

This stress is kept constant now simulating the intermediate stress along the preferred direction and the third stress is increased to the desired value. The injection tube is now connected to the injection system and the data acquisition system records all data during the course of fluid injection.

3.3.1 Scaling analysis

As explained before the scaling laws are applied to establish a correspondence between field and lab hydraulic fracturing tests. The injection rate, fluid viscosity and the total time required for the fracture to propagate through the sample are the output of the scaling analysis, which are used to design a lab hydraulic fracturing experiment. As discussed in Chapter 2 the scaling laws are developed based on energy dissipation during fracture growth. Sample and wellbore size, hydro-mechanical properties of the sample and corresponding field properties are the input into the scaling model and viscosity, flow rate, and the injection time are output of the model. An example will be presented later on how to apply scaling laws for a hydraulic fracturing lab test design.

Viscose dominated propagation regime

The reference to apply the scaled time of experiment is when fracture initiation starts and this is defined as the time at which the wellbore pressurization rate reaches a maximum value. Fracture breakdown is usually defined as the time at which wellbore pressure reaches to its maximum value (Lhomme, 2005) and fracture initiation typically occurs before this breakdown point. The scaling period is valid for the time from initiation until stopping the injection of fluid. To have viscose dominated fracture propagation (see chapter 2); following condition should be met during fracture propagation (de Pater, 1994):

$$K_{Ic} < 2P_n\sqrt{\frac{r_f}{\pi}} \tag{3.3}$$

where r_f is fracture radius and P_n is fracture net pressure.

For viscous dominated propagation regime, the dimensionless toughness parameter of a Penny-Shaped fracture can be calculated as (Detournay, 2004):

$$\kappa = K'\left(\frac{t^2}{\mu'^5 Q_o'^3 E'^{13}}\right)^{1/18}, \tag{3.4}$$

where Q'_o is flow rate and t is the experiment time. Other material properties are defined as:

$$K' = \left(\frac{32}{\pi}\right)^{1/2} K_{IC}, \qquad E' = \frac{E}{1-\nu^2}, \qquad \mu' = 12\mu. \tag{3.5}$$

Here, μ is fracturing fluid viscosity, E is the rock Young's modulus, and ν is Poisson's ratio. In equation 3.4, the fracture propagation will be viscose dominated if κ is below one whereas it is toughness dominated when dimensionless toughness number exceeds four. In contrast with Equation 3.3, the dimensionless toughness parameter is time dependent: this means that fracture regime may change from one type to another as time evolves. Also the propagation regime was checked against another criterion proposed by Bunger (2005). In this method the evaluation criterion is based on three characteristic times of leak-off, toughness, and viscosity.

Applied scaling laws

In Figure 3.17 the plot of scaling analysis results for a 10cm sample is shown. In this figure, the left and right vertical axes correspond to the right and left hand side of Equation 3.3, respectively. For each scaled injection rate and specific viscosity, the value of left hand side axis must be larger than the fracture toughness (shown as horizontal dash line). The graph was plotted for an experiment time of 20-800s and final fracture length considered to be 85% of half-length of the sample.

In Figure 3.17 five iso-time lines corresponding to 20, 80, 200, 500, and 800s for different fracturing fluid viscosities are shown as long dashed-dot lines. From this figure, it can be seen that all fracturing fluids can be used for flow rates of greater than 0.03cc/min but this is limited due to other conditions that need to be met. The flow rate should be chosen in a way that fracturing fluid behaves Newtonian when it travels in the injection lines. The dashed section of curves belonging to fracturing fluid with viscosities of 19,580,000 cp and 2,445,000 cp are in this range (see 6th column of Table 3.1).

Other curves corresponding to other viscosities are in this range too. The fracturing fluid should also behave Newtonian when it moves within the fracture plane. Figure 3.18 shows the graph of dimensionless width versus dimensionless time for the first 205s of fracture propagation after the initiation moment. This figure also includes the corresponding time and width of the dimensionless values. From this graph, the average fracture width (for the first 205s) is approximately 0.06mm.

This limits the use of fracturing fluids with higher viscosities considering the minimum injection rate capacity of the existing pumps, i.e. 0.001cc/min. This flow rate limit increases the experiment time extensively, which is practically not favourable. In addition, choosing higher viscosity fluids increases the fluid lag length (Garagash and Detournay, 2000) which which we also wish to avoid. Based on the above discussion, a fracturing fluid with a viscosity of 20,000 or 97,700cp may be used for the purpose of this study. The chosen flow rate and fracturing fluid viscosity should satisfy the conditions of viscous dominated fracture growth (i.e. $\kappa > 1$) where the dimensionless fracture toughness (κ) value is calculated from equation 3.4.

For the injection rate of 0.1cc/min and fracturing time of 100s, the dimensionless fracture toughness for fracturing fluid viscosity of 97,700cp and 20,000cp is calculated to be 0.47 and 0.73, respectively which shows that both options result in a viscose dominated fracture propagation regime. However, a conservative choice, fracturing fluid of 97,700cp was selected for the lab test design. Taking these parameters the available time for the fracture to propagate within the sample before terminating the test is calculated to be around 1.5 minutes. This point is shown as a black solid dot in Figure 3.17.

The above design was also checked against the criterion developed by Bunger et al. (2005) and Bunger (2005) and resulted in having a viscous dominated propagation regime. The time during which the fracture travels this far depends on the chosen fluid parameters (i.e. viscosity, injection rate etc.). From the data monitoring stand point we prefer to maximise this time: this requires using larger viscosities but a smaller injection rate. However, the increase in fluid pressure (resulted from larger viscosity) should satisfy the above mentioned conditions.

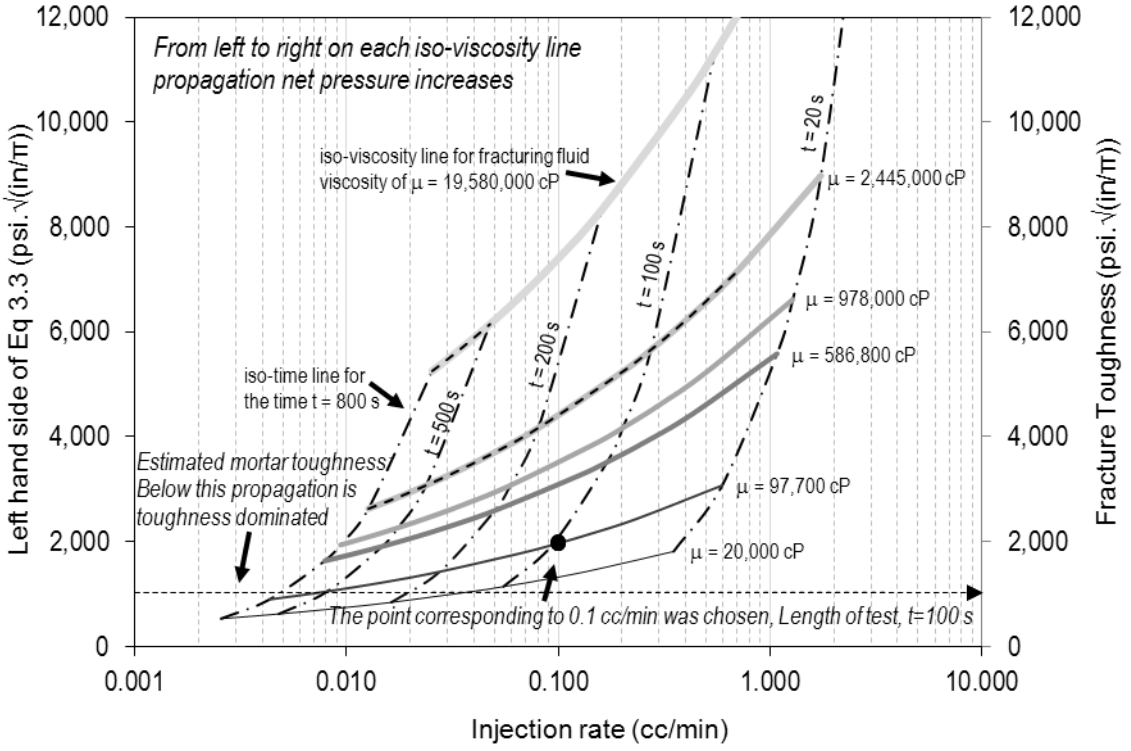

Figure 3.17 Scaling analysis of hydraulic fracturing lab experiments on a 10 cm sample.

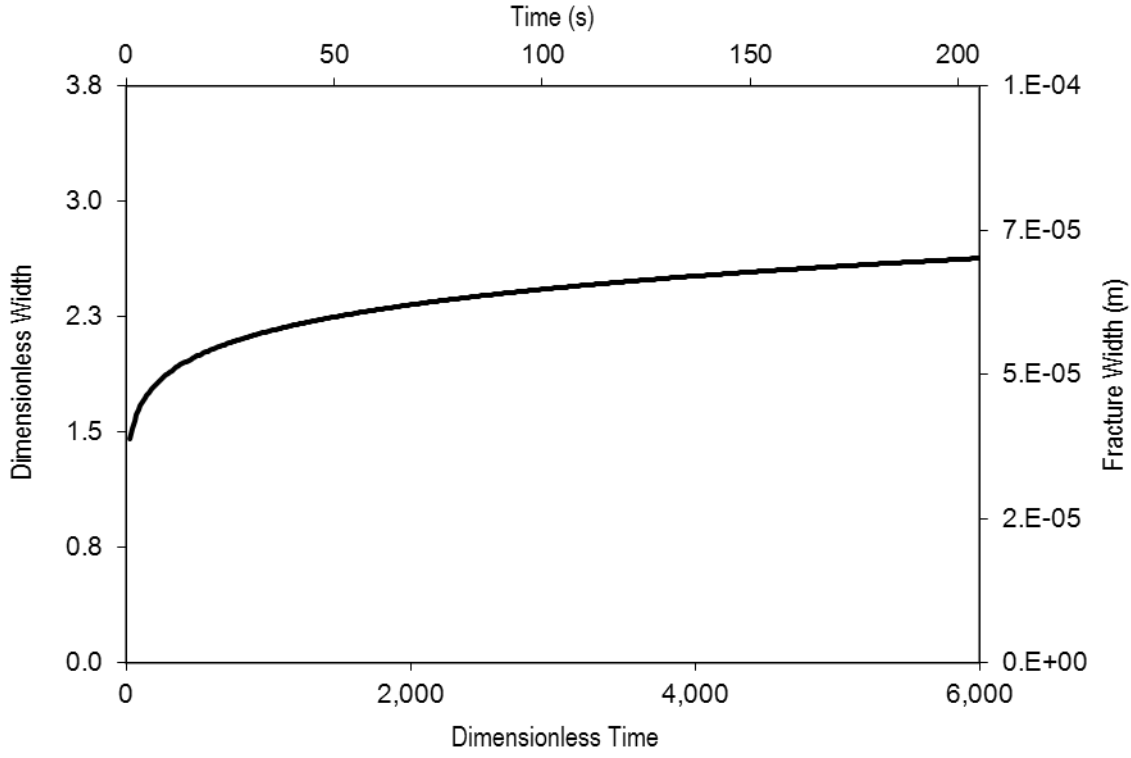

Figure 3.18 Dimensionless time versus dimensionless width for scaled hydraulic fracturing using a 10 cm sample.

Fracturing test interpretation

Figure 3.19 shows the pressure-time curves corresponding to both inj1 (bold grey) and inj2 gauges, i.e. wellbore pressure (bold black), that resulted from the scaled hydraulic fracturing experiments of the 10cm sample. The data were smoothened using moving average method in order to eliminate some parts of the recorded noise. The pressure drop between the pressure transducer inj2 and middle of the wellbore was neglected in our calculations. These two points are approximately 20-25cm apart. From Figure 3.19 it is seen that a breakdown pressure of about 2980 psi (20.5 MPa) was required to hydraulically fracture the sample (from transducer inj2, which is equivalent to wellbore pressure). This is the pressure to overcome both tensile strength of the rock and the induced hoop stresses.

Although we were able to monitor the slope of the wellbore pressure (pressurization rate) curve during the course of experiment, we were unable to distinguish the moment of fracture initiation, i.e. the time at which the wellbore pressurization rate is maximized. The reason is evidently shown in Figure 3.19 where the pressurization rate curve does not indicate a clear maximum. Alternatively, the time at which the pressure difference between gauges inj1 and inj2 starts to increase from a constant value of 50 psi (or its derivative changes from zero to a positive value) may be taken as initiation pressure in the absence of aforementioned evidence. As it show in Figure 3.19, the initiation time is considered as the time at which the pressurization curve, pressure difference between inj1 and inj2, and derivative of pressure difference between inj1 and inj2 start to deviate from plateau condition (straight line).

Some of these curves were not available during the time of the experiment and therefore a breakdown pressure at t =1530s was used as the reference pressure. This resulted in some errors in our calculations which resulted in the induced fracture approaching the sample boundary, i.e. the fracture was not contained from one side. However, the fracture, as expected, propagated along the maximum horizontal stress direction. The difference between the initiation and breakdown pressure was about 167s: this is larger than 100s which was the calculated time for fracture propagation and hence confirms why the fracture was not contained within the sample.

The fluid viscosity and injection rate should be modified based on the fact that they are functions of pressure. To simplify the problem, the pressure along the injection lines and the displacement chamber was considered to be the same as the wellbore pressure (i.e. reading at inj2). The actual injection rate and viscosity can be corrected for different pressures using the following equations (de Pater et al., 1994):

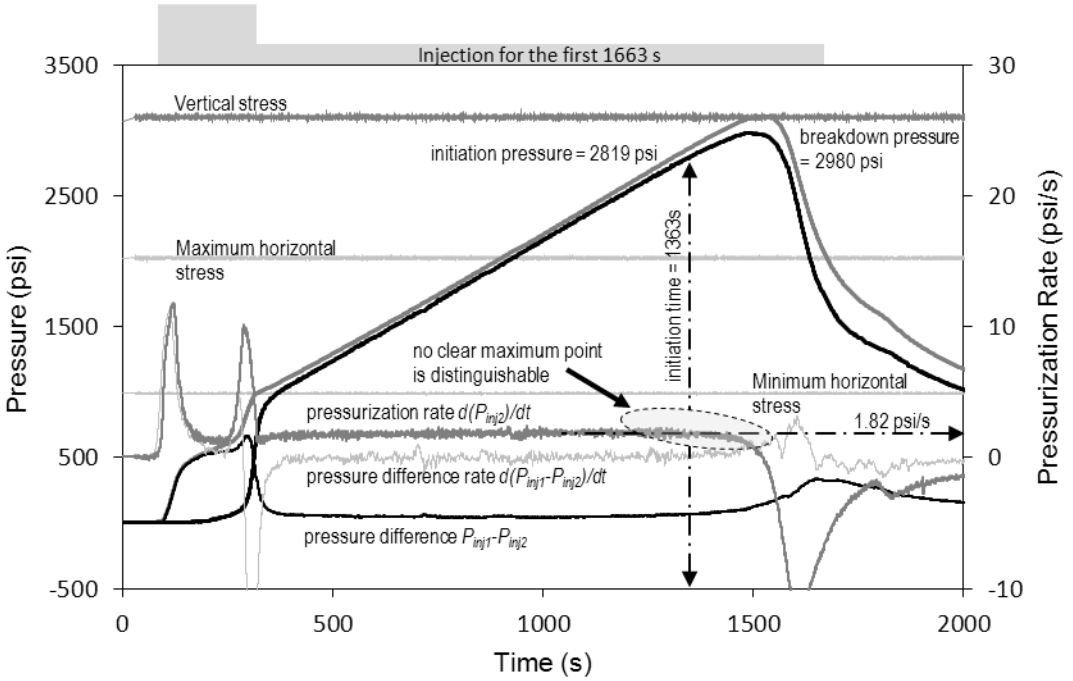

Figure 3.19 The pressure-time curve corresponding to hydraulic fracturing experiment of a 10 cm sample.

$$i_{corr} = i - p'(V_{sys}C_{sys}) \tag{3.6}$$

$$\mu_p = \mu_{atm}\left(1 + 6.5 \cdot 10^{-6} p\right). \tag{3.7}$$

In above equations i_{corr} is the corrected injection rate, p' is borehole pressurization rate, V_{sys} is the total fluid volume of the system, C_{sys} is system compressibility, and μ_p is corrected viscosity. Equation 3.7 shows the pressure (in psi) dependency of viscosity (cP). The constant value of this equation came from table 3.1. Figure 3.20 shows the plot of dimensionless pressure versus dimensionless time for the model, laboratory raw data and the corrected data. The corrected data shows a better match with the model. The product of V_{sys} .C_{sys} can be calculated as the average of wellbore pressurization rate (i.e. 1.82 psi/s) before the initiation (see Figure 3.19) and the flow rate.

The above explanation shows the procedure used in this study to design a lab scale hydraulic fracturing experiment. The hydraulic fracturing test based on calculations given in Figure 3.17 was conducted on a 10cm intact mortar sample. The same procedure was applied to test samples ranging in size from 10 to 20 cm.

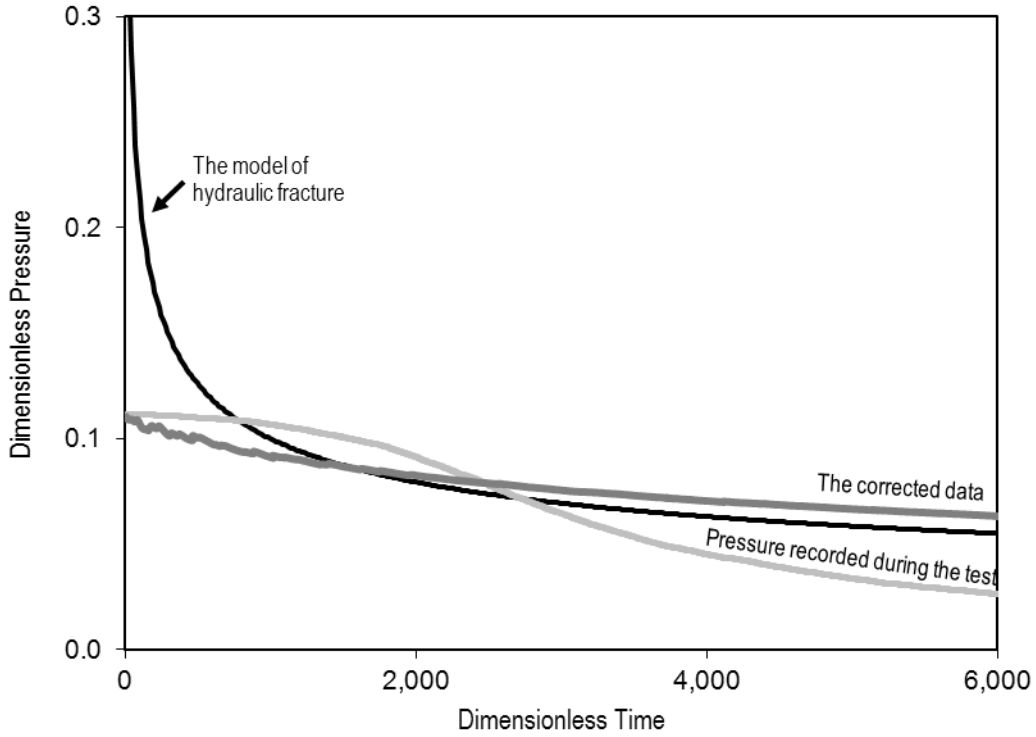

Figure 3.20 Comparison between the corrected dimensionless pressure from experiment and the predicted pressure from the model.

The design of a hydraulic fracture test in a sample having one or two interfaces would be similar except for the induced fracture length. In this case, the hydraulic fracture will be designed for fracturing length equal to the distance between the hole and the interface to ensure that the hydraulic fracture can grow to intersect the interface. This interaction mechanism is explained in further details in the next Section.

3.4 Hydraulic fracture and natural interface interaction

Different parameters affect the interaction between the hydraulic fracture and natural interface. Amongst those, the importance of the magnitude of horizontal stresses (in a stress regime where vertical fractures are formed) and specially the magnitude of the deviatoric stress (see chapter 2) are emphasized as important by many other studies (Blanton, 1986; Warpinski and Teufel, 1987). In this study, we are not aiming to study this parameter again but we need to establish a framework determining stresses to be

applied on the sample considering our equipment limitations, analytical interaction criteria, and sample sizes. TTSC uses four horizontal rams and one vertical one with limited maximum load capacity. The same load applied on different sample sizes will produce different stress on the surface of the samples.

Stress condition

Knowing aforementioned fact and considering the point that stress will not be scaled in our scaling procedure, the horizontal and vertical stresses should be chosen based on the biggest sample size that will be tested. Sample sizes of 10 and 15cm were chosen for the interaction study. So the maximum stress of 2100 and 7200psi could be applied on the samples in horizontal and vertical directions respectively. Finally the stress of 1000, 2000, ~3000 psi were chosen for the minimum horizontal, maximum horizontal and vertical stresses for almost all the tests.

Knowing the hydro-mechanical properties of the sample (Table 3.2) and the stresses, the interaction between a hydraulic fracture and a natural interface can be predicted using different analytical criteria discussed in Chapter 2. The net fracturing pressure (fracturing pressure minus minimum in-situ stress) at the moment of interaction is important for one of the criteria (W&T). As fracturing condition were kept unchanged for all interaction scenarios (different angle of approach, filling material, and different sample sizes), the expected range of net pressure can be estimated using a series of fracturing tests. One example of these tests is shown in figure 3.21. This graph shows the whole process of initiation, breakdown and a long propagation. It also shows a period of no injection and reopening of the fracture.

From this, a tensile strength of 1680 psi (11.6MPa) can be calculated which is around three times bigger than the value previously calculated. This may be because of wellbore geometry (very small wellbore).Hydraulic fracture will reach an interface while the fluid pressure is in the range of 1400-2000psi which provides a range for the fracture net pressure of 400-1000psi (see figure 3.21). This range also was confirmed in other tests and in mathematical modeling (scaling analysis).

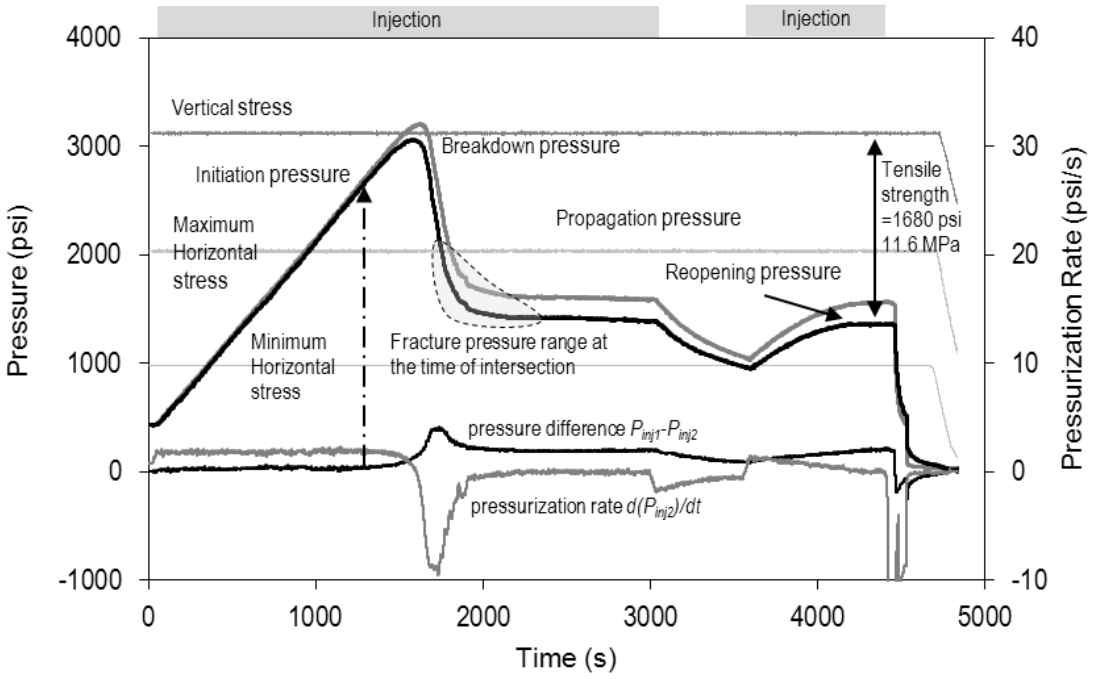

Figure 3.21 An example of processed fracturing test results. This graph shows initiation, breakdown and a long propagation period. It also shows a period of shut in followed by reopening of the fracture.

Blanton criterion (Blanton, 1986)

The Blanton interaction criterion (Eq. 2.2) can be plotted knowing the friction coefficient and tensile strength of the rock. Also, a *b* value is needed, which can be calculated using equation 2.6. This criterion for the friction coefficient of 0.698, tensile strength of 510 psi (see table 3.2), and the value of *b* using equation 2.6 is plotted in figure 3.22. Also, two other plots corresponding to the *b* values of 0.4 and 0.6 are shown in the figure.

Different scenarios of predicted interaction can be seen for a differential stress (deviatoric stress) of 1000psi and angle of approach of 30°, 60°, and 90°. Blanton's criterion predicts crossing will occur for 60° and 90° and opening for 30° of angle of approach. Some other pressure deviatoric stresses were chosen to see the effect of an increase in deviatoric stress. These points (experiment condition) are shown using solid black circles. However, this increase of deviatoric stress does not change the predicted interactions for low and high angle of approaches.

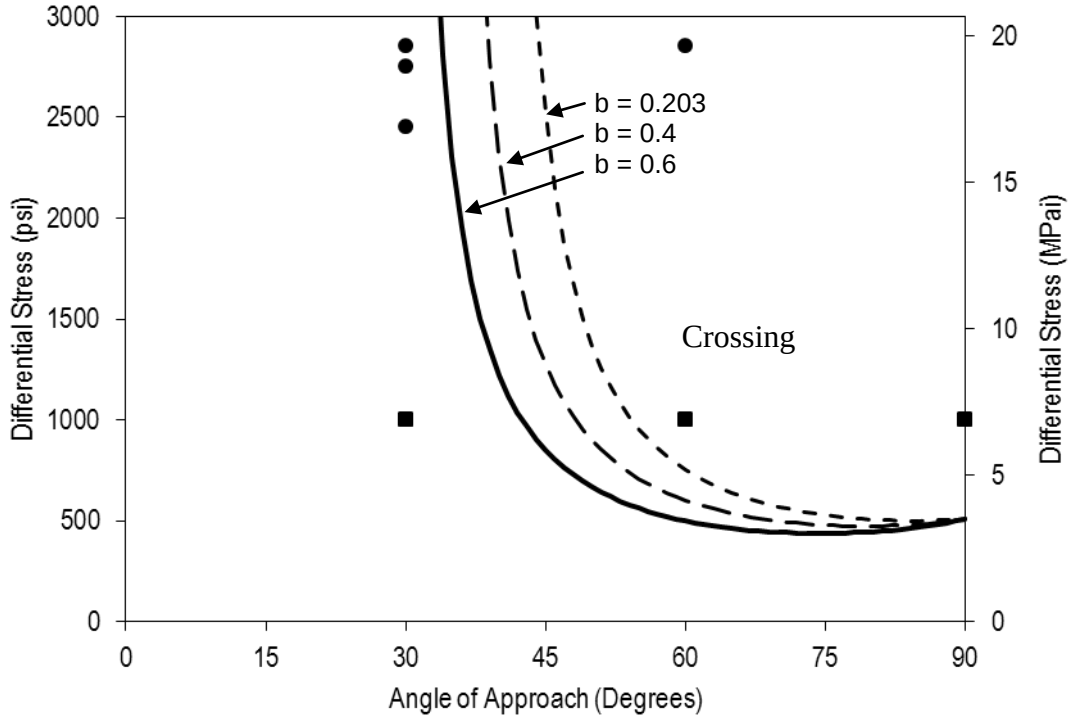

Figure 3.22 Blanton's predicted interaction for different test conditions.

Warpinski and Teufel's criteria (1987)

W&T criterion distinguishes between arresting by opening (Eq. 2.7) and arresting by shear slippage (Eq. 2.8) or continued growth after crossing. The criterion was plotted for three net pressures of 1000, 700, and 400 psi (6.9, 4.8, 2.8 MPa) using a friction coefficient of 0.698 for each of infill material (different fracture cohesion). The W&T criterion for opening depends on the fracturing net pressure and angle of approach which would be a similar case for all filling material. This was plotted in dashed lines in three figures of 3.23 (white glue), 3.24 (cement), 3.25 (Brown glue and Black glue). For low angles and low deviatoric stress W&T criterion predicts opening of the interface. Depending on the fracture net pressure, for low angle and high deviatoric stress or for high angles and low deviatoric stress it predicts different scenarios. Opening is not predicted to occur for interfaces with high angle of approach and a hydraulic fracture propagating in high deviatoric stress medium.

For a friction coefficient of 0.698, the magnitude of normal stress on the fracture plane is big enough to prevent any slippage at angles of approches greater than 55.2° and, as discussed in Chapter 2, a natural interface having an angle of approch of 0° has no slippage capability. Consiquently, slippage (arresting) will be discused only for the angles betweeb 0-55.5° for which its occurance depends on the friction coefficient,

fracture net pressure, and shear strength. White glue has such a big shear strength (26 MPa) that shear slippage is suppressed for low to moderate deviatoric stress (see solid lines in figure 3.23) which is not the case for the conducted experiment. So within the the range of 0-55.5° angle of approach, slippage should not be expected.

Conversely, the Brown and Black glues are weak. They have a low shear strength that made them the potential candidate for studying interactions leading to shear slippage for the angles ranging from 0° to 55° (see figure 3.24). In these cases, the calculated value of the left hand side of the equation 2.8 would always be negative for all net fracturing pressures. These negative values suggest that slippage will be a dominant interaction in these cases. For cemented interface interacting with a propagating fracture with a net pressure of 1000 or 700 psi, sllipage is predicted to be a possible interaction as well (see figure 3.25). For the case of net pressure equal to 400 psi, the area below the grey solid line (figure 3.25) is small andthis limits the chance of a non-crossing fracturing condition. . As a result, although the values of left hand side of equation 2.28 is this case would be positive (shown in firgure 3.25), again the slippage would be possible for the angles ranging from 0-55.5°.

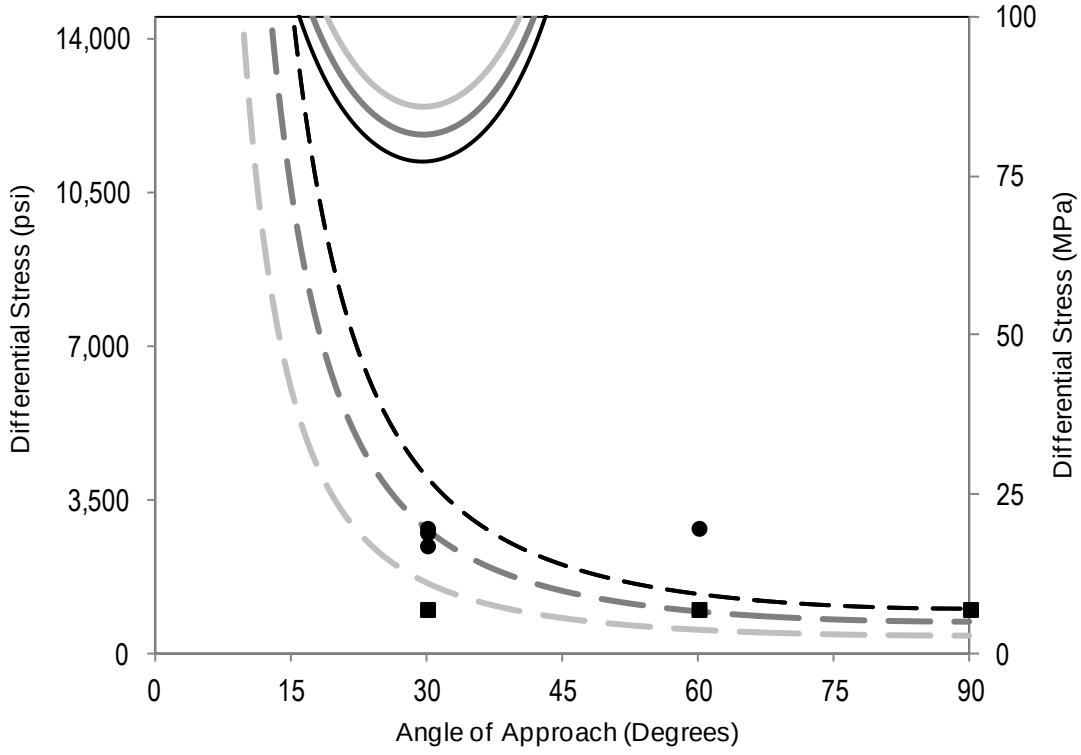

Figure 3.23 Warpinski and Teufel's criterion applied to predict interaction mode for an interface with shearing strength of 26 MPa (white glue) in different deviatoric stresses and angles of approach.

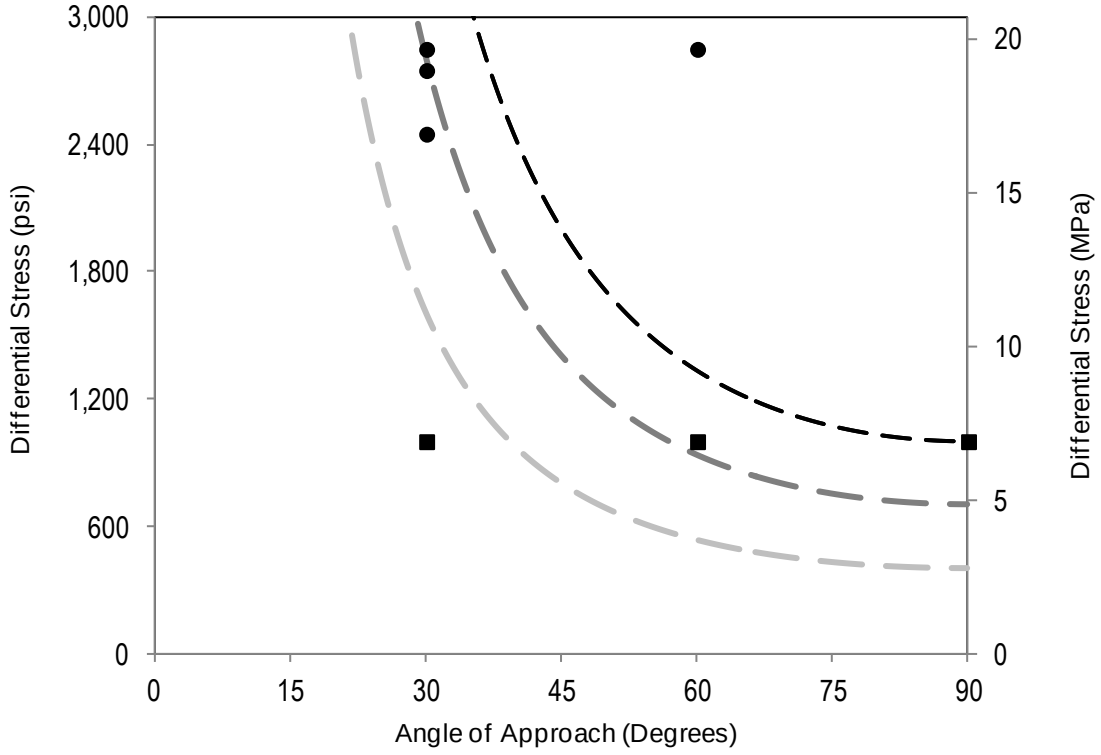

Figure 3.24 Warpinski and Teufel's criterion applied to predict interaction mode for two interfaces with shearing strength of 1 and 0.5 MPa (black and brown glues respectively) in different deviatoric stress and angles of approach.

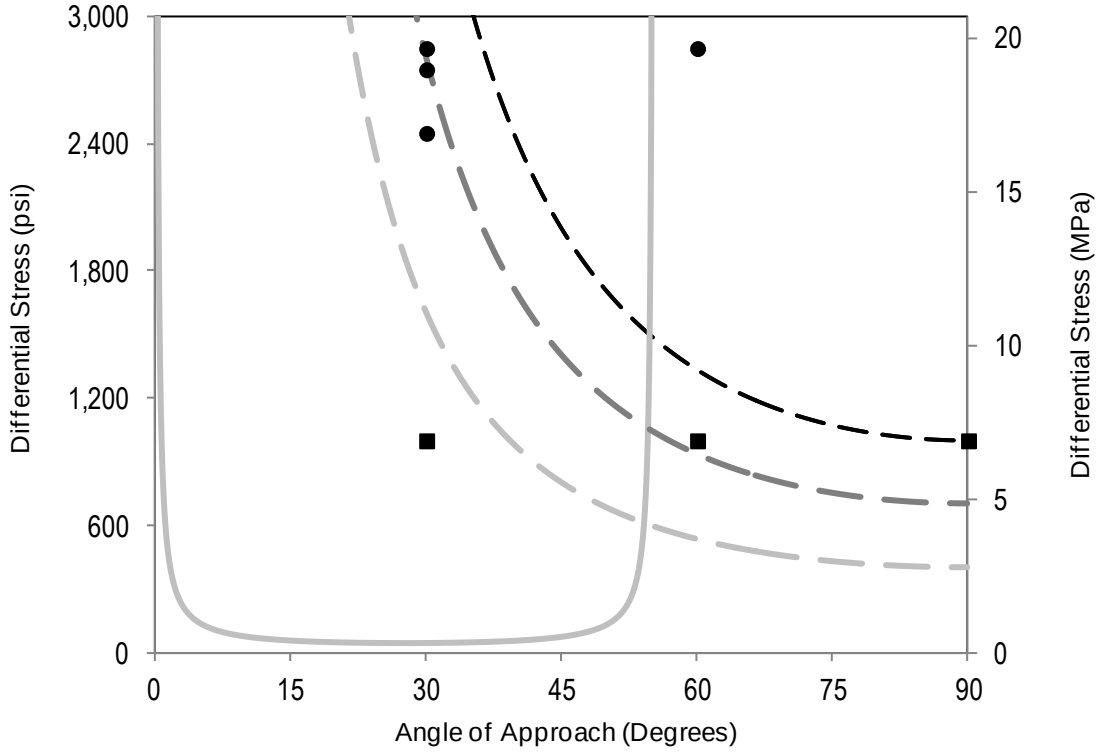

Figure 3.25 Warpinski and Teufel's criterion applied to predict interaction mode for an interface with shearing strength of 2 MPa (cement) in different deviatoric stresses and angles of approach.

Modified Renshaw and Pollard

As mentioned in Chapter 2, a graphical comparison between different angles of approaches is not possible in interaction analysis using the modified R&P model. However, a comparison can be done for one specific angle of approach and for different ratios of shear strength over normal stress on the interface plane (or maximum horizontal stress which applies for the orthogonal cases). Figure 3.27 shows the corresponding modified R&P curve for the ratio 0 (solid bold line, original R&P criterion), 0.17 (small dashed line), 0.255 (long dashed line), and 0.291 (solid thin line) for an orthogonal intersection.

Also, the equivalent condition for orthogonal experiments is shown in the figure. The cross markers show the condition for the ratio 0.255 and should be compared with the small dashed curve. The square marker is for a ratio of 0.17 and the rectangular marker is for a ratio of 0.291. The square marker is just on the line (a little above) showing both crossing and arresting might be possible for the case. The rectangular marker is far below its corresponding line, indicating a strong arresting condition. Two of the cross markers are located above the 0.255 line indicating a crossing condition, one cross is on the line and one below the line, indicating arresting.

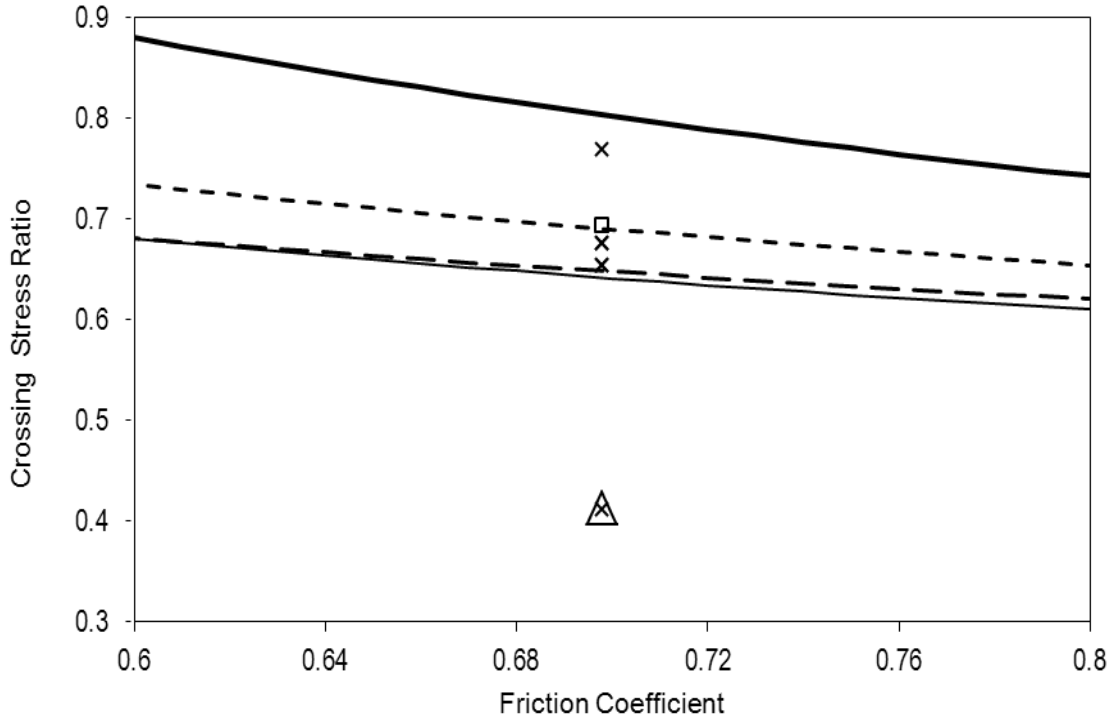

Figure 3.26 Modified Renshaw and Pollard criterion applied for four different ratios of 0 (solid bold line), 0.17 (small dashed line), 0.255 (long dashed line), and 0.291 (solid thin line) is plotted for the angle of approach of 90˚. The markers show the condition of different experiments. The marker above the line shows crossing and the ones located below belong to the arresting scenarios.

It is to be noted that the vertical axis of the graph is not logarithmic in order to magnify the small difference. The graph also covers a small range in comparison to figure 2.13 in chapter 2. The model prediction for other angles of approach are shown in a table (see table 3.3) rather than a graph.

Fracturing results and comparison with analytical criteria

Hydraulic fracturing experiments were conducted on samples with the angles of approach ranging from 30° to 90°. The different cohesive material of strong and brittle (white glue), strong and resilient (Black glue), weak and brittle (cement), and weak and resilient (Brown glue) were used as filling material for synthetic interfaces. The glued interface will not have fluid conductivity so no offsetting interaction will be expected for such samples. Offsetting has rarely happened in our tests. One example of offsetting is shown in figure 3.28. In this experiment, the hydraulic fracture approached to the interface with angle about 70° (it was designed to be 60°) and then opened the interface for 0.5 cm. Then it reinitiated from the other side of interface and continued propagation.

Generally, the result showed a good agreement with the available literature and analytical criteria when hydraulic fracture intersects a brittle interface (white glue and cement). The white glue that has strong shear strength, for the high angle of approach experiment, resulted in a complete crossing only on one side and a minor crossing over a very small section of the other side. It is possible that the hydraulic fracture would cross the interface on the side with partial crossing if the test had been continued (see figure 3.28). Arresting with minor evidence of crossing was the interaction observed for the intermediate angle of approach case.

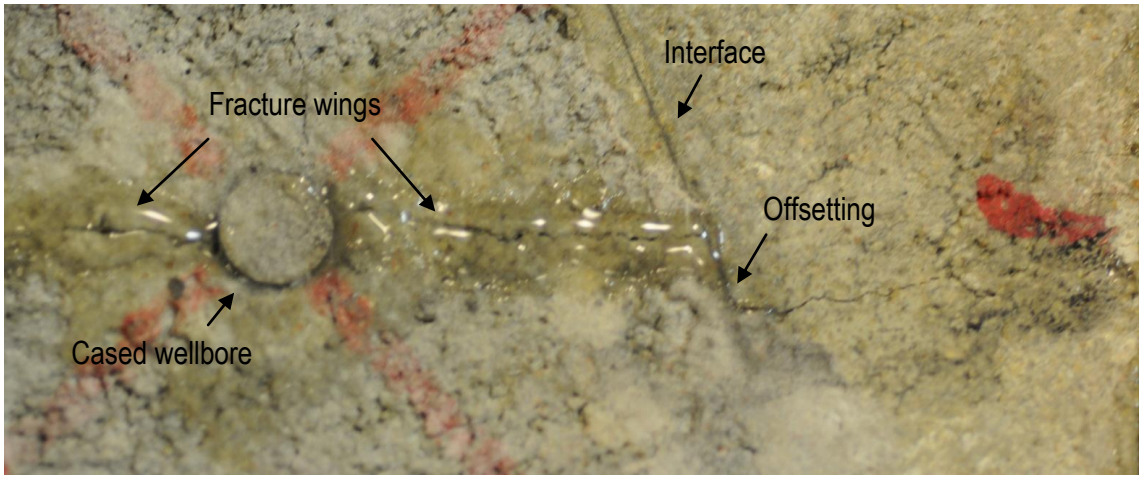

Figure 3.27 An example of offsetting interaction that happened in one of experiments

The shear slippage on this strong interface is unlikely (from analytical approach, see figure 3.23) and a crossing result should happen for this case as well, however; the crossing interaction requires continued growth of the hydraulic fracture. Growth was limited because the fracture leading edge reached the top boundary of the sample resulting in a partial premature crossing. This sort of temporary arresting does not fit into the category of arresting by slippage or opening and we prefer to call it temporary arresting because of sample size limitations. For lower angles of approach, the hydraulic fracture propagated toward the intersection point and then partially opened the interface before continuing the extension parallel to interface (see Figure 3.30). Two more examples of such an interaction in the samples of 10 cm size are shown in Figure 3.31.

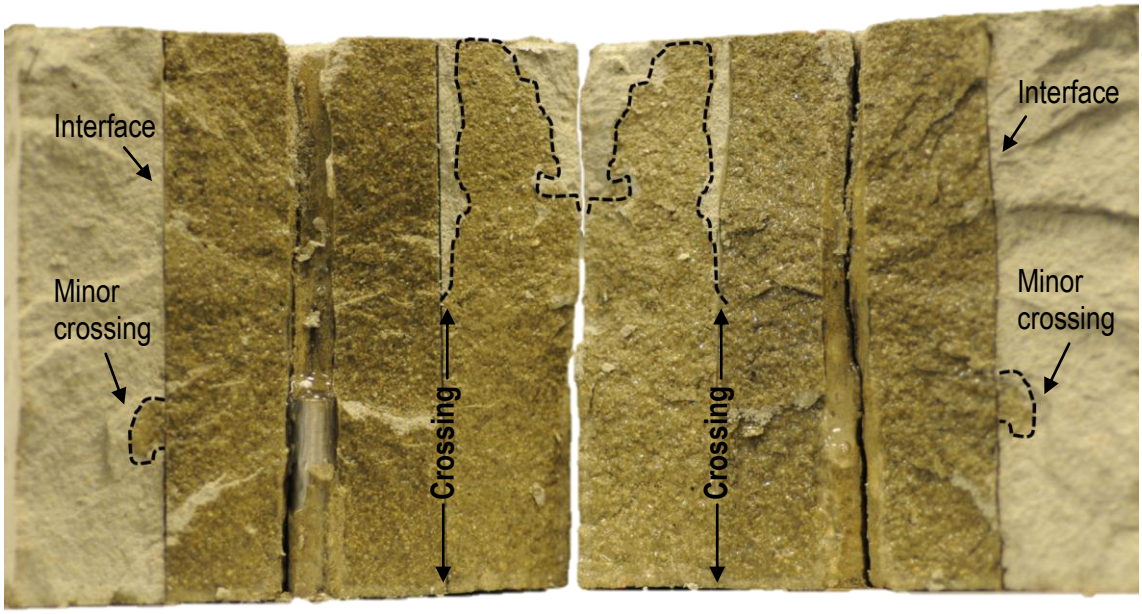

Figure 3.28 Crossing and arresting interactions for strong brittle interface using high angle of approach.

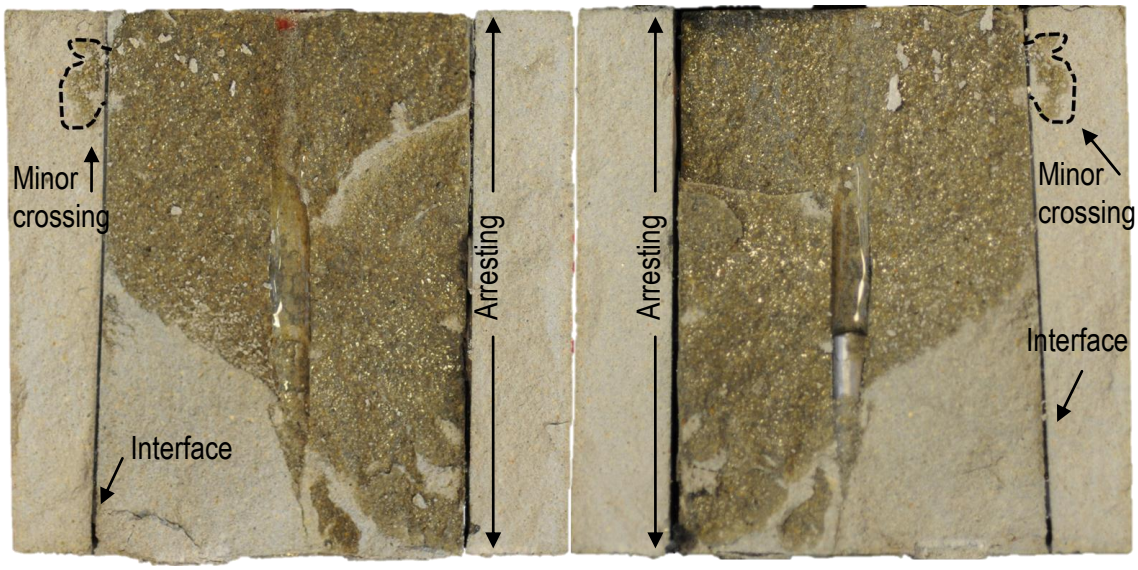

Figure 3.29 Arresting interaction for strong brittle interface using moderate angle of approach.

Figure 3.30 Opening interaction of strong brittle interface in low angle of approach.

Figure 3.31 Opening interaction that happened in hydraulic fracturing propagating toward the strong brittle interface in low angle of approach in 10 cm samples.

The interactions using the cemented interfaces (brittle and weak) were in agreement for majority of experiments with the analytical criteria and results in available literature. This agreement was 100% for low angles of approach, meaning that hydraulic fractures were arrested by the interface or the fractures opened the artificial interface for these low angle cases (see figure 3.32). The size of the sample (15 or 10 cm) did not have an obvious effect on the resultant interaction, however; the hydraulic fracture is able to intersect the interface before it reaches to the boundaries for bigger samples (see figure 3.32). The most problematic case for this kind of interface was the moderate angle of approach. Hydraulic fractures seldom intersected the interface at the designed angle and the actual angle of intersection was typically higher in most of the cases. Nonetheless, the higher angle of intersection did not promote crossing as half of experiments that were conducted using such angle ranges were arrested or opened. Figure 3.33 shows a sample with a 60° cemented interface that has been split open. The hydraulic fracture was arrested one side and partially crossed the other interface. On the other hand some of the tests, such as the one shown in figure 3.34, exhibited a complete crossing scenario. In this test, both of the interfaces were crossed by the hydraulic fracture.

All possible interaction scenarios occurred for orthogonal interface cases. However, the majority of them crossed the interface, at least from one side. Figure 3.35 shows one example of a complete crossing case for which the hydraulic fracture crossed both orthogonal interfaces. In this case, the hydraulic fracture did not grow into the interface. Figure 3.35 (middle) shows a fragmented sample with a 90° interface with interfaces crossed and opened by the hydraulic fracture. One of the discontinuities in this sample

arrested the propagating fracture. In this particular test, the hydraulic fracture opened both of the orthogonal interfaces at the bottom of the sample, but in the upper part of the sample the fracture crossed one interface and was arrested on the other one. The crossing and opening interaction have taken place in the left interface (figure 3.35, top) and arresting and opening have occurred on the other side (figure 3.35, bottom).

All of the hydraulic fracture experiments that were designed using glue on the interfaces that deforms plastically showed almost the same results regardless of interface filling materials or angle of approach. The hydraulic fractures were arrested in all cases and in some cases a small portion of the interface was opened with fracturing fluid. This is because the plastic interfaces could not transfer the tensile stress generated by the fracture to the other side of interface and this acts to arrest the propagation even in high angle of approach or high (one case, see figure 3.23-3.25) deviatoric stress cases. These plastic interfaces work as a barrier to shear stress.

Figure 3.36 shows one example of a 60° black glued interface in a 10cm sample that has been split apart along the fracture plane. The hydraulic fracture was clearly arrested and no sign of crossing were observed. The condition was almost the same for the interface that was bonded using the brown glue. The hydraulic fractures were arrested again at the interface because the interface-glue cohesion in these cases was weaker compared to the black glued interface. The hydraulic fractures in most of the experiments opened a small section of the interface. This is shown in figure 3.37 where, while both of hydraulic fracture wings were arrested at the interface, a small opening has occurred along the right hand side interface.

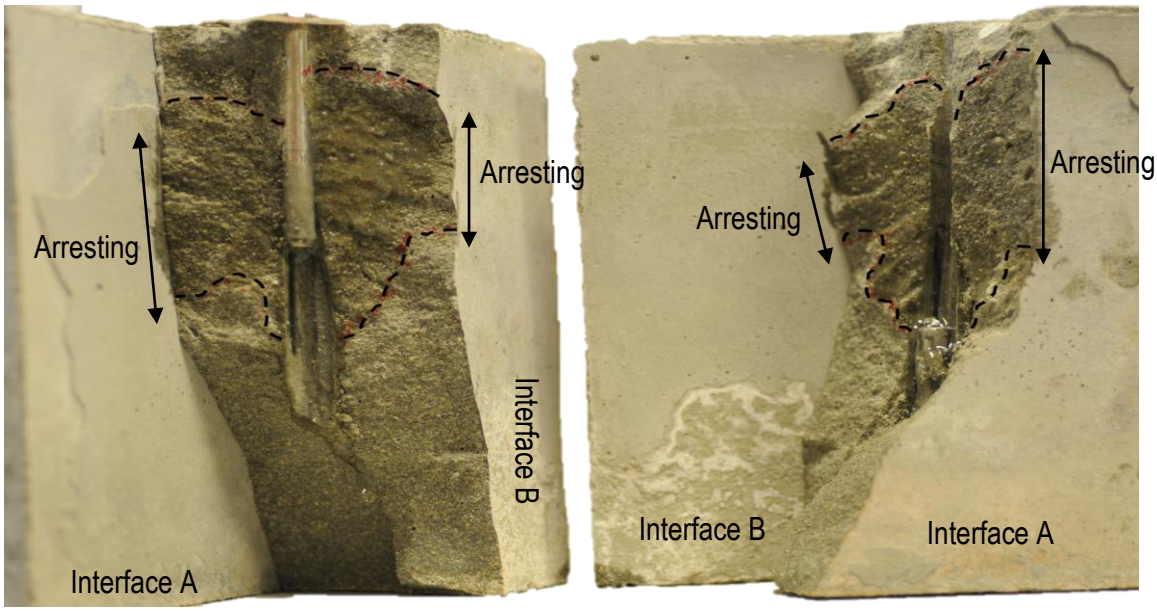

Figure 3.32 Hydraulic fracture that was arrested by a low angle cemented interface.

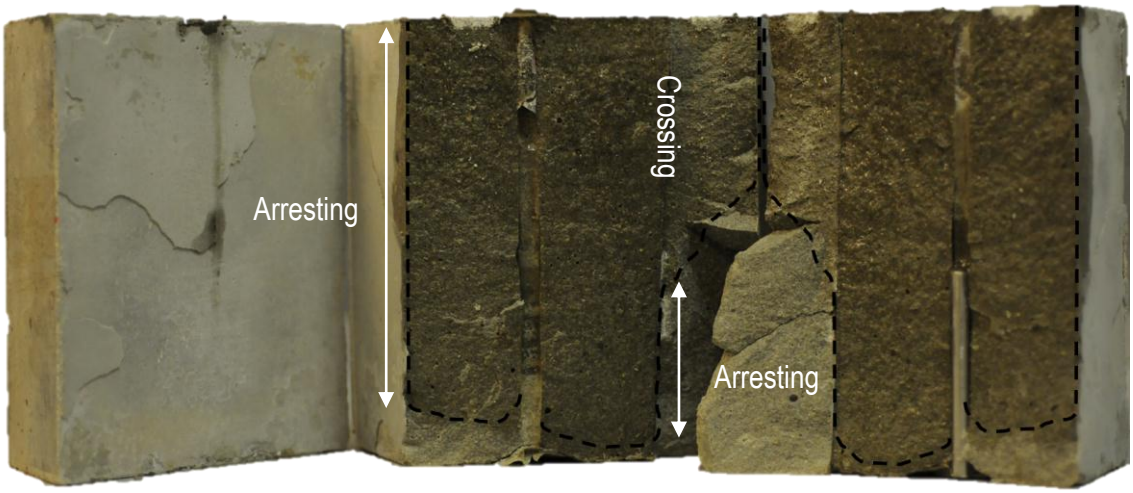

Figure 3.33 Hydraulic fracture that was arrested on one side and partially crossed the other side for the 60˚cemented interface.

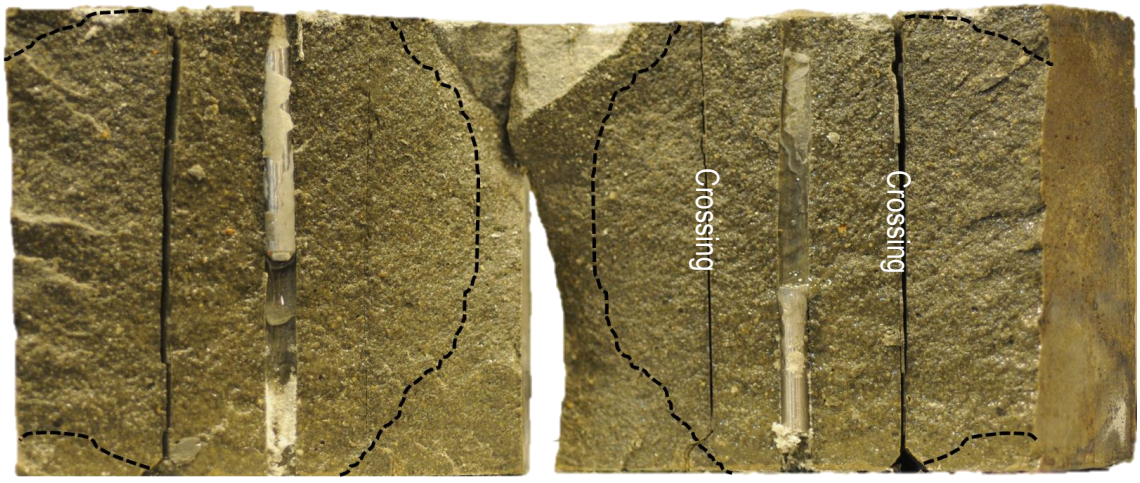

Figure 3.34 Hydraulic fracture that crossed both of 60˚cemented interfaces.

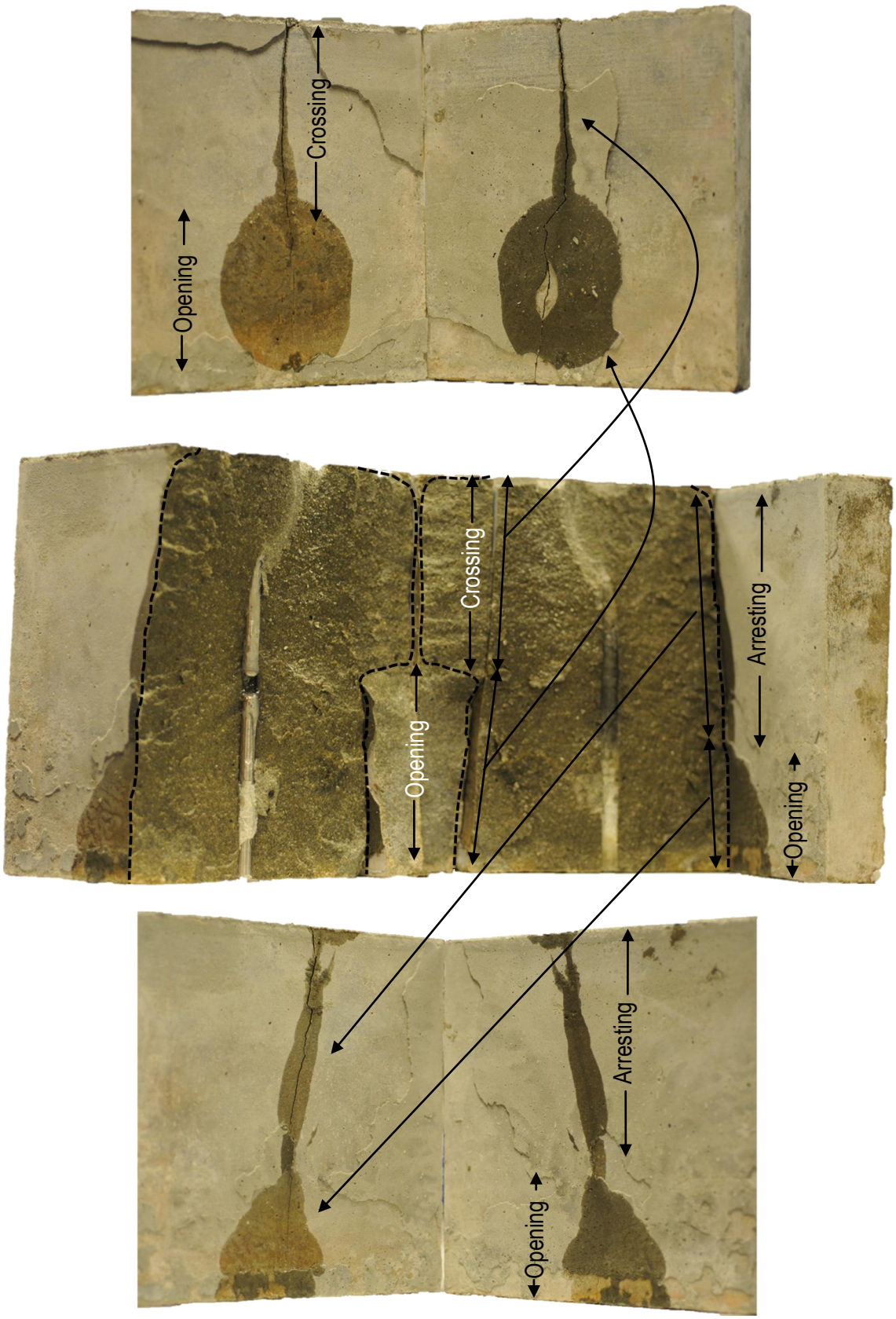

Figure 3.35 Hydraulic fracturing experiment conducted on the sample of 15 cm cube of cement having two orthogonal cemented interfaces. Fracture opened (bottom section of both interfaces) and crossed (top section of left hand side interface) the interfaces. The natural interface arrested the hydraulic fracture in top section of right hand side interface as well.

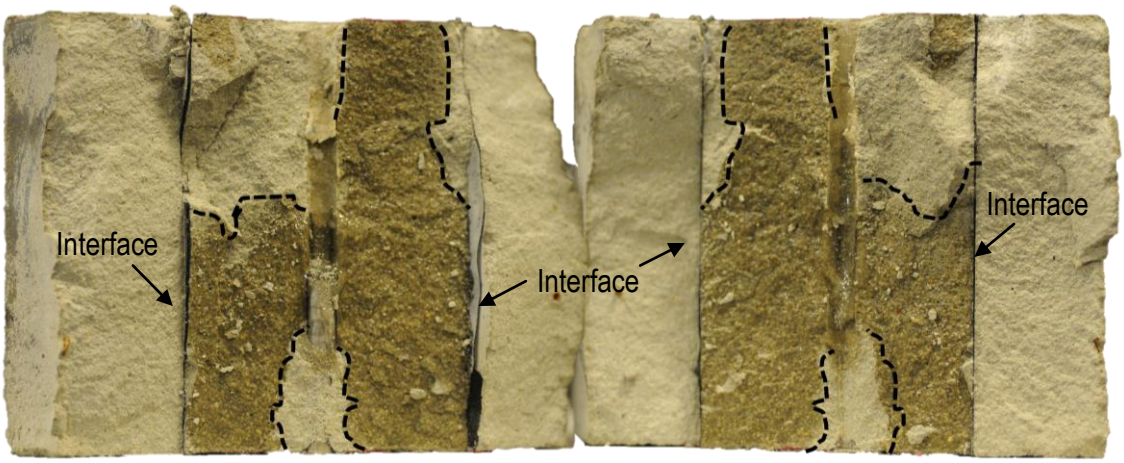

Figure 3.36 Hydraulic fracturing experiment conducted on the cube sample of 10 cm cement having two 60° black-glued interfaces. Similar to the other test of this type of interface, hydraulic fracture was arrested by interfaces.

Figure 3.37 Hydraulic fracturing experiment conducted on the sample of 10 cm cube of cement having two orthogonal brown-glued interfaces. The fracture has arrested by both of interfaces. A small opening section is observed on the left hand side interface.

3.5 Comparison between the analytical criteria and experiment results

In this section, the experimental results will be compared to analytical criteria. It should be noted that the modified R&P criterion just distinguishes between crossing and not crossing while Blanton's formula differentiates among opening and crossing interactions. In addition, the W&T criterion discriminates between a wider range of interaction including arresting, opening, and crossing. Because W&T criterion needs detailed data about fracture net pressure, three net pressures of 1000, 700, 400psi were considered for the final interaction prediction. These pressures were chosen based on the mathematical model (scaling laws) and observed pressure decline in the experiment after the breakdown.

Based on these facts, the probability of the net pressure of 1000 psi at the time of intersection is high and it is possible for an intersecting fracture to have a net fracturing pressure around 700 psi. The above mentioned investigation also shows that the net pressure of 400 psi at the moment of intersection is very unlikely. This means that the pressure decline time (from net breakdown or net initiation pressure) to the net pressure of 400 psi is much higher than the predicted value (and also observed) considering the time required for fracture to intersect the interfaces.

The results of experiments and the predicted interaction of analytical criteria are shown in Table 3.3 with the dark shaded cells showing where the criterion prediction and experiment results were similar. The intensity of cell colour indicates the accuracy of the prediction with a darker shade corresponding to a more accurate prediction. Keeping in mind that in each experiment there were two interfaces present and the resultant interaction may be different in each. For the brittle (stronger) interfaces almost all the models showed a good prediction. The diversity of prediction was more scattered for non-brittle interfaces. The results show that W&T criterion will work very well if net pressure is predicted accurately.

However, relying only on a mathematical model for net pressure prediction is prone to error and few preliminary fracturing tests should be carried out before running the experiments on the final sample. Having an accurate prediction, W&T model may be used for non-brittle interfaces as well. It should be highlighted that this model is very sensitive to the value of net pressure and choosing a wrong value may produce a very poor prediction (see the results of net pressure equal to 400 psi). The modified R&P criterion shows slightly better results than the Blanton formula, but both of them have very poor prediction on non-brittle interfaces.

Table 3.3 Comparison between the experiment results and interaction prediction of analytical criteria.

Sample	Experiment result	Blanton	Modified R&P	W&T 400 psi net pressure	W&T 700 psi net pressure	W&T 1000 psi net pressure
15cmCement90	Crossing	Crossing	Crossing	Crossing	Crossing	Crossing or Opening (marginal)
15cmCement90-2	Arresting	Crossing	Crossing	Crossing	Crossing	Crossing or Opening (marginal)
10cmCement90	Test failure	Crossing	Crossing	Crossing	Crossing	Crossing or Opening (marginal)
10cmCement90-2	Crossing	Crossing	Crossing	Crossing	Crossing	Crossing or Opening (marginal)
10cmCement60	Opening	Crossing	Crossing	Crossing	Crossing	Opening
10cmCement60-2	Crossing	Crossing	Crossing	Crossing	Crossing	Opening
15cmCement60	Arresting + Crossing	Crossing	Crossing	Crossing	Crossing	Opening
15cmCement60-2	Opening	Crossing	Crossing	Crossing	Crossing	Opening
10cmCement30	Opening	Opening	Not Crossing	Arresting or Opening	Arresting or Opening	Arresting or Opening
15cmCement30	Arresting	Opening	Not Crossing	Arresting or Opening	Arresting or Opening	Arresting or Opening
10cmWhite90	Arresting + Crossing	Crossing	Crossing	Crossing	Crossing	Crossing or Opening (marginal)
10cmWhite60	Arresting + Crossing	Crossing	Crossing	Crossing	Crossing	Opening
10cmWhite30*	Arresting + Opening	Opening	Not Crossing	Crossing	Opening	Opening
10cmWhite30-2*	Opening	Opening	Not Crossing	Crossing	Crossing	Opening
10cmBrown90	Arresting + Opening	Crossing	Crossing	Crossing	Crossing	Opening + Arresting (marginal)
10cmBrown60	Arresting + Opening	Crossing	Crossing	Crossing	Crossing	Opening
10cmBrown30*	Opening	Opening	Not Crossing	Arresting or Crossing	Opening or Arresting	Opening or Arresting
10cmBlack90	Opening	Crossing	Crossing	Crossing	Crossing	Opening + Arresting (marginal)
10cmBlack90-2	Arresting + Opening	Crossing	Crossing	Crossing	Crossing	Opening + Arresting (marginal)
10cmBlack60	Arresting	Crossing	Crossing	Crossing	Crossing	Opening
10cmBlack60-2*	Arresting	Crossing	Crossing	Crossing	Crossing	Crossing

*Tests with higher deviatoric stress than 1000 psi

3.6 Summary

The first part of this chapter presented the detailed results of measurements of the hydro-mechanical properties of the samples. This information was used later to generate the scaling laws and predict the fracture net pressure at the time of intersection. Then test procedures and the experimental equipment and loading of the sample was described. The scaled hydraulic fracture design was used to conduct the experiments and the measured pressure data was corrected to see how accurately it matches with the model. The stress condition of the test was determined and different predictions of interaction criteria were analysis. Finally the predicted interactions were compared with laboratory test results. Of the criteria tested, the W&T criterions provided the most consistent match between predicted and measured crossing interaction but requires an accurate knowledge of net pressure. It was shown that analytical interactions works well for brittle interfaces better. In addition, relying on these analytical interactions would not result a consistent prediction.

4 Numerical simulations of interaction mechanisms

The discussions given in the previous chapter demonstrates how performing a simple lab experiment could be time consuming and costly. This constrains our ability to repeat the tests in order to obtain some valid conclusions. Simulating a problem numerically is a widely used approach which can be used to simulate a lab experiment. Once the model is calibrated and validated against a set of experiments, sensitivity analyses can be done over a range of different model parameters. Considering high speed computers being available these simulations takes a very small amount of time compared to a lab experiment. Also, performing full size modeling (for example, hydraulic fracturing of large scale as performed in a well) which is not possible in the laboratory, can be easily performed using a numerical simulator.

Within the past decades several numerical methods have been proposed to model an elastic continuum (e.g. finite element (FEM), boundary element (BEM) and finite difference (FDM)) and to model a discontinuum (i.e. distinct element method (DEM)) media (Jing, 2003). To integrate the advantages of different methods, hybrid methods have also been proposed, such as FEBEM. Further developments resulted in so called pseudo continuous methods for modeling highly fractured medium (Sakurai, 1991).

In this research we use a DEM package to simulate the interaction of a hydraulic fracture with a natural fracture. The existence of induced and natural fractures within the model is a clear reason for such selection. Simplified 2D models have been developed in this study using the particle flow code (Potyondy and Candall, 2004) software for which a number of FISH codes were developed. In this Chapter after giving a brief review of different numerical models the simulation procedure in PFC^{2D} is explained. Then the method for rock hydro-mechanical validation and calibration will be discussed. This will be followed by presenting and interpreting the results of various models developed to simulate the interaction of a hydraulic fracture with a natural fracture.

4.1 Numerical methods

4.1.1 Boundary element method (BEM)

BEM is a faster computing approach comparing to FEM, as it uses fewer elements in discretizing the problem. The fracture surface and the boundary between rocks of different elastic properties (if any) are the only areas that need to be discretised in this method. Simple structured mesh generation is employed in BEM, which simplifies re-meshing as the hydraulic fracture propagates and numerically the BEM reduces the dimension of the problem by one degree. In addition, BEM is applicable for elastic (hard) rocks and dynamic problems.

With respect to the applications of this study, i.e. interaction mechanism, the BEM discrepancy in modelling a discontinue medium may be overcome by considering the two sides of an interface (e.g. crack as two laying boundaries). Alternatively, BEM accompanied with discontinuity displacement method (DDM) could be employed. DDM was developed by Crouch (1976) to manage the two coinciding boundaries of a crack (two surfaces of a crack) which was considered as a big issue in conventional BEM method. DDM was later used for modelling variety of applications (Napier 1999; Bobet and Einstein, 1998; Whittaker et al., 1992).As a third approach one may use the hybrid FEBEM method which integrates the advantages of the two method. Although BEM applications have been extended to nonlinear solid mechanics (Nicolazzi et al., 2005) and mesh free BEM (Liu and Gu, 2004), it still suffers in modelling non-homogenous media or a propagating fracture. A comprehensive list of the advantages and disadvantages of BEM may be found in Manolis and Polyzos (2009) and Katsikadelis (2002).

Two BEM software were found suitable for the simulations purpose in this study. FRACOD^{2D} which was developed based on the work of Shen (1993) has been used for variety of rock mechanical problems. The difficulty, however, is that the source code is unavailable to public hence no changes can be made to simulate some specific cases required in our studies. In particular, modelling fluid flow inside the fracture channel and adding fluid-mechanical coupling into the code were the essential modifications needed in current work. HYFRANC3D is a 3D code written in FORTRAN programming language that solves the deformation of an elastic medium based on BEM and fluid flow equations using a FEM.

In each step of fracture propagation, BE calculation is performed on external software called BES and fluid solution for equilibrium fracture propagating pressure is converged in an iterative manner (Carter et al., 2000).Implementing the natural interface into code in order to study the effect of interaction between the interface and a hydraulic fracture needs full access to the source code which was not available for us.

4.1.2 Finite method

The ability of installing the gravitational load and in situ stresses in several nonlinear heterogonous materials with complicated boundary condition and geometries has made FEM a flexible and powerful numerical tool for research (Jing and Hudson, 2002). Also, a complete set of model regional details like geological information with its all complexities, directional formation characteristics, different fault zones, and preexisting excavation can be enclosed into model directly (Jing and Hudson, 2002). Conventional FEM approaches have some drawbacks. These shortcomings result from their inherent continuum assumptions which form unstable condition when extensive fracture opening or element disconnection is happening (Jing, 2003). Table 4.1 shows some of drawbacks associate with FEM and their solutions.

Table 4.1 Examples of FEM numerical modeling of hydraulic fracturing.

It is difficult to model	Solution
Large stress gradient around discontinuities	Increase the number of elements
Large deformation	Remeshing or using mesh free method
Crack growth	Remeshing or element separation

It was recommended that as newer developed FDM methods (i.e. Finite Volume Method (FVM) and Finite difference time domain (FDTD)) were able to address some of its shortcomings like simulating nonlinear solid behaviour (Jing and Hudson, 2002) and heterogeneous media (Yee, 1966). However, it still is unable to simulate the fracture in an accurate way.

4.1.3 Discrete element method (DEM)

DEM was firstly introduced by Born and Huang (1954) and their first application in geo-mechanics was reported by Cundall (1971). He modeled macro-mechanical behavior of the rock by keep tracing of micro-changes of particles. This was further applied to study the types and mechanism of rock failure in distinct bonded granular materials (Cundall and Strack, 1979, Bruno and Nelson, 1991) and their mechanical behavior (Ting and Corkum, 1988).

The DEM was also used to investigate the stress induced porosity and permeability changes in granular materials (Bruno, 1994). Several similar applications have been reported since then looking at different aspects of simulation, for example, Cook and Jensen (2002), Konietzky (2002), Shimizu et al. (2004), Detournay et al. (2008), and Sainsbury et al. (2011). Table 4.2 shows some examples of numerical modeling of hydraulic fracturing related simulation in DEM.

Table 4.2 Examples of DEM numerical modeling of hydraulic fracturing.

Petroleum geomechanics application	Reference
Slurry generated fracture	Bruno et al. (2001)
Hydraulic fracturing propagation	Thallak et al. (1990, 1991b) Al-Busaidi et al. (2005) Gumbsch (1995) Schlangen and van Mier (1995)
Mixed mode fracture toughness of Colombia granite	Lee et al. (2006)
Tensile failure response	Yao and Kim (1996)

In general, the use of DEM based numerical simulators is more appropriate for rock mechanics related applications considering that the rock mass media is prone to discontinuities to different degrees. In a DEM problem the formulation is based on grain to grain interaction where the movements are governed by Newton's second law. This has made the DEM to be considered a simpler method than those (e.g. FEM) for which complicated constitutive relations are to be solved. For fracture propagation applications, in DEM the crack path is created through a debonding process. The debonding occurs as the stress on the contact exceeds the contact strength.

In DEM the density and extent of micro bond breakage are the factors used to evaluate the macro damage, crack initiation and propagation. This offers a much simpler concept of crack evolution without a need for complex remeshing or node separation as is involved in continuum based methods. DEM identifies the grains individually by its

contact characteristics, mass and moment of inertia. The movement of particle is estimated based on the contact model(s) that represent(s) the contact behaviour between the grains. The displacement and force of individual micro particles and their interaction via the particle-particle contacts will generate the macro mechanical rock behaviour (PFC^{2d} manual, 2008).

4.2 PFC^{2D} code

PFC^{2D} was used in this study for simulation of the interaction between the hydraulic fracture and natural interface. PFC^{2D} is a DEM based numerical code which was developed by Itasca consulting group (PFC^{2D}, 2008). A PFC^{2D} representation of an intact rock sample is an assembly of particles with specified statistical size distributions of gains particles (balls) and their bonding (Potyondy and Cundall, 2004). These particles are generated with an automatic particle generator with their radii being distributed uniformly between two radius values. The circular disks (in 2D) represent the total mass and grain volume of the model which is a numerical representative of an intact rock sample. Once the bond is installed into the neighboring particles, the overall mechanical behavior of the assembly is dominated by the micro-properties for particles and bonds (Wang et al., 2003).

The run time for each model increases significantly as the number of particles increases and therefore an optimized model should be chosen with reasonable particle size which gives the level of accuracy required depending on the modelled medium properties. The PFC code has been used to simulate several rock mechanics problems such as biaxial experiments of a rock specimen in laboratory (Potyondy and Cundall, 2004), failure around a circular opening under biaxial compression (Fakhimi et al., 2002), perforation (Sarmadivaleh et al. 2010), and hydraulic fracturing (Sarmadivaleh and Rasouli 2010).

The breakage of the bond between each couple of rock particles (disks in this case) and its direct effect on grain motion represents the failure (or micro crack). Thus, the rock deformation is the resultant of the accumulated individual bonds rupture and fracture propagation is a dynamic process of coalescing of neighbouring micro cracks. Simulating the micro behaviour of the rock mass makes the code a reliable tool for predicting the micro-mechanisms damage. This ability should be highlighted when micro failure mechanism plays a major role in the rock mechanical event. An example

of this phenomenon is studied here, where micro mechanisms of energy dissipation in creation of new surfaces and propagation of fracture tip is so important. The code provides the ability to track this mechanism.

On the other hand, a strong coupling between the mechanical part of the code and fluids on the pore space or fractures is developed. Although the developed code is able to consider the effect of pore fluid on reduction of mechanical strength of the rock, this detail was not implemented in our numerical modelling. This was because our experimental samples were concrete with very low permeability and that the fracturing fluids used in the lab had a very high viscosity (see Chapter 2): these extensively reduce the amount of fracture leak-off volume. However, the developed model is able to track the possible leak-off path and apply the subsequent reduction in effective stresses. The 2D limitation of the model in well described in software manual (2008) and Pruiksma and Bezuijen (2002).

4.2.1 Model generation in PFC

As was mentioned in the previous subsection, PFC^{2D} models the particles as circular disks which may be bonded together. Sample generation in PFC^{2D} comprises of four major steps. These are random particle generation, isotropic stress installation, elimination of floating particles, and bond installation (Potyondy and Cundall, 2004). The bonds having specific strength parameters and stiffness are installed into the adjacent particles. At end of these steps, a bonded assembly of particles with some magnitude of in-situ trapped stress is generated with a defined porosity. An example of generated particles' assembly and trapped in-situ stress is shown in Figure 4.1 (left). In this figure, thicker black lines along the ball-ball or ball-wall contact lines represent the magnitude of contact stress at that contact (Itasca, 2008).Now the sample is ready for installation of two independent stresses. The stresses are installed by setting up a servo control ball movement mechanism for all boundary balls. These two stresses represent the maximum and minimum horizontal stresses (σ_H, σ_h). Figure 4.1 (right) shows the generated sample after stress installation corresponding to two independent horizontal stresses of 1 and 5 MPa, respectively.

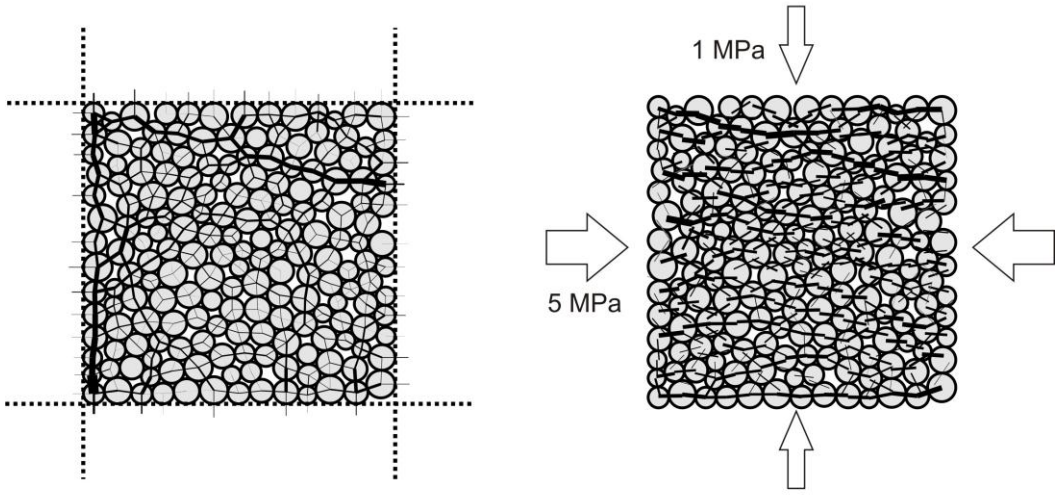

Figure 4.1 The generated assembly of particles with trapped in-situ stress (left), state of the stress on the sample after installing two independent horizontal stresses of 1 and 5 MPa (right). The scales on stress magnitude in left and right figures are not equal.

The assembly of particles is generated with some specific statistical parameters such as ball statistical size distributions, number of particles, and porosity. Figure 4.2 shows an example of ball size distribution histogram corresponding to a sample with minimum and maximum grains radii of 1 and 1.66 mm, respectively. The mechanical porosity is defined as the ratio of void space between the ball particles and total area of assembly.

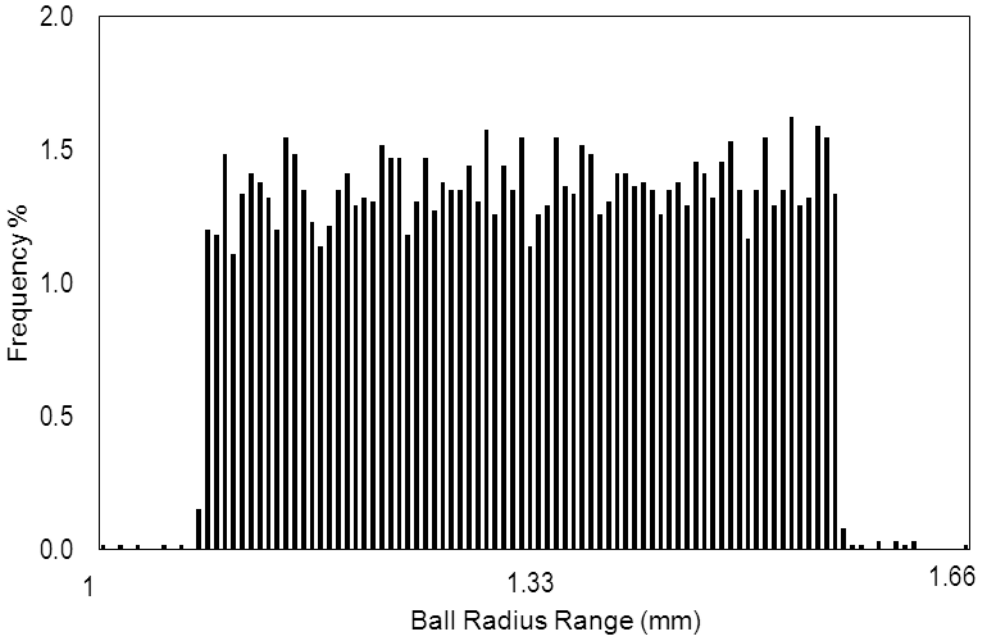

Figure 4.2 An example of ball size distribution histogram.

The code solves two sets of equations: one for calculation of the forces and momentum applied on the balls - this is the mechanical part of the code - and another for computation of fluid flow which is the hydraulic part. During model evolution these two parts are integrated allowing calculations of forces applied to the balls and subsequent changes in pore volume (domain) and pore throat (conduit). This is a poro-elastic simulation approach.

To determine the geometry of the pore space, the links between the particles are spotted by either of these two methods. First the positive compression force among each pair of grains is detected meaning that particles are in direct contact. Second the existence of bond (either contact or parallel bonds) between each couple of particles is tracked. Any closed loops of linked (bonding or contacting) particles generate a pore volume. The middle picture in Figure 4.3 shows a schematic for the structure of balls (disks) with their domains and conduits. The left picture in this figure is an example of how four balls may generate a domain, whereas the right picture shows the way that one aperture connects two domains on two sides of a contact between a couple of particles.

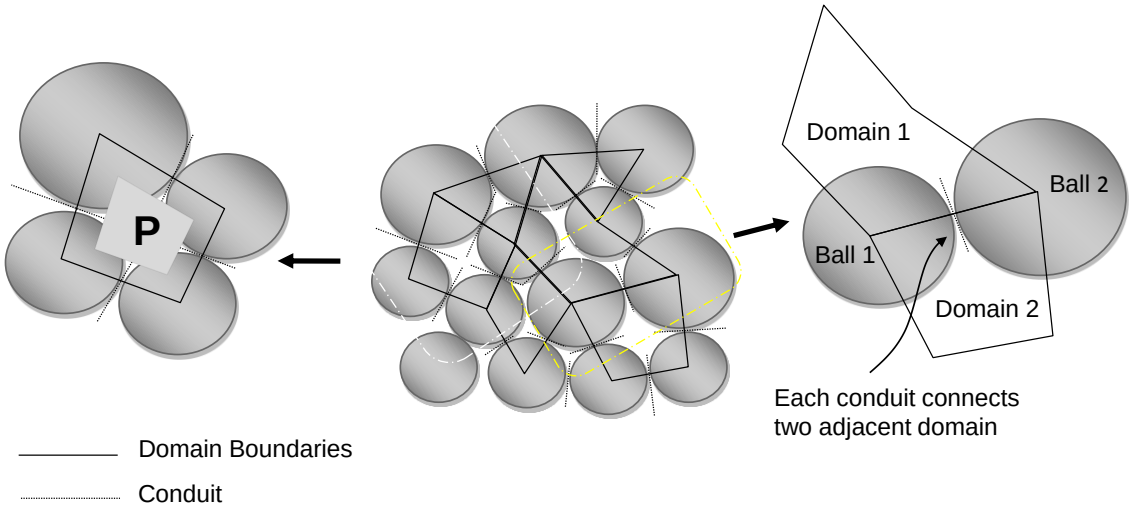

Figure 4.3 Schematic of particle assembly, domain, and conduits generated by PFC^{2D} code.

It is to be noted that the third dimension length of the model (particle and domain as well as the conduits) in PFC^{2D} is considered to be unity, so the calculated area for the pore spaces (domains) are equivalent to their volume. The total domains areas represent 100 percent of pore volume of the sample. The area and pressure of domains are used for mass conservation calculation of the fluid flow. Calculating each individual domain area based on this method will result in the total pore volume of approximately equal to

the bulk volume. Here, the hydraulic (real) porosity (ϕ_h) is introduced to calculate a multiplication coefficient for domain volume in which the total pore and domain volume in specimen and numerical code become equal. The schematic of initial and final domain volumes that should be calculated in order to consider the rock real pore space volume is shown in Figure 4.3 (left picture).

The pressure communication of neighboring domains is facilitated using several pore throats. These conduits are responsible for all fluid flow and have a volume of zero. In contrast to the reality where pore space and pore throats occupy some volume and contribute in fluid flow, in this code all pore volume belongs to the domains and the fluid movement only occurs inside the conduits. The properties of each conduit are defined based on the contact of two balls and connects two unique domains. The diagram of one of these conduits is also shown in Figure 4.3 (right side) where it connects the domain one and two together. Each domain is connected to one or more domain. The pressure change in a domain is given by (PFC^{2D}, 2008):

$$\Delta P = \frac{K_f}{V_d}\left(\sum q\Delta t - \Delta V_d\right), \tag{4.1}$$

where K_f is the fluid bulk modulus , V_d is domain volume, Σq is the sum of the total fluid flow into the domain in time step Δt, and ΔV_d is the domain volume change due to particle movement in each time step (PFC^{2D}, 2008).

The pore pressure of a domain exerts a hydrostatic stress on all balls that create the domain and integrates the pore pressure effect (stress or force) with mechanical response of the model. On the other hand, each individual ball will experience different (either in magnitude or direction) fluid force from its nearby domains which results in a net hydraulic force on the ball. The ball will tend to displace and apply the net force to the neighboring balls. This changes the geometry of the domains (ΔV_d) and accordingly the pore pressure. The change of pressure is calculated based on fluid bulk modulus. For each time step calculation, these iterations should be performed several times in order to achieve equilibrium. This iteration process is computationally very expensive and cannot be done using the ordinary computers and therefore in most cases we implemented a simpler approach in order to calculate the domain volume (V_d) and its change during last time step (ΔV_d).

An approach that was used here to facilitate a faster process is to consider four different types of pore spaces (domain). Except for the wellbore (type one) and its

adjacent domains which are type two (stave domain), the rest of domains are from type four which will not considered for fluid calculation at the start of simulation (see the top left side of figure 4.5). If the pressure of any slave domain (type two) exceeds a threshold, it converts to type three (master domain) and then its entire neighbouring domains that are in type four (no flow calculation) category convert to type two (slave domain). Figure 4.5 shows the evolution of this phenomenon at the time passes. Two different stresses applied on the model before the injection process so the shape of pressure evolution is elliptical with major axis in the direction of maximum horizontal stress. The model is much faster at early time when the number of domains which are involved in fluid flow calculation is low.

It gets slower when state of more and more domains changes from type four to others. This is an example for injection into the sample without fracture generation. However; the same algorithm will be applied in the case of fracturing. Type one domain is the wellbore shown by big black dot. Type two (slave) pore spaces are the boundary domains of darker area of the sample while type three (master) pore spaces occupy the area between the well bore and boundary domains (type two). The rest of domains are type four (lighter colour area) which will not contribute in flow calculation.

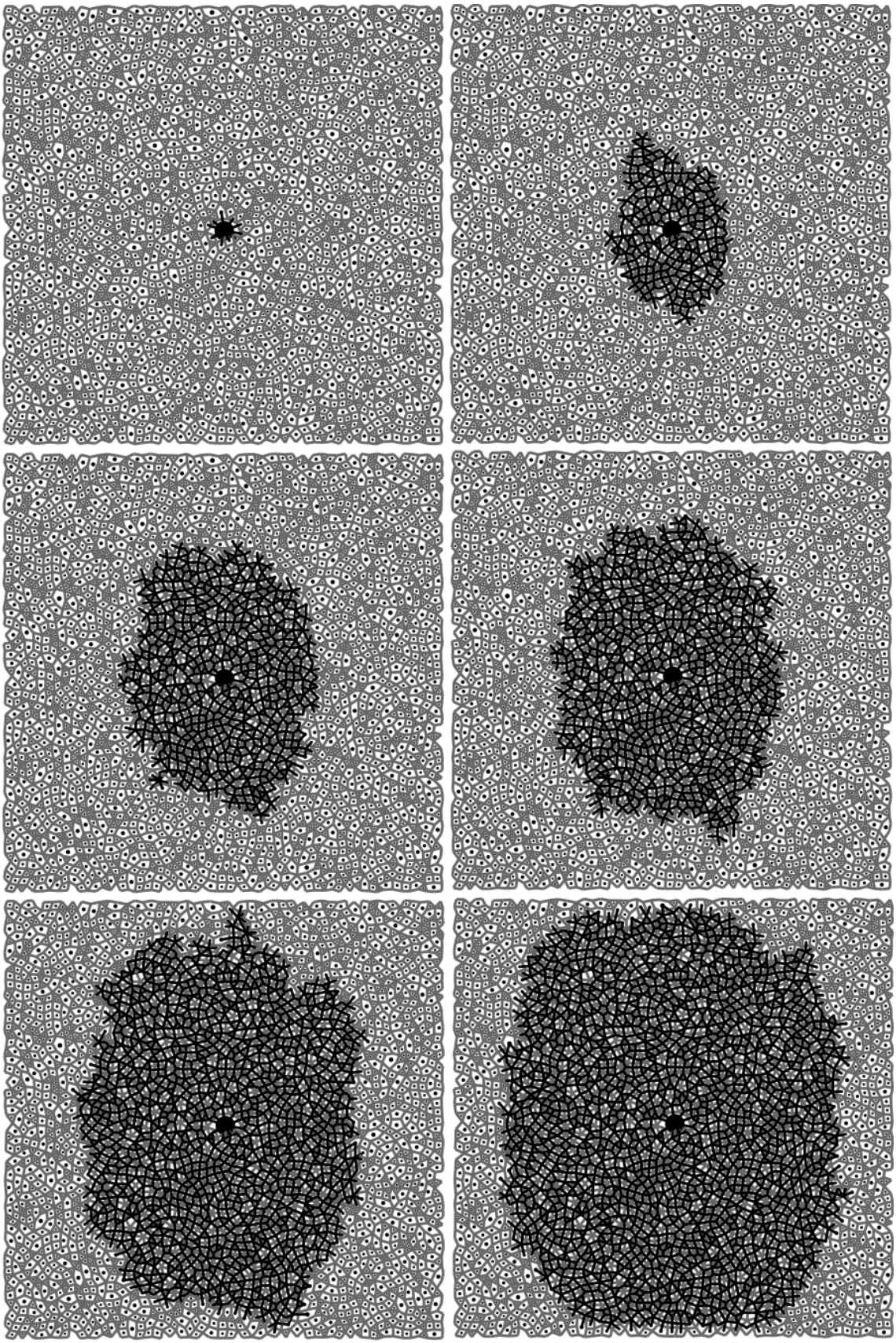

Figure 4.4 Schematic of fluid calculation evolution (top to bottom) of particle assembly with domain (gray closed shape), pore volumes magnitude (black dots), well borehole (single large black dot in the middle), and conduits (black lines) generated for fluid flow simulation.

The volume of fluid that is transferred per unit of time for each conduit between two specific domains is given by (PFC^{2D}, 2008):

$$q = ka^3 \frac{(p_2 - p_1)}{L}, \tag{4.2}$$

where k is the mobility value equal to the ratio of conduit micro permeability over fluid viscosity and (P_2-P_1) is the pressure difference between two domains. Here, L is defined as the length of conduit that is equal to sum of two balls radii that are governing the conduit aperture (a). The most important source of instability in this code comes from the smallest domains which may raise the need for very small time steps for calculation. The pressure change of a small domain as a result of a big time step and consequently a big unrealistic transfer of fluid volume will be very high. To bypass this deficiency, one approach has been to use equal ball radii to have equal domain volume. However, this assumption makes the code much unrealistic because the model is no longer considers the grains interlocking and the same time an identical pore space properties are present all over the model.

A good practice tried here was to implement the random nature of particle sizes distribution of the assembly into fluid flow calculation. For the fluid flow calculations between the two domains, the concept of fluid flow in parallel plats was used (Equation 4.2). This concept needs the calculations of conduit's initial aperture. For this purpose, the aperture thickness corresponding to each conduit was considered as a function of the minimum volume of the two domains connected by that conduit. A multiplication coefficient (C_a) is used for permeability calibration (this will be explained in future sections). The initial aperture (a_o) of each conduit can is given by:

$$a_o = C_a \times \left(\frac{\min(V_{d2}, V_{d1})}{L} \right). \tag{4.3}$$

This random initial conduit property provides a much numerically stable and realistic model. Using this initial aperture thickness calculation, the smallest domains are connected to adjacent pore spaces with the thinnest aperture. This narrow conduit stops large fluid flood due to bigger time steps.

Figures 4.5 and 4.6 show the histograms of the pore space volume and conduit aperture of the assembly of the particles which was shown in Figure 4.2. From these two figures one may conclude that the effect of smaller domain volumes is more significant than larger volumes for determining the conduit aperture.

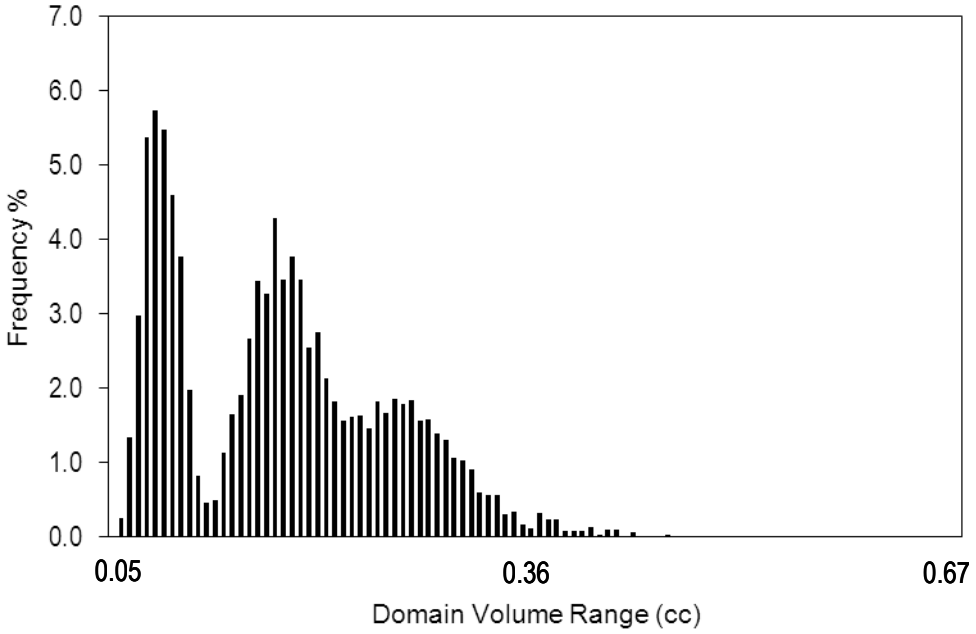

Figure 4.5 An example of domain volume histogram.

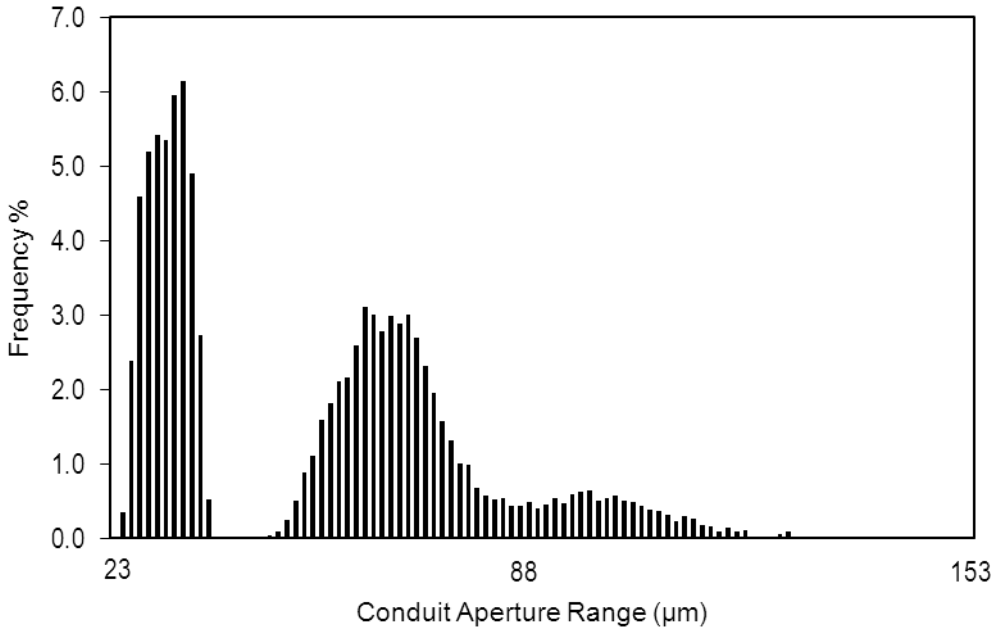

Figure 4.6 An example of conduits aperture histogram.

The micro properties that were assigned to the model (i.e. contacts, balls and bonds) should be chosen in a way that desired macro mechanical properties for assembly is achieved. These macro properties were measured using laboratory tests and reported in Chapter 3. The procedure for selecting the proper micro mechanical properties is explained in the next section.

4.2.2 Hydro-mechanical time step calculations

A characteristic mechanical time step calculation is necessary for each cycle of PFC^{2D} as it uses explicit time integration for equation of motion. The time step must not exceed a critical value ($t_{critical}$) in order to sustain the stability. PFC^{2D} calculates this time step using translational and rotational stiffnesses, and mass and moment of inertia of each particle. The actual mechanical time step is a fraction of this value that can be set by user (PFC^{2D}, 2008).

The fluid and mechanical coupling in PFC^{2D}, as was explained before raises the need for critical fluid time step calculation. For this purpose, firstly we need to introduce a characteristic fluid time step for each domain *i*. Equation 4.1 is rearranged in order to find the fluid time step of each domain (Δt_i), which is shown as:

$$\Delta t_i = \frac{V_{di}}{K_f}\frac{\Delta P_i}{\sum q_j} + \frac{\Delta V_{di}}{\sum q_j}, \tag{4.4}$$

where Σq_j refers to summation of the total fluid coming from all adjacent domains which causes a volume change of ΔV_{di} in domain *i*. Σq_j can be calculated using equation 4.2. It is worthwhile mentioning that Equation 4.2 is for fluid flow rate calculation in each conduit connecting domains *j* and domain *i*. Introducing equation 4.2 into 4.4 we will have:

$$\Delta t_i = \frac{V_{domain\,\mathrm{i\,old}}}{K_f}\frac{(p_{domain\,\mathrm{i}} - p_{domain\,\mathrm{i\,old}})}{k\sum_{j=1}^{n}\frac{a_j^3(p_{domain\,\mathrm{j}} - p_{domain\,\mathrm{i\,old}})}{L_j}} + \frac{(V_{domain\,\mathrm{i}} - V_{domain\,\mathrm{i\,old}})}{k\sum_{j=1}^{n}\frac{a_j^3(p_{domain\,\mathrm{j}} - p_{domain\,\mathrm{i\,old}})}{L_j}}, \tag{4.5}$$

where *"old"* refers to a property of domain (volume or pressure) in the previous time step calculation.

The critical fluid time step ($t_{critical\ fluid}$) would be the minimum value of all characteristic time steps (Δt_i) in each fluid cycle. Figure 4.7 shows the detailed graphical representation of equation 4.5 for domain *i* with four neighbouring domains (*n=4*).

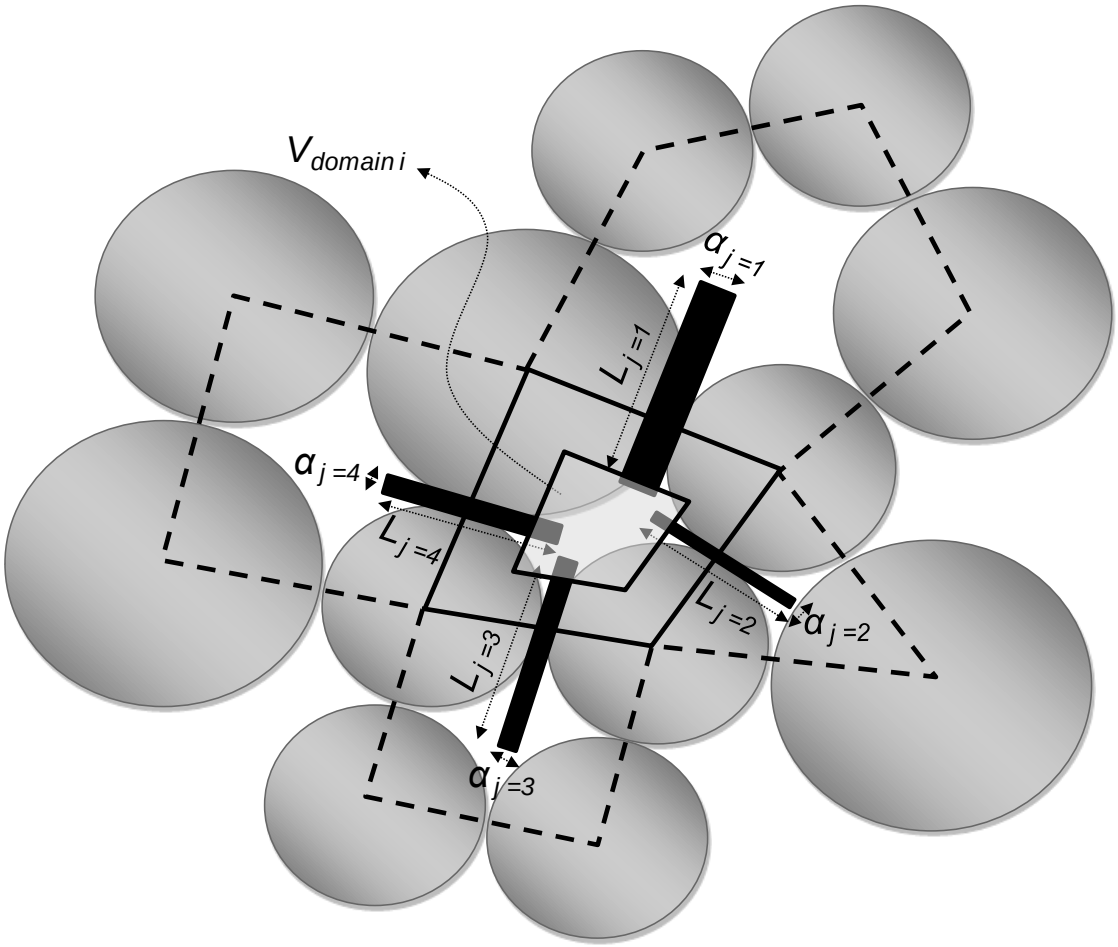

Figure 4.7 Graphical representation of parameters encountering in fluid time-step calculations for one domain.

If critical fluid time step is less than that of critical mechanical time step, fluid time step should be taken for both of mechanical and fluid calculation and for each mechanical step one fluid cycle should be performed. However, if critical mechanical time step is less than the fluid one, critical mechanical time step would be proper value for mechanical calculation and for each fluid cycle, the following number of mechanical steps ($N_{mech\ to\ fluid}$) should be applied:

$$N_{mech\ to\ fluid} = abs\left(\frac{t_{critical\,\mathrm{fluid}}}{t_{critical}}\right). \tag{4.6}$$

Then the new fluid timestep will be

$$t_{critical\,\mathrm{fluid}} = N_{mech\ to\ fluid} \times t_{critical}. \tag{4.7}$$

4.3 Hydro-Mechanical validation and calibration of the model

The PFC^{2D} manual covers several examples of models mechanical validation (PFC^{2D}, 2008). The hydro-mechanical calibration and validation of hydraulic part of the code will be studies in this section. The capability of the code to reproduce small scale hydro-mechanical behavior of the rock sample is demonstrated, through the simulations of triaxial experiments and fluid flow measurement. Here the process of comparing macro parameters of sample in the model and experiment is referred to as the "hydro-mechanical" calibration.

Input parameters of the PFC^{2D} code are at micro scale, so these parameters should be chosen in a way to represent mechanical and hydraulic properties of the numerical model (macro) as closely as possible to laboratory specimen (i.e. mortar). The process that was applied here is a trial and error practice in which micro parameters are changed and the response of model (hydro-mechanical properties) is monitored. The idea here is to generate a numerical representation of the sample that has a set of hyro-mechanical properties as close as possible to the experimental sample. It is to be noted that the relation between UCS value of the numerical sample and micro parameters of PFC^{2D} code has already been suggested by Jong and Lee (2006) and Yoon (2007). However, the micro parameters that were used in our study were different and more complicated; so the common trial and error method was used here.

4.3.1 Model hydraulic validation and calibration

The fluid flow behavior in the model is validated against analytical calculations of diffusivity equation for a simple Darcy test for a rectangular plug with sealed top and bottom boundaries. In this test the inlet and outlet fluid pressure of the sample will be kept constant and flow rate and pressure distribution will be monitored. When the inlet and outlet flow rate become equal, the steady state condition is achieved and the corresponding macro permeability of the model can be measured. This permeability is a function of specific micro hydraulic properties and stress (this will be explained later). One of these micro parameters is micro mobility factor (*k)* which is considered to be constant for all conduits in each model. This factor represents the ratio of micro permeability of the conduits (m^2) over fluid viscosity (Pa.s). So if the micro permeability of a conduit is got doubled while the fluid viscosity is decreased to half, the resultant permeability of sample should not change. The micro mobility and

multiplication coefficient (C_a) will be adjusted thorough a trial and error procedure in the way that model macro permeability becomes equal to the experimental sample permeability. In addition to permeability, hydraulic porosity of the numerical model should be equal to the porosity of the experimental specimen.

The fluid flow validation of the model against the analytical solution for both transient and steady state condition was confirmed in this study by conducting the Darcy test simulation on a rectangular sample. Initial pore pressures of all domains (pore spaces) were set to be zero and inlet and outlet pressures of the sample were fixed to be 5 and 0 MPa, respectively for the entire test period. The view of generated model for this test is shown Figure 4.8. It also shows the pore fluid pressure distribution (diameter of black circles) along the sample at the time of steady flow.

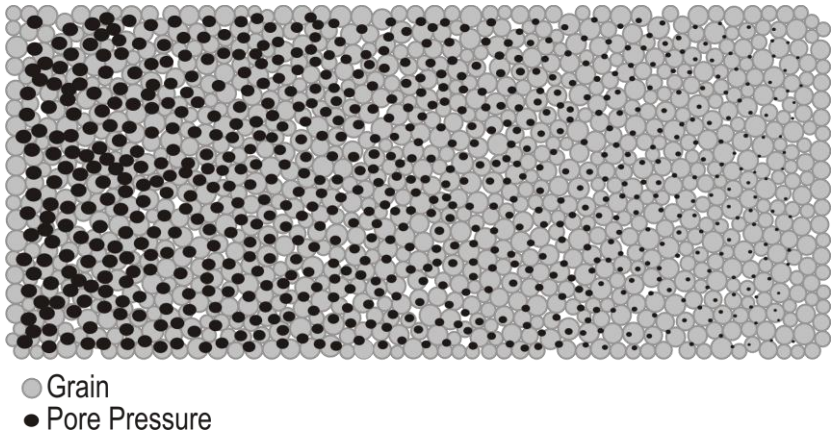

Figure 4.8 Simulation of Darcy test on a rectangular sample. The grains are shown by gray circles. The magnitude of pressure in each pore space is shown by the size of black circles.

The partial differential equation (PDE) that describes the above problem is given by:

$$\frac{\partial P}{\partial t} = \frac{1}{K_p}\frac{\partial^2 P}{\partial x^2},\ 0 < x < L, \tag{4.8}$$

where:

$$K_p = \frac{k_{ma}}{\mu c \phi}. \tag{4.9}$$

Here, K_p [$M^2.s^{-1}$] is defined as piezometric conductivity, c is the compressibility or consolidation coefficient, μ is fluid viscosity, ϕ is porosity and k_{ma} is macro (inherent) permeability. In Equation 4.8, x is the distance from the inlet point. The boundary conditions in this example are:

$$P(L,t) = 0.0, \qquad P(0,t) = 5Mpa \qquad t > 0, \tag{4.10}$$

and initial condition is:

$$P(x,0) = 0.0, \quad 0 \le x \le 0.06. \tag{4.11}$$

The solution for Equation 4.8 considering the above mentioned initial and boundary conditions is given by:

$$P(x,t) = 822.5x + \sum_{n=1}^{\infty}\left(-98.7\,\frac{\sin(0.06n\pi) - 0.06n\pi\cos(0.06n\pi)}{n^2\pi^2}\right)e^{-\frac{n^2\pi^2 t}{0.0075}}\sin\left(\frac{n\pi x}{0.06}\right). \tag{4.12}$$

The dimensionless form of this equation is used for the analysis purposes. This is given by:

$$P_D(x_D,t_D) = x_D - \frac{2}{\pi}\sum_{n=1}^{\infty}\frac{(-1)^n}{n}e^{n^2\pi^2 t_D}\sin(n\pi x_D), \tag{4.13}$$

where P_D, x_D, t_D are dimensionless pressure, length, and time, respectively. Figure 4.9 shows the solution of equation 4.13 for different dimensionless times and distances. Figure 4.10 shows how dimensionless pressure evolution along the sample in different dimensionless time agrees very closely with the analytical solution. The cross sectional flow rates (in the cross sections perpendicular to flow direction) of inlet, outlet and in the middle of the sample were monitored during the flood test and compared with those of analytical results. Differentiating Equation 4.13 with respect to X_D, the equation of dimensionless flow will be obtained as:

$$q_D(x_D,t_D) = 1 - 2\sum_{n=1}^{\infty}(-1)^n e^{n^2\pi^2 t_D}\cos(n\pi x_D). \tag{4.14}$$

This equation was solved for three dimensionless lengths of 0, 0.5, and 1.0 which correspond to the sample inlet, middle section, and outlet, respectively. The flow rate was also calculated for the entire period of the experiment at these three points in numerical simulations. The results are plotted in Figure 4.11 showing a very good agreement.

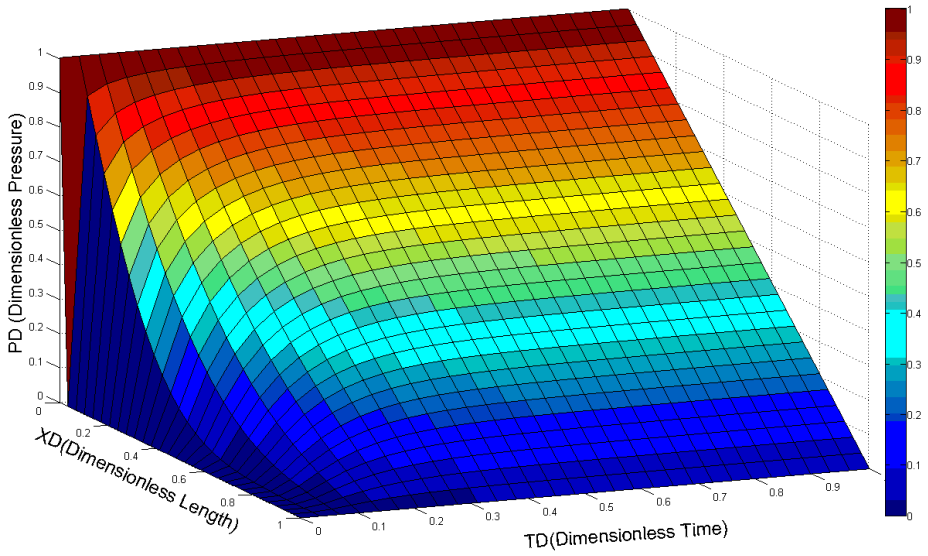

Figure 4.9 Time evolution of pressure along the length of the sample in different dimensionless times.

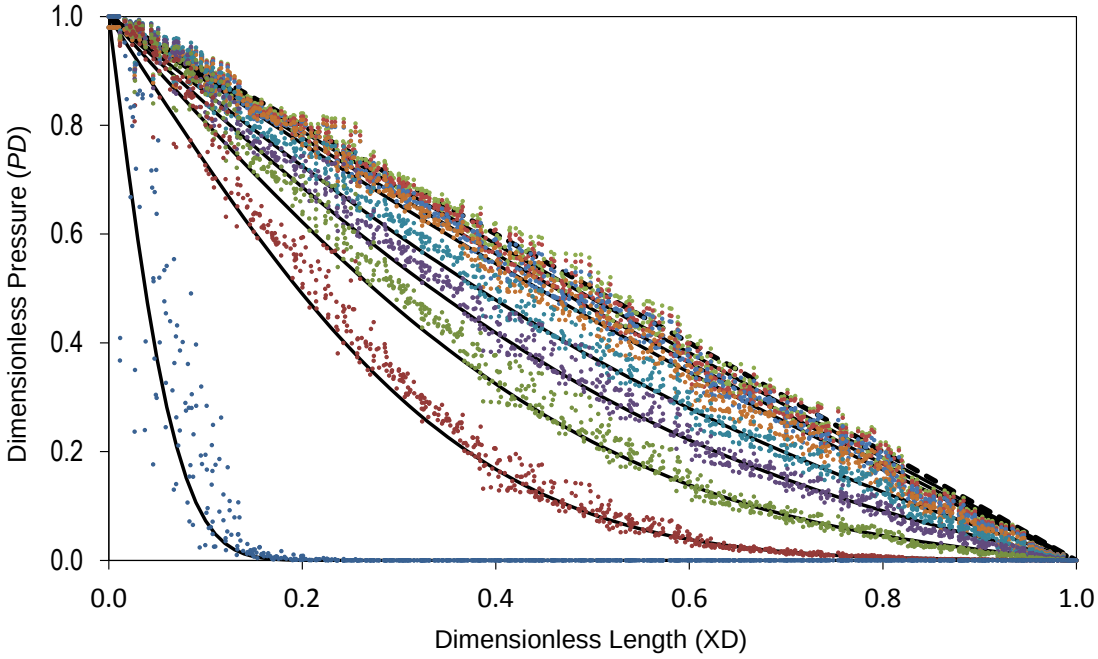

Figure 4.10 Changes of pressure along the length of the sample for different dimensionless times of 0.001555, 0.041992, 0.082429, 0.122865, 0.163302, 0.203739, 0.244175, 0.284612, 0.325049, and 1.000000 (steady state). Solid lines are the analytical solution of the problem based on Equation 4.9 and the dots are the pore pressures along the sample. Different colors show different dimensionless times. Dashed line shows the analytical solution for the steady state condition (Darcy law).

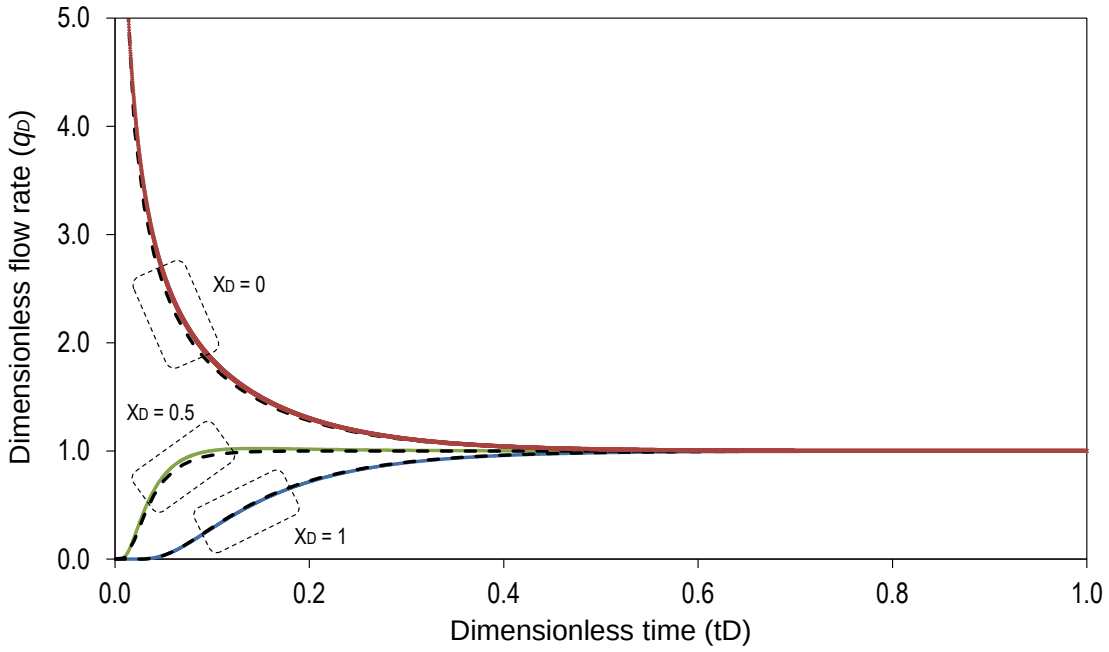

Figure 4.11 Changes of dimensionless flow rates at three different points of inlet (X_D=0), middle section (X_D=0.5), and outlet (X_D=1.0) of the sample. The colored points are the results of numerical simulation and the dash lines are the analytical solutions from Equation 4.10. For t_D > 0.6, all 6 graphs become almost identical showing numerical and analytical solutions being in a steady state mode.

4.3.2 Model mechanical calibration

In this subsection, the macro mechanical properties of the numerical code are calibrated based on micro properties as are used in numerical simulations. Table 4.3 lists different tests used for calibration of various the macro mechanical properties.

Table 4.3 Proposed tests used to calibrate macro mechanical properties in PFC[2D].

Macro properties	**Test method**
Uni-axial Compressive Strength (UCS)	Unconfined compression test
Confined Compressive Strength	Biaxial test
Tensile Strength	Direct and Brazilian tensile test
Fracture Toughness Test	Semi Circular Bend Test and middle-tension panel[1]

[1]*Anderson 1991*

Table 4.4 lists different tests proposed for calibrating the macro (experiment) versus PFC[2D] model (micro) properties. Calibration of the micro input parameters of the numerical model with macro experimental values is a complicated and time consuming task. Some of the tests listed in Table 4.4 were designed specifically for the purpose of

this study. More information about the procedure of these tests can be found from PFC^{2D} manual (2008).

Table 4.4 The experimental and corresponding numerical macro hydro-mechanical properties of mortar sample.

Test	Types of matching	Matched parameter	Value for cement	
			Experiment	Numerical
Uniaxial compression[1]	**Mechanical**	UCS psi (MPa)	11,530±750 (79.5)	11,300 (78)
		v	0.197± 0.02	0.21
		E psi (GPa)	$4.018\times10^6 \pm 2\times10^5$ (27.74)	5.51×10^6 (38.0)
Confined compression[1]	**Mechanical**	Φ (Degree) [4]	43.3	44.5
		σ_c psi (MPa) [4]	2524 (17.3)	2565 (17.7)
		v	0.197 ± 0.01	0.20
		E psi (GPa)[5]	35 ± 4	42
Fracture toughness	**Mechanical**	KIC_D psi.in½ (MPa.m½)	-	510 (0.561)
		KIC psi.in½ (MPa.m½)	710±200 (0.78)	-
Direct tensile strength	**Mechanical**	T_{0D} psi (MPa)	-	710(4.9)
Brazilian tensile strength	**Mechanical**	T_{0B} psi (MPa)	510±200 (3.5)	2600(18)
Hydraulic fracturing reopening	**Mechanical**	T_{0ro} psi (MPa)	1680 (11.6)	-
Linear flow[2]	**Hydraulical**	K (mD)	0.018±0.005	0.0061
Porosity[3] **and pore size distribution measurements**	**Hydraulical**	Φh (%)	14.7±1	14.6
		D pore space max (µm)	1000	460
		D pore space min (µm)	1	120
		D ave. pore space (µm)	-	231
		D pore throat max (µm)	-	154
		D pore throat min (µm)	-	23
		D ave. pore throat (µm)	1	53.3

[1] The numerical and experimental uniaxial and confined compression tests may be performed under Drained and Undrained conditions for an ideal Hyro-Mechanical matching.

[2] Linear or Darcy test provides permeability and conductivity of the sample which may be highly dependent on stress direction and magnitude. Thus a numerical stress sensitive linear flow test will provide a more realistic permeability results.

[2] Linear permeability may match with the results of ambient or confined core permeability tests.

[2] Water was used in numerical test with a viscosity of 10^{-3} Pa.s. Transient gas (nitrogen) permeability was used for laboratory sample.

[3] This is a hydraulical porosity. This porosity is totally different from the mechanical porosity and is equal to real specimen (cement in this case) porosity. The difference between the mechanical and hydraulical porosities values is due to the 2D nature of the simulation used here.

[4] Internal friction angle and intact rock cohesion based on Mohr-Coulomb failure envelope corresponding to 400, 700, 1400psi confining pressures.

[5] Corresponding to a confinement of 1400psi.

The main difficulty in conducting the above tests was the design of a rock with very low permeability and moderate porosity with high mechanical strength similar to the mortar used for laboratory tests in this work (see Chapter 3). The maximum, minimum, and average values of these two properties are shown in Table 4.4. The wide differences between the model and specimen pore space and throat sizes (maximum, minimum, and average values) are due to different number of particles present in the model and that of the real sample. However, other micro properties like permeability were assigned to the model such that this difference becomes negligible. During the simulation, conduit

aperture will change depending on the applied force on the particles and existing domain pressures.

Table 4.5 shows the micro properties of the sample corresponding to the numerical model. As we used the parallel bond contact, an increase or a decrease in number of particles will not affect the simulation results noticeably. However, based on the available computational resources, the optimum least particle size diameter and the biggest sample size dimension should be decided upon before doing the simulation. It is worth mentioning that applying the fluid flow and parallel bond model available in PFC^{2D} increases the simulation time significantly.

Table 4.5 Micro parameters used in PFC^{2D} for sample generation.

Property	Value
Bulk density lb/ft3 (kg/m3)	129.8(2080)
Minimum particle radius (mm)	0.5-1.0
Particle size ratio	1.66
Ball Contact Young's Modulus psi (GPa)	4.35×10^6 (30)
Ball normal to shear stiffness ratio	1.5
Ball friction coefficient	0.5
All contact bond strength values psi (MPa)	0.0
Parallel bond Young's Modulus psi (GPa)	4.35×10^6 (30)
Parallel bond normal to shear stiffness ratio	1.5
Mean value of parallel bond normal strength psi (MPa)	1450 (10)
Standard deviation of parallel bond normal strength (MPa)	0.0
Parallel bond mean value of cohesion psi (MPa)	10,870 (75)
Parallel bond shear angle (degree)	30

4.3.3 Stress dependency of permeability

It is well known that the rock permeability is stress dependent (Bruno, 1994). In fractured rocks the permeability of the fracture plane is also a function of far field stress magnitudes as well as the orientation of principal stresses with respect to the fracture plane. In PFC^{2D} code, the aperture of conduits is recalculated in each time step when fluid analysis is undergoing in order to consider the type (tension or compression) and magnitude of the new stresses applied to the conduits. The aperture size, for the compression case, is calculated as (PFC^{2D}, 2008):

$$a = \frac{a_o F_o}{F + F_o}, \tag{4.11}$$

where a_o is given in equation (4.3), and F_o is the value of the compressional force F, applied to the conduit resulting to its aperture reducing to half of a_o. Equation (4.11) shows that the applied stresses reduce the aperture size and hence the conduit capacity

to pass the flow (see equation 4.2). Therefore, the measured permeability in the model is expected to reduce as a result of increasing applied stresses on the sample. The reduction of hydraulical properties of the rock sample under stressed conditions has been reported in many published experimental tests (e.g. Chierici et al., 1967; Thomas and Ward, 1972; Bruno, 1994).

Figure 4.12 shows comparison of numerical model estimation permeability and hydraulic porosity that was used in the simulation as solid squares. It was explained earlier that the hydraulic porosity is the one that will contribute into the fluid flow calculation. Once it sets at the beginning of the simulation, it can be calculated based on pore volume change. However; this type of porosity measurement need lots of iterations. Avoiding this time consuming process, in each simulation the macro porosity (hydraulic porosity) value of the entire model is given to the model as an input. Also, the analytical solution of porosity (solid gray line) and permeability (dashed gray line) are given in figure 4.12 based on equations 3.1 and 3.2. So the porosity values are identical to analytical solutions, whereas there is some discrepancy in the case of permeability. This is because anisotropic stresses were applied in the simulations while the developed analytical models are for the case of isotropic state of stresses: applying anisotropic stresses was found to make the sample more permeable in one direction comparing to the second direction. (see Figure 4.4).

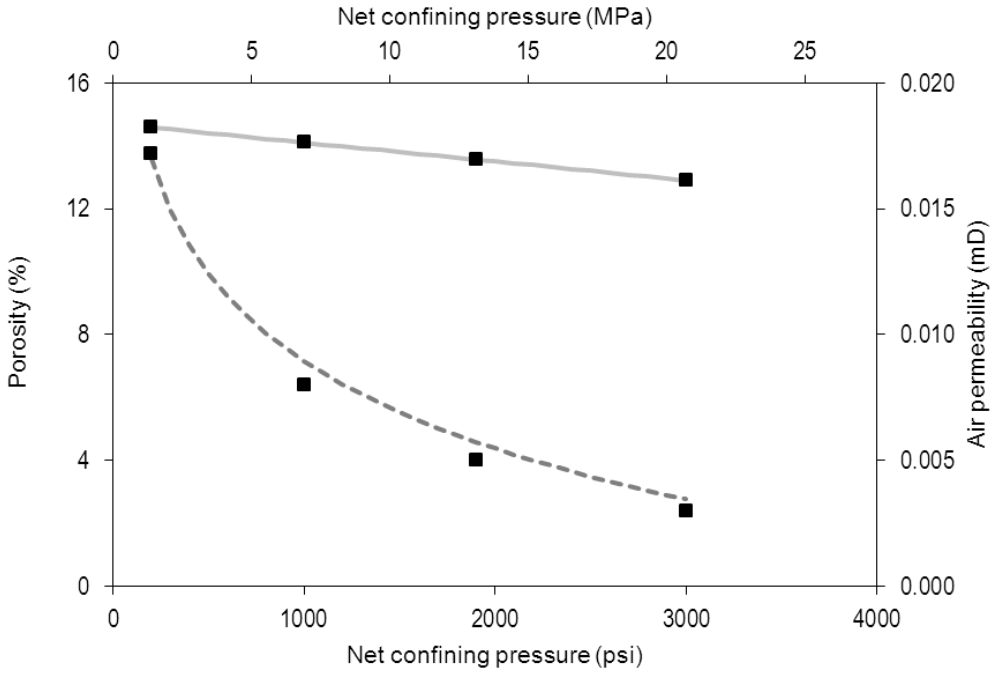

Figure 4.12 Calibration of estimated permeability of the samples from simulation against analytical solutions. The porosity variation considered to be identical to analytical solution.

4.4 Modeling natural interfaces

Modeling a discontinuity plane in PFC^{2D} was one of the most challenging parts of the simulations. This requires comprehensive knowledge of the interface properties (i.e. cement-cement characteristics) but very limited information was available in this case. Shear and normal stiffness of the interface together with its cohesion are some of the interface properties that are needed for simulating an interface. In our lab experiments, as explained in the previous Chapter, the interface friction was measured at different normal stresses; however, no tangential or normal displacement measurement of fracture plane was carried out on the sample due to practical limitations of the TTSC. This avoided the possibility of estimating interface normal and shear stiffness. Therefore, the required interface properties were extracted from the literature (e.g. Kulhawy, 1975) for cases close to our experiments. . Most of the reported cases were for gas filled fractures whose shear stiffness were obtained through direct shear tests. The experimental set up for estimation of the normal stiffness is more complicated than that of a shear test and consequently the available data reported for normal stiffness is less comparing to shear stiffness. In this situation, one approach is to estimate the normal stiffness through existing empirical relationships between the two stiffness and some rock parameters. Sayers and Kachanov (1995) proposed an analytical formula for the ratio of shear (K_{shear}) to normal (K_{normal}) stiffness as a function of Poisson's ratio (ν):

$$\frac{K_{shear}}{K_{normal}} = \frac{1-\upsilon}{1-\frac{\upsilon}{2}}. \tag{4.12}$$

Similarly, Liu et al. (2000), based on the planar distribution of small isolated areas of slips, proposed below relationship:

$$\frac{K_{shear}}{K_{normal}} = 1-\frac{\upsilon}{2} \tag{4.13}$$

based on equations 4.12 and 4.13, the theoretical range for the stiffness ratio will be approximately 0.902-0.891. This is reasonably close to the ratio of one which is commonly used for gas (dry) filled fractures. Other ratios have been reported by other researchers based on their lab experimental results (e.g. Lubbe et al., 2008, reported a ratio of 2), however, we chose a value of 0.9 in this study as it has been reported in majority of literatures. A shear stiffness of 0.5 $\times 10^{13}$ Pa/m (Möllhoff and Bean, 2009)

was used for our interfaces. Considering the ratio of 0.9, the normal stiffness will be 0.55×10^{13} Pa/m.

The natural interface in this thesis was modeled using the Smooth Joint model in PFC^{2D} which considers different failure criteria, and has cohesion, friction and other fracture (interface) properties as its input. Further information about the theoretical aspects of such modeling can be found in PFC^{2D} manual (2010).

4.5 Simulation of fracturing propagation

After the excavation of the wellbore in the middle of sample and installation of the pore (if any) and wellbore fluid pressures, the model is ready for simulation of a hydraulic fracturing. The hyro-mechanical properties of the model are tabulated in Table 4.4. The flow rate in this test which was carried out on a 15cm cube sample was 0.1 cc/min and the far-field stresses applied to the model boundaries were 20 and 10 MPa, respectively. Figure 4.13 shows the evolution of a hydraulic fracture in PFC^{2D} simulation. Fracturing fluid pressure profile along the fracture length for the final stage of fracturing test is shown in the top left part of Figure 4.13. The diameter of black circles represents the magnitude of fluid pressure at each point. The highest pressure values are observed at the wellbore with the lowest ones at the tip of the fracture and leak-off zones.

The maximum opening of the hydraulic fracture was estimated to be approximately 0.9 mm. The displacement vectors are shown in the top right side in Figure 4.13 which shows an outward fluid movement from fracture to the formation. The fracture plane footpath may be traced as locations where grain to grain contacts are disconnected in the model. It is important to note that the adjacent grains, at the beginning of hydraulic fracturing, are forced against each other due to applied in-situ stresses and the bonding process. This results in grains separation which defines the fracture propagation path as is shown in bottom left side of Figure 4.13.

To simulate the lab experiments, a high fracturing fluid viscosity was applied which resulted in a very limited leak-off zone around the fracture plane, as is shown by the affected dark pores in the bottom right side of Figure 4.13. The fracture propagation, as is seen from Figure 4.13 is along the maximum horizontal stress direction. The fracture propagation may start in a different direction but corrects itself to the direction of maximum stress here (generally the least resistance direction) soon when the local propagating resistance changed. It is to be noted that the local conditions during fracture

propagation may change due to the change in ball sizes, pore space, and other micro hydro-mechanical properties; however, the general direction of fracture propagation at a distance enough far from the wellbore should remain along maximum horizontal stress direction in this particular case.

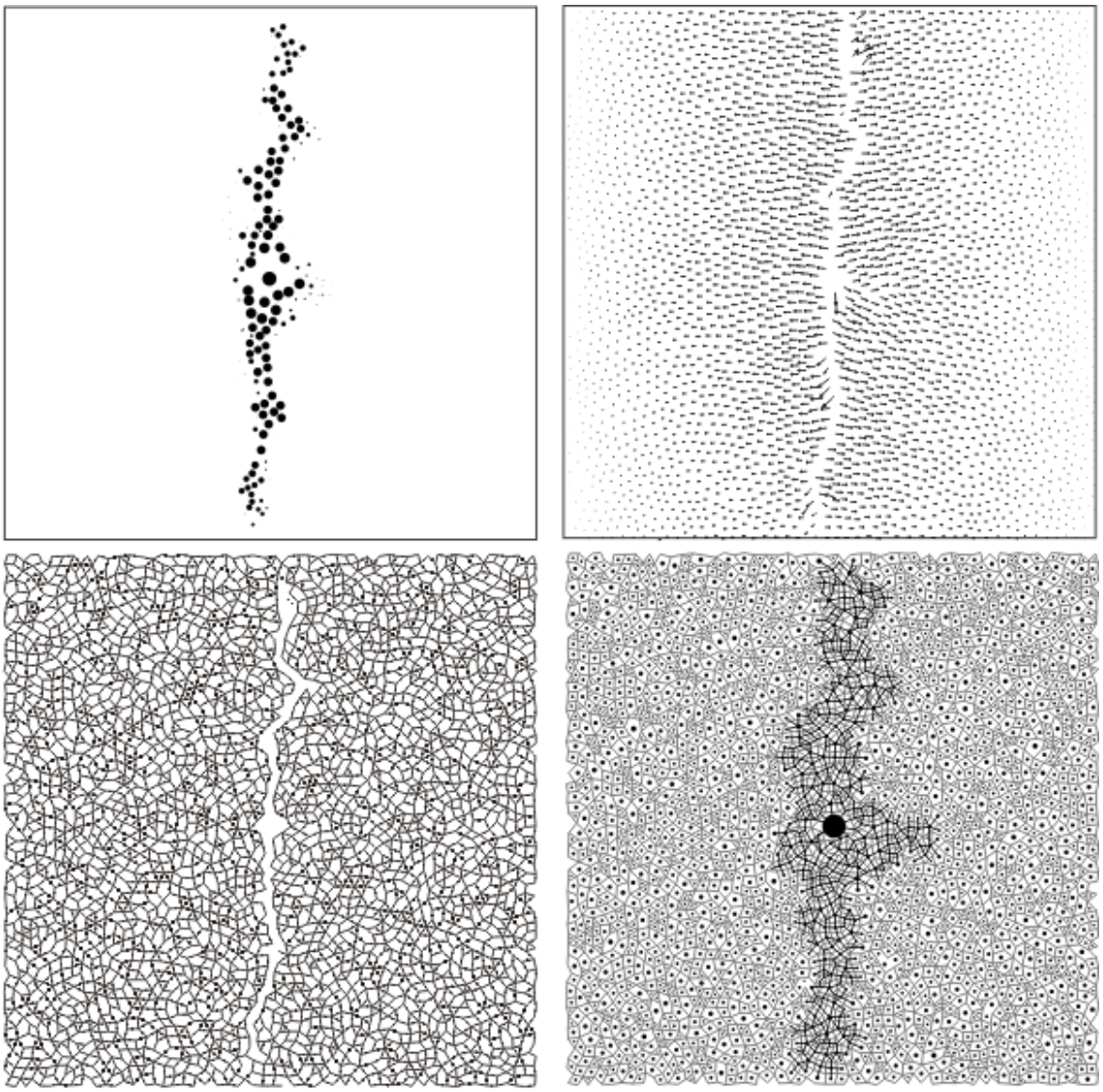

Figure 4.13 Fracture fluid pore pressure (top left), displacement balls (top right), ball contacts (bottom left), and area of pore space that was encountered into fluid calculation (bottom right).

4.6 Effect of different parameters on interaction mechanism

A wide range of parameters affects the interaction process. Here, the impact of few of these parameters on interaction mechanism will be studied qualitatively. These parameters include interface friction coefficient, cohesion, and the angle of approach. Also, the superimposed effect of these parameters will be investigated. For this purpose,

two straight natural interfaces with similar properties and angle of approaches with respect to the hydraulic fracture plane were considered for simulations. The propagation distances (this is the distance between the wellbore and the intersection point of natural and hydraulic fractures) in all models were kept constant.

However, it was observed that some of the hydraulic fractures did not propagate perfectly along a straight line resulting in slightly lower or longer distances. As was explained earlier in Chapters 2 and 3, when the hydraulic fracture approaches a natural interface, the magnitude of the stress that is transferred from one side of the natural interface (the side at which the hydraulic fracture exists) to the other side is the factor which determines whether the fracture is able to cross the interface or not.

The magnitude of the stress depends on the shear stress applied at the interface. The shear stress itself depends on three factors: friction coefficient of the natural interface, its shear strength, where the shear strength is due to cohesion between the two sides of the interface, and the normal stress applied on the interface plane which is function of in-situ stresses magnitude and the angle of approach. The effects of these factors will be studied in the following subsections.

4.6.1 Friction of the natural interface

Frictional force acting on the interface is a product of the projected component of the far field stresses applied normal to the interface plane (σ_n) and the friction coefficient of the plane. To ensure that the hydraulic fracture crosses the interface, an approach angle of 90° was chosen in our models (Warpinski & Teufel, 1987). The results of a simulation model using PFC^{2D} shown in Figure 4.14 indicate that an induced fracture will stop upon approaching a frictionless and cohesion-less natural interface: the interface behaves like a barrier as its friction coefficient is zero.

Particles displacements can be used as an illustration of stress transfer in the model. Figure 4.14 (right) shows the displacement vectors in the model during fracturing simulation. The fracture path can be easily distinguished from this figure. As it can be seen, particles which are located on the side of the induced fracture are displaced outwards and in opposite directions. Particle displacements are completely different in two sides of the natural interfaces.

Displacement vectors are much larger at the interior sides of the natural interfaces than those on the exterior sides. Undisturbed displacement vectors shown on the top and bottom sides of model confirm that fracture propagation was stopped once approached

the natural interface. Particles on the fractured side of model are arranged with a displacement component parallel to the natural interface and outward from the hydraulic fracture plane while other particles are arranged mostly normal to the natural interface.Nonetheless; the displacements on outer parts is not well pronounced here meaning that two zones of undisturbed stress present at top and bottom sides of the model.

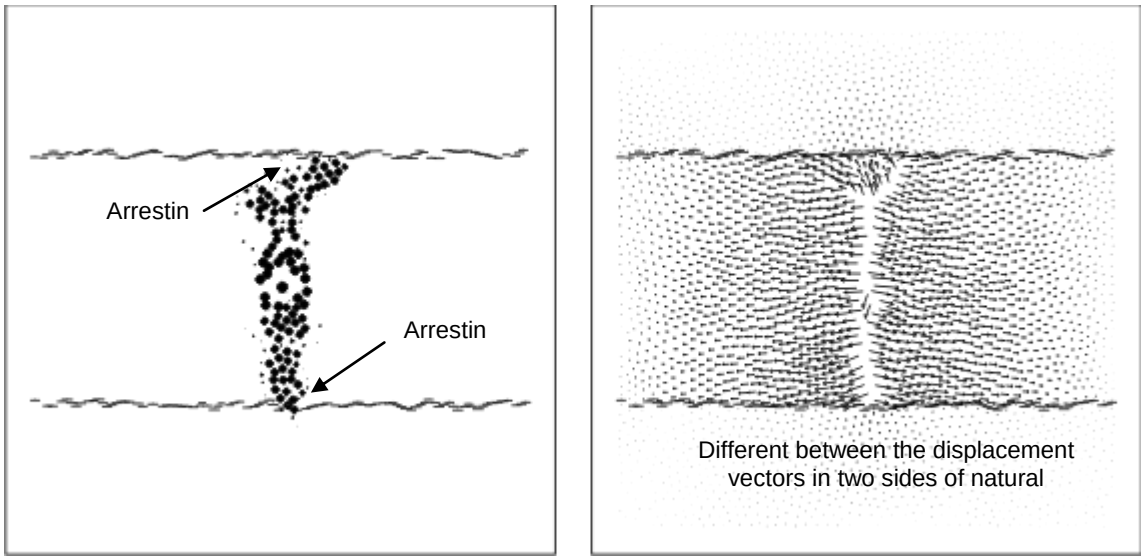

Figure 4.14 Interaction of a hydraulic fracture when approaches a frictionless and cohesion-less interface at 90 degrees (left), Scaled displacement vectors of particles (right).

In the next step, the friction coefficient was increased slightly; the hydraulic fracture crossed the natural fracture in the upper side (see top Figures in 4.15) but was arrested by the lower interface. This observation may be interpreted as a result of the fact that when the interface frictional properties are not strong and the hydraulic fracture crosses one interface, the pressure will be released inside the crossed interface which avoids the other wing of fracture to cross the second interface. Similar observations were made in some of experimental tests carried out in the lab (see Chapter 3). It is interesting to note the extent of particles displacement at the intersection point in the upper interface in Figure 4.15. It is seen how the width of the hydraulic fracture reduces after it intersects the interface: this demonstrates the important effect of the interface properties on hydraulic fracture propagation. In this model the friction coefficient was 0.5.

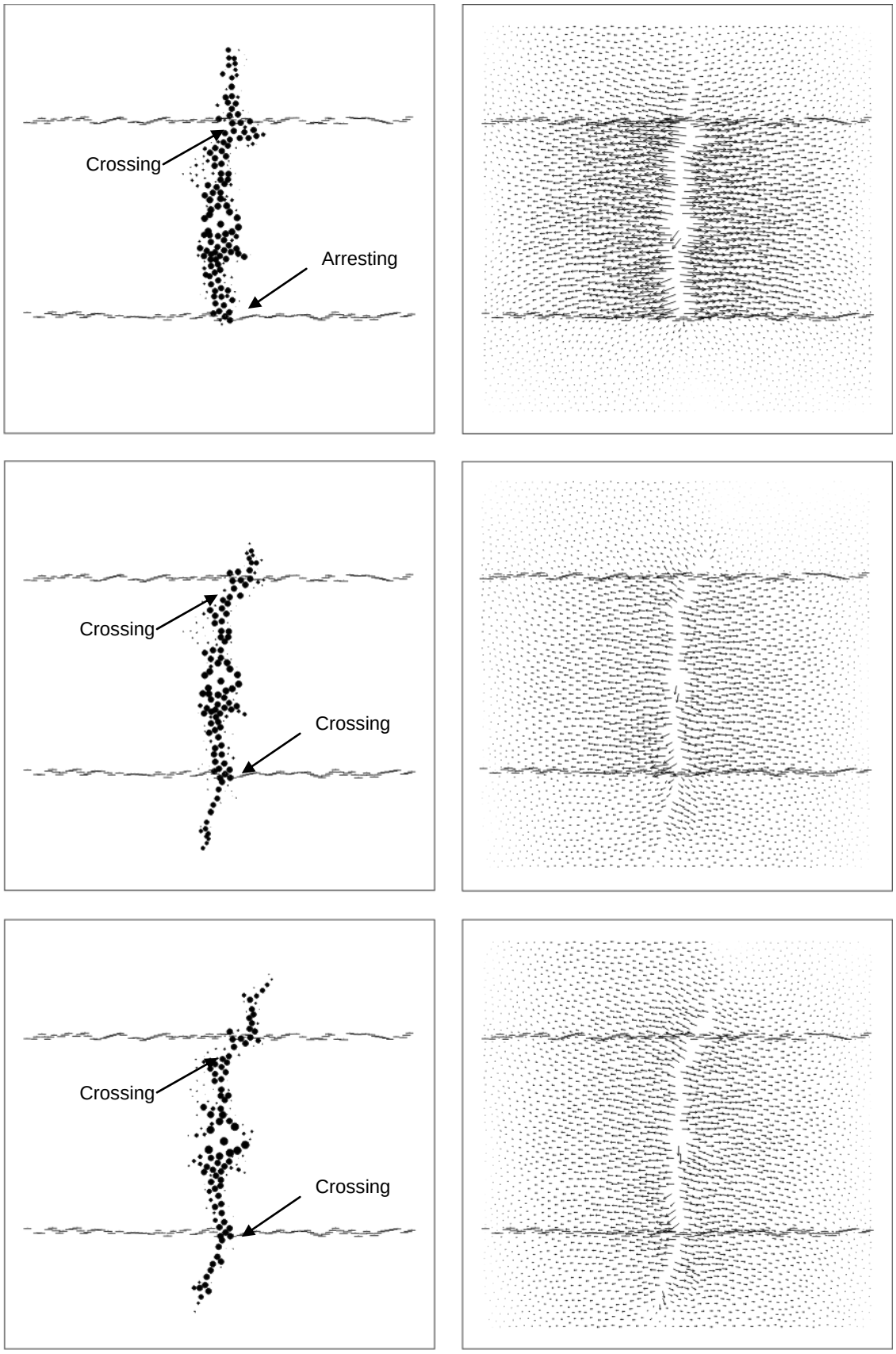

Figure 4.15 A hydraulic fracture starts to cross the cohesion-less interface with a friction coefficient of 0.5 and an approaching angle of 90 degrees from one side (top two figures). The crossing interaction occurs in both interfaces when friction coefficient increased to 0.7 (middle figures). Two perfect crossing modes were the dominant interaction when friction coefficient was increased (bottom figures).

Increasing in friction coefficient of interfaces to 0.7 the crossing interaction occurred in both interfaces (see Figure 4.15, middle section). However, in this case the upper interface experiences a non-mature crossing mode. A further increase of 0.3 in friction coefficient resulted in pure crossing in both interfaces (see bottom section in Figure 4.15). A detectable displacement boundary (e.g. top models in Figure 4.15) was not observed here indicating that the friction of the natural interface caused the fracture to fully cross the interface. This shows that interface friction properties was high enough resulting in the interface to behave similar to an intact rock. These results demonstrate the significance of the interface friction coefficient on the behavior of a hydraulic fracture approaching a natural interface.

4.6.2 Shear strength of the interface

Generally, natural interfaces are expected to have less shear strength than that of the rock body. However, when the natural interfaces are filled with strong cement, their shear strength can be as high as that of the rock body. In this study, for interpretation purposes, in most models the natural interface was assumed to be weakly cemented to represent a lower shear strength compared to the rock body. To analyze the effect of natural interface shear strength, a 60º and cohesion-less interface with a friction coefficient of 0.5 were considered for fracturing simulation. It was seen earlier that this type of interface is likely to undergo the crossing mode at 90º angle of approach. Friction coefficient of 0.5 was considered here as a starting point as no crossing was expected to occur beyond this value (see discussions in section 4.6), in particular for lower angle of approaches. The results were compared with another fracturing simulation in a model that has two cohesive (interface that has shear strength) natural interfaces having an angle of 30° with respect to the minimum horizontal stress direction (i.e. an angle of approach of 60°).

Figure 4.16 shows the model results corresponding to two tests where the hydraulic fractures interact with two types of interfaces of zero (top figures) and 5 MPa (bottom figures) shear strength, respectively. It was observed that the hydraulic fracture did not cross the frictional interface as the angle of approach decreases from 90º to 60º even when it intersected the interfaces in an orthogonal angle of approach (see Figure 4.16, top). This is while the hydraulic fracture crossed the natural interface with a higher shear strength (see Figures 4.16, bottom).

This shows how the lack of enough frictional strength for the interface plane may be compensated for by some bonding material which allows transferring adequate tensile stress from one side of the interface to another. So based on numerical simulation results, it is concluded that friction coefficient and shear strength of natural interfaces can work in a interchangeable manner: this means that the inadequate effect of one parameter may be compensate by larger influence of another parameter.

However, the friction existing between the two sides of an interface plane is usually a permanent property which is present even after a shear displacement taken place but with a different magnitude. It should also be noted that if the applied shear stress caused by a hydraulic fracture exceeds the shear strength of the natural interface plane, the shear strength (bond) will fail permanently: this is the main difference between these two interface properties (friction and cohesion).

4.6.3 Effect of angle of approach

In order to investigate the effect of the angle of approach, a sensitivity analysis was performed by keeping all parameters constant except the orientation of the natural plane which determines the angle of approach. A similar practice was presented in Figure 4.7 when the angle of approach was changed from 60º to 90º. A natural interface with the frictional and cohesive properties similar to crossing scenario presented in the last subsection (Figure 4.23, bottom) where considered and the angle of approach was changed from 60º to 30º. The analysis results are given in Figure 4.17 for the latter angle of approach. From the results of this figure and Figure 4.7 t is seen that the hydraulic fracture could cross the interface at an approach angle of 60° but was arrested when the angle reduced to 30º. This shows the significance of the angle of approach on interaction results.

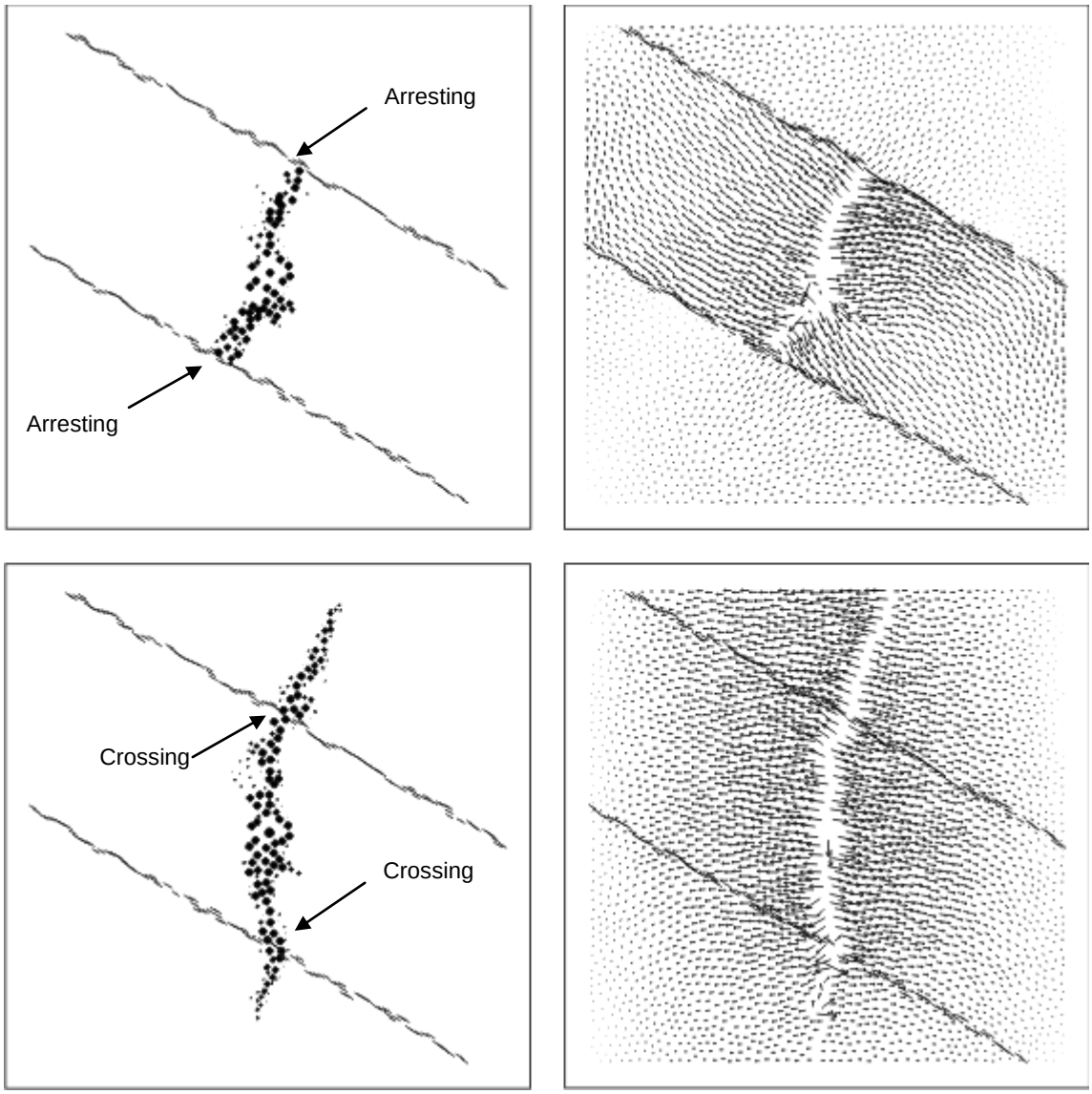

Figure 4.16 A hydraulic fracture interacts with two types of frictional natural interfaces with an angle of approach of 60° where the interface has no shear strength (top) and shear strength of 5 MPa (bottom).

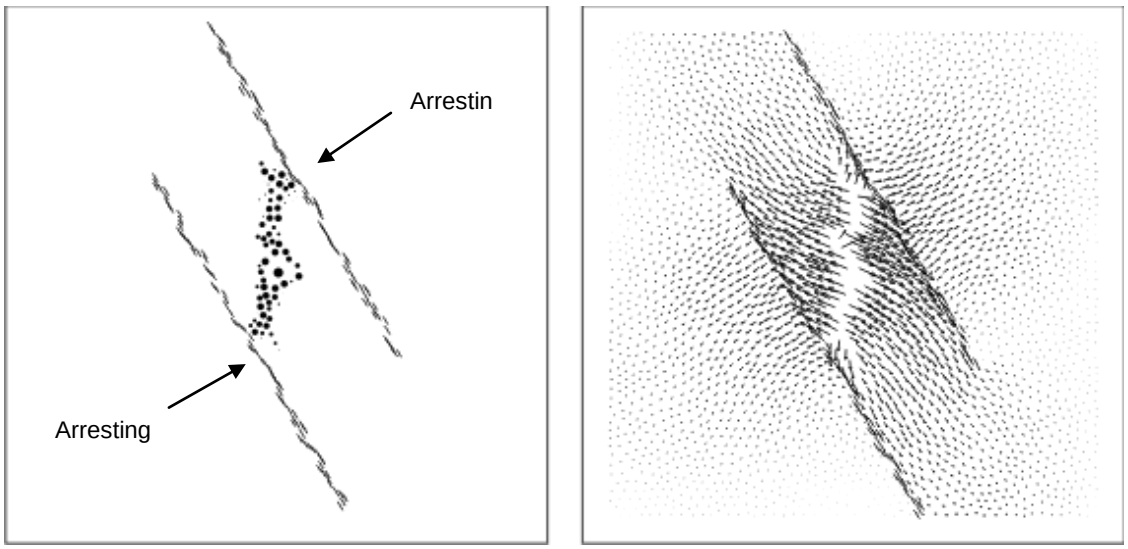

Figure 4.17 Hydraulic fracture interaction with a cohesive natural interface with an angle of approach of 30°. For given conditions the fracture was arrested at its intersect with the natural interface.

4.6.4 Superimposed effect of all parameters

To study the combined effect of friction coefficient, angle of approach, and shear strength of the interface, 36 different extreme cases were simulated. Angles of approach of 30°, 60°, and 90° were considered for in these simulations. Friction coefficients were assumed to be 0, 0.5, 0.7 and 1.0. Also, high (5MPa), moderate (2.5MPa) and zero and values of shear strength were considered for each model. The analysis results indicated that except the case when the interface shear strength is high, in zero friction coefficients, arresting is the dominant interaction mechanism. When the friction coefficient increased to 0.5 the interface with an angle of approach of 90º allowed the hydraulic fracture to cross. When the friction coefficient increased further, crossing was observed at 60° angle of approach but at 30° angle no crossing was observed even when the friction coefficient was high. Also, while friction coefficient was kept high, the shear strength was increased significantly for angle of approach of 30° but again no crossing was observed. However, the latter case was also not comparable with an intact rock model.

The above analysis concludes that perhaps as it is unlikely to have zero friction coefficients for the natural interfaces in real situations, the fracture will cross the interface at a 90° angle of approach. As the angle of approach decreases, the chance for crossing reduces. In order to have crossing to happen at smaller angles of approach, the friction coefficient must be increased. For example at 60° angle of approach crossing can happen depending on the value of friction coefficient. The results obtained in this study show a good qualitative agreement with previously published works (Blanton 1986, Renshaw & Polard 1995, Zhou et al. 2008) and our laboratory experiments for brittle weak interfaces (see Chapter 3).

In this study the effect of horizontal stress magnitude changes was not considered in the models. However, this factor influences the hydraulic fracture and natural interface interaction considerably. Apart from the stress magnitudes, stress contrast can also affect the results of a fracturing job considerably (See Chapter 2).

4.7 Summary

The results presented in this study showed the capability of PFC^{2D} for simulation of interaction between a hydraulic fracture and a natural interface. The simulation results for different angles of approach, interface friction coefficient, and shear strength showed that the interaction results are sensitive to any combination of these parameters. High angle of approach and high friction coefficient values will increase the chance for crossing mode. However, hydraulic fracture tends to become arrested when both the angle of approach and friction coefficients are low. There is a threshold for the angle of approach for any rock type below which hydraulic fracture will be arrested by the natural interface in any circumstances. This depends on many factors, some of which were studied here. It was also shown that if the natural fracture is filled, the resultant shear strength of the natural interface can be influenced but except when the shear strength is high it is not as important as the interface friction coefficient. The results of this study were in good qualitative agreement with a large quantity of our laboratory experiments (see Table 3.3) and other numerical and experimental work reported in the literature (See Chapter 2).

5 Conclusions and recommendation

In this thesis, different scenarios of interaction between cohesive natural interfaces intersected by a propagating hydraulic fracture at different angles of approach have been investigated. Analytical and experimental studies in conjunction with 2D numerical simulations were performed. The conclusions reached as a result of this study are presented in Sections 5.1 and 5.2 with Section 5.3 outlining future research that should be undertaken as a continuation of this work.

5.1 Analytical criterion and experimental studies

- A new analytical criterion was developed that can be used to predict the interaction between a hydraulic fracture and an interface that includes the effect of interface cohesion, friction coefficient, and orientation. The results obtained from this criterion were found to compare reasonably to the published experimental laboratory tests.
- The results presented in this thesis indicate how natural interface properties may affect the interaction behaviour. Also, it was shown that analytical solutions which have been developed based on a number of simplified assumptions are unable to predict the outcome of complicated interactions except for the case of an interface filled with weak brittle material. Therefore, care should be taken when only analytical criteria are used for predicting the outcome of interactions in laboratory tests or full size fracture treatments.
- It is very important to bear in mind the importance of sample preparation and experimental set up in when interpreting laboratory results. The experience obtained from lab experiments carried out in this study indicates how a simple error during sample preparation can lead to a failed test. For example, cutting the notch before running a hydraulic fracturing test was found to be very important in the laboratory to aid the fracture initiation process.
- Various hydro-mechanical properties (UCS, porosity, tensile strength...) of the sample must be estimated or measured before conducting the hydraulic fracturing

experiment. A series of tests was conducted on a wide range of cylindrical samples to establish a good knowledge of the hydro-mechanical properties of the samples prepared for hydraulic fracturing experiments.

- In order for a hydraulic fracturing experiment to represent the field conditions, scaling laws must be applied to design the test. In this study, scaling laws were applied in all experiments to predict the fracture growth regime and net pressure at the time of intersection.
- Many factors are involved in the interaction scenarios that arise as a hydraulic fracture grows toward an interface. These factors may influence the results in a number of ways depending on the given conditions. These factors are coupled meaning that the strength of one may affect the other. Therefore, special care should be taken when general conclusions are made from the laboratory experiments because laboratory conditions impose a restriction on the range of the parameters involved and some processes cannot be represented realistically in the lab.
- The experiments show that interaction results may be completely governed by the hydro-mechanical properties of the filling material (Casas et al., 2006a). Experiments with a brittle weak interface produced results that agreed most closely with the prediction offered by analytical criteria. The study showed that crossing may not be observed in the majority of cases when interaction of hydraulic fracture and an interface filled with elastic material is investigated. A few cases using high deviatoric stress showed that the resistance of such an interface to fracture penetration is beyond the prediction ability of existing analytical criteria or common expectations discussed in the published literature.

5.2 DEM Numerical simulations

- DEM numerical simulations were performed for the purpose of this study. Few attempts have been made in using discrete element method for simulation of interaction mechanism (Itasca, 2008; Zhao and Young, 2009). DEM was found useful in this study. This is because the model can easily include a natural interface which changes the intact rock to a discontinuum rock and DEM is indeed designed for modeling a discontiuum media.
- Similar to laboratory tests, hydro-mechanical properties of the sample should be determined adequately before running a numerical simulation. However generating

a high UCS and low tensile strength (similar to cement sample properties) in the DEM model is difficult. This was achieved in model generation of this study.

- In some of simulations, it was observed that the induced fracture plane tended to run parallel to the interface plane when it was approaching the intersection point. This was seen in some laboratory tests too. The reason for this is thought to be that that the current DEM model reflects the local condition of each individual point very well. So the propagation path is determined based on local micro resistance of fracture. These two facts highlight the applicability of the model for numerical simulation of interaction mode. Also, stress change that is expected to occur near an interface will play an important role in change of local resistance.
- Stress dependent and directional permeability is established in the model. So in addition to fracture channel fluid flow (which is mostly in the direction of maximum horizontal stress), the leak-off direction is stress dependent. This stress dependent permeability was also seen in simulating a well test involving pure injection.
- The results of simulation included cases that considered different scenarios using samples with various angles of approach, interface friction coefficients or shear strengths, which showed that interaction results are sensitive to a combination of these parameters and in many cases these factors could work interchangeable.
- It was seen that a high angle of approach and a high friction coefficient led to crossing mode. However, the hydraulic fracture tends to become arrested when both the angle of approach and frictional strength are low. Also, it was observed that there is a threshold for the angle of approach for any simulation condition below which hydraulic fracture will be arrested by the natural interface in all circumstances. This depends on many factors some of which were studied in this work.
- The results of this study were in good qualitative agreement with most of our laboratory work, especially for weak brittle interfaces. The results also agreed reasonably well with other numerical and experimental work reported in the literature. The laboratory results did not fit the Renshaw and Pollard crossing criterion without a significant adjustment to their criterion. This adjustment involved considering different angle of approaches and cohesive interface.

5.3 Recommendations for future work

- The number and types of different hydro-mechanical tests that were conducted for estimating properties of sample were, in some cases (e.g. fracture toughness test), limited in this study. Performing more of such tests before conducting the hydraulic fracturing experiments is recommended. This would allow a more valid interpretation of results where there is discrepancy with what is expected from other methods.
- It is very important to make sure that stress on the sample in uniformly distributed. This may be considered as the main advantage of using flat jack over hydraulic ram for applying the stress on the sample. However, considering the deficiencies associated with flat jacks, including their regular failure during operation, their needs for systematic calibration, and their non-effective surface area are factors that make use of flat jacks more complicated for these types of applications. On the other hand very big hydraulic rams are required to apply high stresses on large samples which, in turn, require large supporting frames. The uniformity of distributed stresses on the sample should be examined in each test. This may be done by acoustic transmission (check if sound velocity is similar in all cross sections) or by instrumenting the ram plates through which the stresses are applied to the sample. This could be implemented by mounting stain gauges on the plates which apply the stress on the sample. Alternatively, strain gauges may be embedded inside the sample body or on its surface. Fracture pressure analysis during and after the fracturing test may be used for this purpose as well, especially by checking the closure pressure and fracture geometry to obtain an average normal stress acting on the fracture.
- Numerical simulation and laboratory tests showed that different factors that are affecting the interaction may work interchangeably. However; the details of this relationship is unknown. There might be some relationship between the properties of the sample or test procedure. It is recommended that more laboratory studies be conducted to decode this relation.
- Although DEM model used here offers a strong ability to study the interaction mechanisms, it is subjected to some shortcomings. The model presented in this study was a 2D model meaning that a third dimension exists but model properties do not vary in this direction. The length of this dimension may be considered to be

unity or any other value. In this study, we did not investigate the influence of the third dimension of the model on the results. More general form of this problem comes from the fact that the interaction problem in our laboratory tests and in full size field cases is in fact 3D and therefore, 3D simulations are suggested to be conducted as a continuation of this study.

- It is recommended to use the results of different methods, i.e. analytical, experimental and numerical, to make any conclusions regarding the interaction mode. The combination of these methods provide a better view of the problem and hence a more valid conclusion.
- This study was focused on synthetic samples. The scaling laws applied for hydraulic fracturing design in these samples were those presented by de Pater (1994) and some others. It would be interesting to test real samples (e.g. tight sandstones or shale) and develop scaling laws appropriate for these types of rocks.
- Although in this study samples with 10, 15 and 20cm sizes were tested experimentally, it is advisable to perform the experiments on samples with other sizes to establish correlations for the size effect: this would enable us to extrapolate the results to the field scale and compare to the log derived hydraulic fracturing properties.
- It is advised to revalidate the scaling laws that were applied in this study to assess their applicability for current test procedure, equipment, and prepared samples. This requires a comprehensive acoustic monitoring of fracture growth during an experiment along with some wellbore displacement measurements.

Reference

Adachi, J., Siebrits, E., Peirce, A., and Desroches, J., 2007, Computer simulation of hydraulic fractures: International Journal of Rock Mechanics & Mining Sciences 44, 739–757.

Adachi, J.I., 2001, Fluid-Driven Fracture in Impermeable and Permeable Rock: PhD Dissertation, University of Minnesota.

Adachi, J.I., and Detournay, E., 2002, Self-similar Solution of a Plane-strain Fracture Driven by a Power-law Fluid: Int J Numer Anal Meth Geomech, v. 26, p. 579-604.

Adachi, J.I., and Detournay, E., 2007, Plane-strain Propagation of a Fluid-driven Fracture: Finite Toughness Self-similar Solution: Int J Fracture 2007.

Ahmed, U., Strawn, J., Wilson M., and Schatz, J., 1983, Effect of stress distribution on hydraulic fracture geometry: a laboratory simulation study in one meter cubic blocks: SPE 11637SPE/DOE Low Permeability Gas Reservoirs Symposium, 14-16 March, Denver, Colorado.

Akulich, A.V., and Zvyagin, A.V., 2008, Interaction between Hydraulic and Natural Fractures: Fluid Dynamics, v. 43, no. 3, p. 428-435.

Al-Busaidi, A., Hazzard, J.F., and Young, R.P., 2005, Distinct Element Modeling of Hydraulically Fractured Lac du Bonnet Granite: Journal of Geophysical Research, v. 110, B06302.

Amadei, B. and Stephansson, O., 1997. Rock Stress and Its Measurement: Chapman & Hall.

Anderson, G.D., 1981, Effects of Friction on Hydraulic Fracture Growth near Unbonded Interfaces in Rocks: SPE Journal, v.21, No.1, SPE 8347: p. 21-29.

Anderson, T.L., 1991, Fracture Mechanics: Fundamentals and Applications: Boca Raton, CRC Press.

Athavale, A.S., and Miskimins, J.L., 2008, Laboratory Hydraulic Fracturing Tests on Small Homogeneous and Laminated Blocks: The 42nd U.S. Rock Mechanics Symposium (USRMS), June 29 - July 2, San Francisco, CA.

Azeemuddin, M., Ghori, S. G., Saner, S., and Khan, M. N, 2002, Injection-induced hydraulic fracturing in a naturally fractured carbonate reservoir: a case study from Saudi Arabia: Paper SPE 73784 presented at the SPE international symposium & exhibition on formation damage control, Lafayette, Los Angeles, 20–21 February.

Barree, R.D. and H. Mukherjee, 1996, Determination of Pressure Dependent Leakoff and Its Effect on Fracture Geometry: SPE 36424.

Behrmann, L.A., and Elbel, J.L., 1991, Effect of Perforations on Fracture Initiation: Journal of Petroleum Technology, v. 43, no. 5, p. 608-615.

Berumen, S., Tiab, D. and F. Rodriguez, 2000, Constant rate solutions for a fractured well with an asymmetric fracture: Journal of Petroleum Science and Engineering, v. 25, pages: 49-58.

Beugelsdijk, L. J. L., and de Pater, C. J., 2000, Experimental Hydraulic Fracture Propagation in a Multi-Fractured Medium: SPE Asia Pacific Conference on Integrated Modeling for Asset Management, Yokohama, Japan, SPE Paper No. 59419.

Blair, S. C., Thorpe, R.K., 1989, Laboratory Observations of the Effect of Geological Discontinuities on Hydrofracture Propagation: Proceedings of the 30th US Symposium on Rock Mechanics, Morgantown.

Blanton, T.L., 1982, An experimental study of interaction between hydraulically induced and pre-existing fractures: SPE 10847, presented at the SPE/DOE unconventional gas recovery symposium, Pittsburgh, 16–18 May.

Blanton, T. L., 1986, Propagation of Hydraulically and Dynamically Induced Fractures in Naturally Fractured Reservoirs: SPE UGTS, Louisville, SPE Paper No. 152618.

Bobet, A., Einstein, H., 1998, Fracture Coalescence in Rock-type Materials under Uniaxial and Biaxial Compression: Int. J. Rock Mech. Min. Sci. v. 35, p. 863-888.

Born, M., and Huang, K., 1954, Dynamic Theory of Crystal Lattice, Oxford.

Branigan, P.T., Peterson, R.E., Warpinski, N.R., and Wright, T.B. 1996, Characterization of Remotely Intersected Set of Hydraulic Fractures: Results of Intersection Well No. 1-B, GRI/DOE Multi-Site Project: Paper SPE 36452 presented at the SPE Annual Technical Conference and Exhibition, Denver, 6–9 October.

Britt, L.K. and C.J. Hager, 1994, Hydraulic fracturing in a naturally fractured reservoir: SPE 28717, presented at the SPE international petroleum conference and exhibition, Veracruz, Mexico, 10–13 October.

Bruno, M.S., and Nelson, R.B., 1991, Microstructural Analysis of the Inelastic Behavior of Sedimentary Rock: Mech. Mater., v. 12, no. 2, p. 95-118.

Bruno, M.S., 1994, Micromechanics of Stress-induced Permeability Anisotropy and Damage in Sedimentary Rock, Mechanics of Materials, v. 18, p. 31-48.

Bruno, M.S., Dorfmann, A., Lao, K., and Honeger, C., 2001, Coupled Particle and Fluid Flow Modeling of Fracture and Slurry Injection in Weakly Consolidated Granular Media: Proceedings of 38th U.S. Symposium on Rock Mechanics: Rock Mechanics in the National Interest, 7 – 10, July, Washington D.C., v. l, p. 173-180.

Bunger, A., 2005, Near-surface Hydraulic Fracture: PhD Dissertation, University of Minnesota, Minneapolis.

Bunger, A., Detournay, and E., Jeffrey, R., 2005a, Crack Tip Behavior in Near-Surface Fluid-Driven Fracture Experiments', Comptes Rendus Mécanique, v. 333, p. 299-304.

Bunger, A., Detournay, E., and Jeffrey R., 2005b, Application of Scaling Laws to Laboratory-Scale Hydraulic Fractures: Alaska Rocks 2005, The 40th U.S. Symposium on Rock Mechanics (USRMS): Rock Mechanics for Energy, Mineral and Infrastructure Development in the Northern Regions, Anchorage, Alaska, June 25-29.

Carbonell, R.S., Desroches, J., and Detournay, E., 1999, A Comparison between a Semi-analytical and a Numerical Solution of a Two-dimensional Hydraulic Fracture: Int J Solids Struct, v.36, p. 4869–88.

Carter B.J., Desroches, J., Ingraffea, A.R., and Wawrzynek, P.A., 2000, Simulating Fully 3D Hydraulic Fracturing: M. Zaman, J. Booker and G. Gioda, Editors, Modeling in Geomechanics, Wiley Publisher, p. 30.

Casas, L.A., Miskimins, J.L., Black, A., and Green, A., 2006a, Laboratory Hydraulic Fracturing Test on a Rock With Artificial Discontinuities: SPE paper No. 103617-MS, SPE Annual Technical Conference and Exhibition, 24-27 September, San Antonio, Texas, USA.

Casas, L.A., Miskimins, J.L., Black, A., and Green, S., 2006b, Hydraulic Fracturing Laboratory Test on a Rock with Artificial Discontinuities: paper ARMA/USRMS 06-917, American Rock Mechanics Association Golden Rocks Conference, Golden, CO, June 17-21.

Chierici, G.L., Ciucci, G.M., Eva, F., and Long, G., 1967, Effect of the Overburden Pressure on Some Petrophysical Parameters of Reservoir Rocks: 7th World Petroleum Congress, April 2 - 9, Mexico City, Mexico, 12128.

Chong, K.P., and Kuruppu, M.D., 1984, New Specimen for Fracture Toughness Determination of Rock and Other Materials: International Journal of Fracture, v. 26, p. R59-R62.

Chong, K.P., Kuruppu, M.D., and Kuszmaul, J.S., 1987, Fracture Toughness Determination of Layered Materials: Eng. Fract. Mech. v. 28, no. 1, p. 43– 54.

Chuprakov, D.A., Akulich, A., Siebrits, E., and Thiercelin, M., 2010, Hydraulic Fracture Propagation in a Naturally Fractured Reservoir: Paper SPE 128715-MS presented at the SPE Oil and Gas India Conference and Exhibition, Mumbai, India. DOI: 10.2118/128715-MS.

Chuprakov, D.A., and Zhubayev, A.S., 2010, A Variational Approach to Analyze a Natural Fault with Hydraulic Fracture Based on the Strain Energy Density Criterion: Theoretical and Applied Fracture Mechanics 53, p. 221-232.

Cipolla, C.L., Warpinski, N.R., Mayerhofer, M.J., Lolon, E.P. and Vincent, M.C., 2008, The Relationship Between Fracture Complexity, Reservoir Properties, and Fracture Treatment Design: SPE 115769.

Cleary, M.P., 1980, Comprehensive Design Formulae for Hydraulic Fracturing: SPE paper no, 9259, Annual Technical conference and exhibition of society of petroleum engineering, Dallas, TX, September.

Cook, B.K., and Jensen, R.P., 2002, Discrete Element Methods: Numerical Modeling of Discontinua: Proceeding of 3rd International Conference on Discrete Element Methods, Geotechnical Special Publication No. 117, Reston, Virginia: American Society of Civil Engineers.

Cooke, M.L., and Underwood, C.A., 2001, Fracture Termination and Step-over at Bedding Interfaces Due to Frictional Slip and Interface Opening: Journal of Structural Geology v.23 (2-3) p. 223-238.

Crouch, S.L., 1976, Solution of Plane Elasticity Problems by the Displacement Discontinuity Method: Int. J. Num. Methods Eng. v. 10, p. 301-343.

Cundall, P. A., and Strack, O.D.L., 1979, Discrete Numerical Model for Granular Assemblies: Geotechnique, v. 29, p. 47-65.

Cundall, P.A., 1971, A Computer Model for Simulating Progressive Large Scale Movements in Blocky Rock Systems: ISRM Symp., Nancy, France, Proc. 2, p. 129-136.

Dahi-Taleghani, A., and Olson, J.E., 2009, Analysis of Multistranded Hydraulic Fracture Propagation: An Improved Model for the Interaction between Induced and Natural Fractures: SPE 124884, SPE Annual Technical Conference and Exhibition, 4-7 October 2009, New Orleans, Louisiana.

Dahi-Taleghani, A., and Olson, J.E., 2011, Numerical Modeling of Multistranded-Hydraulic-Fracture Propagation: Accounting for the Interaction between Induced and Natural Fractures: SPE Journal, v. 16, no. 3, September, p. 575-581.

Damjanac, B., Gil, I., Pierce, M., Sanchez, M., Van As, A., and McLennan, J., 2010, A New Approach to Hydraulic Fracturing Modeling In Naturally Fractured Reservoirs: 44th U.S. Rock Mechanics Symposium and 5th U.S.-Canada Rock Mechanics Symposium, June 27 - 30, 2010 , Salt Lake City, Utah.

Daneshy, A.A., 1971, True and Apparent Direction of Hydraulic Fractures: SPE 3226, Drilling and Rock Mechanics Conference, 5-6 January, Austin, Texas.

Daneshy, A.A., 1973a, Experimental Investigation of Hydraulic Fracturing through Perforations: Journal of Petroleum Technology. v. 25, no. 10, p. 1201-1206.

Daneshy, A.A., 1973b, A Study of Inclined Hydraulic Fractures: SPE Journal, v. 13, no.2, p. 61-68.

Daneshy, A.A. 1974, Hydraulic Fracture Propagation in the Presence of Planes of Weakness: SPE 4852, SPE European Spring Meeting, 29-30 May, Amsterdam, Netherlands.

Daneshy, A. A., 2004. Analysis of Off-balance Fracture Extension and Fall-Off Pressures: SPE International Symposium and Exhibition on Formation Damage Control. Lafayette, SPE Paper No. 86471.

Daneshy, A. A., 2005, Proppant Distribution and Flowback in Off-Balance Hydraulic Fractures: SPE Production & Facilities, Feb, p. 41-47.

de Pater, C.J., Cleary, M.P., Quinn, T.S., Barr, D.T., Johnson, D.E., and Weijers, L., 1994, Experimental Verification of Dimensional Analysis for Hydraulic Fracturing: SPE Production & Facilities, Volume 9, Number 4, p. 230-238.

de Pater, C.J., and Beugelsdijk, L.J.L., 2005, Experiments and Numerical Simulation of Hydraulic Fracturing in Naturally Fractured Rock: Alaska Rocks, The 40th U.S. Symposium on Rock Mechanics (USRMS), June 25 - 29, Anchorage, AK.

Dees, J. M., 1995. Highly Overbalanced Perforating: Journal of Petroleum Technology, Volume 47, Number 5, Pages 395-397.

deKetterij, V., R.G., 2001. Optimisation of the Near-wellbore Geometry of Hydraulic Fractures Propagating from Cased Perforated Completions: Delft University Press, Amsterdam.

Detournay, E., 2004, Propagation Regimes of Fluid-driven Fractures in Impermeable Rocks: Int J Geomech, v.4, p. 1-11.

Detournay, C., Hart, R., and Nelson, M., 2008, Proceedings of the 1st International FLAC/DEM Symposium, Minneapolis, August 25-27.

Doe, T. W. and Boyce, G., 1989, Orientation of Hydraulic Fractures in Salt Under Hydrostatic and Non-Hydrostatic Stresses: International Journal of Rock Mechanics and Mining Sciences and Geomechanics Abstracts v. 26(6): p. 605-611.

Dollar, A. and Steif, P.S., 1989, A Tension Crack Impinging Upon Frictional Interfaces. J. Appl. Mech. 56, 291-298.

Economides M.J., Watters L.T., and Dunn-Norman S., 1998, Petroleum Well Construction: John Wiley & Sons, West Sussex, England.

Fakhimi, A., Carvalho, F., Ishida, T., Labuz, J.F., 2002, Simulation of Failure Around a Circular Opening in Rock: International Journal of Rock Mechanics and Mining Sciences, v. 39, p. 507-515.

Fast, R.E., Murer, A.S., and Timmer, R.S., 1994, Description and analysis of cored hydraulic fractures — Lost Hills Field, Kern County, California: Soc. Petr. Eng. Prod. and Fac., p. 107–114.

Freund, L.B., 1990, Dynamic fracture mechanics (Cambridge Monographs on Mechanics): Cambridge University Press, Cambridge, UK.

Garagash, DI, Detournay E., 2000, The Tip Region of a Fluid-Driven Fracture in an Elastic Medium: Journal of Applied Mechanics, March, v. 67.

Garagash, D.I., Detournay, E., 2005, Plane-strain Propagation of a Hydraulic Fracture: Small Toughness Solution: J Appl Mech, 72 v.6, p. 916-28.

Garagash, D.I., 2006, Plane Strain Propagation of a Hydraulic Fracture During Injection and Shut-in: Large Toughness Solutions. Eng Frac Mech, v.73, 4, p.456-81.

Gu, H., and Weng, X., 2010, Criterion For Fractures Crossing Frictional Interfaces At Non-orthogonal Angles: 44th U.S. Rock Mechanics Symposium and 5th U.S.-Canada Rock Mechanics Symposium, June 27 - 30, Salt Lake City, Utah.

Gu, H., Weng, X., Lund, J., Mack, M., Ganguly, U., and Suarez-Rivera, R., 2012, Hydraulic Fracture Crossing Natural Fracture at Nonorthogonal Angles: A Criterion and Its Validation, Volume 27, Number 1, February, p. 20-26.

Gumbsch, P., 1995, An Atomistic Study of Brittle Fracture: Towards Explicit Failure Criteria from Atomistic Modelling: Journal of Material Research, v. 10, no. 11, p. 2897-2907.

Haimson, B., and Fairhurst, C., 1969, Hydraulic Fracturing in Porous-Permeable Materials, Journal of Petroleum Technology, V. 21, no, 7, July, p.811-817.

Hainey, B.W., R.G. Keck, M.B. Smith, K.W. Lynch, and J.W. Barth, 1999, On-site fracturing disposal of oilfield-waste solids in Wilmington field, California: SPE production and facilities, v.14, p.88-93.

Hallam, S.D., and Last, N.C., 1990, Geometry of Hydraulic Fractures from Modestly Deviated Wellbores: Journal of Petroleum Technology, v. 43, no. 6, p. 742-748.

Hopkins, C.W., Rosen, R.L., and Hill, D.G., 1998, Characterization of an Induced Hydraulic Fracture Completion in a Naturally Fractured Antrim Shale Reservoir: Paper 51068 SPE, Eastern Regional Mtg., Pittsburgh, Pennsylvania.

Itasca Consulting Group, Inc., 2008, PFC2D – Particle Flow Code in 2 Dimensions, Ver. 4.0 User's Manual. Minneapolis: Itasca.

Jaeger, J., Cook, N.G., and Zimmerman, R., 2007, Fundamentals of Rock Mechanics: Oxford, UK, Blackwell.

Jeffrey, R. G., Enever, J.R., Phillips, R., Moelle, D., and Davidson, S., 1992, Hydraulic Fracturing Experiments in Vertical Boreholes in the German Creek Coal Seam: presented at the Symposium on Coalbed Methane Research and Development in Australia, Townsville, November 19- 21.

Jeffrey, R.G., Settari, A., and Smith, N.P., 1995, A comparison of hydraulic fracture field experiments, including mineback geometry data, with numerical fracture model simulations: In Proceedings of the Society of Petroleum Engineers Annual Technical Conference and Exhibition, Dallas, 1995. p. 591–606.

Jeffrey, R.G., X. Zhang, and M. Thiercelin, 2009, Hydraulic Fracture Offsetting in Naturally Fractured Reservoirs: Quantifying a Long-Recognized Process: SPE paper No. 119351 in the proceedings of the 2009 SPE Hydraulic Fracturing Technology Conference, The Woodlands, TX, 19- 21 January.

Jeffrey, R.G., Zhang, X., and Bunger, A.P., 2010, Hydraulic Fracturing of Naturally Fractured Reservoirs: Proceedings of Thirty-Fifth Workshop on Geothermal Reservoir Engineering Stanford University, Stanford, California, February 1-3, SGP-TR-188.

Jing, L., Hudson, J.A., 2002, Numerical Methods in Rock Mechanics: Int. J. Rock Mech. & Min.Sci., v. 39, p. 409-427.

Jing L., 2003, A Review of Techniques, Advances and Outstanding Issues in Numerical Modelling for Rock Mechanics and Rock Engineering: Int. J. Rock Mech. & Min.Sci., v. 40, p. 283-353.

Jong, Y.H., and Lee, C.I., 2006, Suggested Method for Determining a Complete Set of Micro-Parameters Quantitatively in PFC2D: Tunnel & Underground Space. Journal of Korean Society for Rock Mechanics, v.16, no. 4, p. 334-346.

Katsikadelis, J.T., 2002, Boundary Elements: Theory and Applications: Elsevier Science Ltd.

Konietzky, H., Editor, 2002, Numerical Modeling in Micromechanics via Particle Methods: Proceedings of 1st International PFC Symposium, Gelsenkirchen, Germany, 6-8, November.

Koshelev, V., and Ghassemi, A., 2003, Hydraulic Fracture Propagation near a Natural Discontinuity: In Twenty-Eight Workshop on Geothermal Reservoir Engineering. Stanford University, Stanford, California.

Kulhawy, F.H., 1975, Stress Deformation Properties of Rock and Rock Discontinuities, Engineering Geology, v. 9, no. 4, p. 327–350.

Lamont, N. and Jessen, F., 1963, The effects of existing fractures in rocks on the extension of hydraulic fractures: Journal of Petroleum Technology, February, p. 203–209.

Lash, G.G., and Engelder, T., 2009, Tracking the Burial and Tectonic History of Devonian Shale of the Appalachian Basin by Analysis of Joint Intersection Style: Geological Society of America Bulletin, v. 121, p. 265–277.

Lecampion, B., and Zhang, X., 2005, Onset of the Interaction between a Hydraulic Fracture and a Natural Joint: Scaling Considerations: ARMA, Alaska, June 25 - 29, Paper 768.

Lee, J.S., Kemeny, J., and Ko, T.Y., 2006, Modified PTS Test and Clump Modeling on Mixed Mode Crack Growth in Granite: Golden Rocks 2006: 50 Years of Rock Mechanics Landmarks and Future Challenges, Proceedings of 41st U.S. Symposium on Rock Mechanics, 19-21, June, Golden, CO, Editors: D.P. Yale, S.C. Holtz, C. Breeds, and U. Ozbay, Paper No. ARMA/NARMS 06-937.

Lhomme, T., 2005, Initiation of Hydraulic Fractures in Natural Sandstones: PhD Dissertation, Delft University of Technology, Delft; the Netherlands.

Lianos, E.M., Jeffrey, R., Hillis, R. and Zhang, X., 2006, Factors influencing whether induced hydraulic fractures cross pre-existing discontinuities: AAPG International conference, Perth, Western Australia, 5–8 November, poster.

Liu, E., Hudson, J.A., and Pointer, T., 2000, Equivalent Medium Representation of Fractured Rock: Journal of Geophysical Research, v. 105, no. 82, p. 2981-3000.

Liu, G.R., Gu, Y.T., 2004, Boundary Meshfree Methods Based on the Boundary Point Interpolation Methods: Eng Anal Bound Elem., v. 28, p. 475-487.

Lubbe, R., Sothcott, J., Worthington, M.H., and McCann, C., 2008, Laboratory Estimates of Normal and Shear Fracture Compliance: Geophysical Prospecting, v. 56, no. 2, p. 239–247.

Mack, M.G., and Warpinski, N.R., 2000, Mechanics of Hydraulic Fracturing: in M. J. Economides and K. G. Nolte (eds.), Reservoir Stimulation: Chichester, England, John Wiley & Sons, LTD.

Manolis, G.D., and Polyzos, D., 2009, Recent Advances in Boundary Element Methods, A Volume to Honor Professor Dimitri Beskos. Springer Science+Business Media.

Meng, C., 2010, Interaction between Hydraulic Fracturing Process and Pre-existing Natural Fractures: Delft University Press: Ph.D. thesis, Delft University of Technology, The Netherlands.

Min, S., Sastry, S.K., Balasubramaniam, V.M., 2010, Compressibility and Density of Select Liquid and Solid Foods under Pressures up to 700 MPa: Journal of Food Engineering v. 96, no. 4, February, p. 568-574.

Mindess, S., Young, J.F., and Darwin, D., 2003, Concrete (2nd Edition): Prentice-Hall, New Jersey.

Mitchell, S.L., Kuske, R., and Peirce, A.P., 2007, An Asymptotic Framework for Finite Hydraulic Fractures Including Leak-off: SIAM J Appl Math 2007.

Möllhoff, M., and Bean, C.J., 2009, Validation of Elastic Wave Measurements of Rock Fracture Compliance Using Numerical Discrete Particle Simulations: Geophysical Prospecting, v. 57, no. 5, p. 883-895.

Murphy, H.D. and Fehler, M.C., 1986, Hydraulic fracturing of jointed formations: SPE 14088.

Napier, J.A.L., 1999, Numerical Studies of Time-dependent Failure and Implications for the Prediction of Time to Failure: Proc. 37th U.S. Rock Mechanics Symposium, Vail, USA, p. 911-917.

Nicolazzi, L.C., Barcellos, C.S., Fancello, E.A., Duarte, C.A.M., 2005, Generalized Boundary Rlement Method for Galerkin Boundary Integrals: Eng Anal Bound Elem., v. 29, p. 494-510.

Olson, J.E., and Dahi-Taleghani, A., 2009, Modeling Simultaneous Growth of Multiple Hydraulic Fractures and Their Interaction with Natural Fractures: SPE 119739, SPE Hydraulic Fracturing Technology Conference, 19-21 January, The Woodlands, Texas.

Ong, S. H., 1994, Borehole Stability: PhD Dissertation, The University of Oklahoma, Norman, Oklahoma, USA.

Peter P. Valkó, 2005, presentation file of Hydraulic Fracturing Short Course: Texas A&M University, College Station, Fracture Design Fracture Dimensions Fracture Modeling.

Potluri, K., 2004, Effect of a Natural Fracture on Hydraulic Fracture Propagation: Master Thesis, The University of Texas at Austin.

Potluri, N.K., Zhu, D., and Hill, A.D., 2005, The Effect of Natural Fractures on Hydraulic Fracture Propagation: Paper SPE 94568-MS presented at the SPE European Formation Damage Conference, Scheveningen, The Netherlands.

Potyondy, D.O., and Cundall, P.A., 2004, A Bonded-particle Model for Rock: International Journal of Rock Mechanics and Mining Sciences and Geomechanics Abstracts, v. 41.

Pruiksma, J.P. Bezuijen, A. 2002, Hydraulic fracturing with distinct element method, External Research Report, Delft Cluster.

Raaen, A.M., Skomedal, E., Kjorholt, H., Markestad, P. and Okland, D., 2001, Stress determination from hydraulic fracturing tests: The system stiffness approach: International Journal of Rock Mechanics and Mining Sciences, v. 38, pages: 529-541.

Rabaa, W., 1989, Experimental study of hydraulic fracture geometry initiated from horizontal wells: SPE 19720, SPE Annual Technical Conference and Exhibition, 8-11 October, San Antonio, Texas.

Rahman, M.M., Aghigi, A., Sheik, A.R., 2009, Numerical Modeling of Fully Coupled Hydraulic Fracture Propagation in Naturally Fractured Poro-elastic Reservoir: SPE 121903, EUROPEC/EAGE Conference and Exhibition, 8-11 June, Amsterdam, The Netherlands,.

Rahman, M.M., Aghigi, A., Sheik, A.R., Syed, A.H., 2010, Effect of Natural Fracture on Hydraulic Fracture Propagation in Naturally Fractured Geothermal Reservoirs: Proceedings World Geothermal Congress 2010, Bali, Indonesia, 25-29 April.

Rasouli, V., and J, B. Evans., 2010, A True Triaxial Stress Cell (TTSC) to Simulate Deep Downhole Drilling Conditions. APPEA journal. v. 50, p. 61–70.

Renshaw, C.E., and Pollard D.D. 1995, An experimentally verified criterion for propagation across unbonded frictional interfaces in brittle, linear elastic materials: International Journal of Rock Mechanics Mining Science and Geomechanics 32, v.3.

Rodgerson, J. L. 2000. Impact of natural fractures in hydraulic fracturing of tight gas sands: Paper SPE 59540 presented at the SPE Permian basin oil and gas recovery conference, Midland, Texas, 21–23 March.

Sainsbury, D., et al., 2011, 2nd International FLAC/DEM Symposium. Melbourne, Australia, 14-16 February.

Sakurai, S., 1991, General Report: Computational Methods in Rock Mechanics: International Congress on Rock Mechanics, Aachen, Deutschland.

Sarmadivaleh, M., and Rasouli, V., 2010. Studying the controlling parameters in Hydraulic Fracturing and fracture containment in tight formations: APPEA journal. v. 50, p. 581-591.

Sarmadivaleh, M., Nabipour, A., Asadi, M., Sabogal, J., Rasouli, V., 2010 Identification of Porosity Damaged Zones around a Perforation Tunnel Based on DEM Simulation. 6th Asian Rock Mechanics Symposium - Advances in Rock Engineering, October, New Delhi, India.

Sarmadivaleh, M., V. Rasouli, V., and A. Nabipour, 2011, DEM simulation of controlling parameters in hydraulic fracture and natural interface interaction: In proceeding of 2nd International FLAC/DEM Symposium, 14–16 February, eds D. Sainsbury et al, 07-03 Melbourne: Australia.

Savitski, A.A., and Detournay, E., 2002, Propagation of a Fluid-driven Penny-shaped Fracture in an Impermeable Rock: Asymptotic Solutions: Int J Solids Struct, v. 39, p. 6311–37.

Sayers, C.M., and Kachanov, M., 1995, Microcrack-induced Elastic Wave Anisotropy of Brittle Rock: Journal of Geophysical Research. v. 100: B3, p. 4149-4156.

Schlangen, E., and van Mier, J.G.M., 1995, Crack Propagation in Sandstone: Combined Experimental and Numerical Approach: Rock Mechanics and Rock Engineering, v. 28, no. 2, p. 93-110.

Scott, T.E., Zeng, Z.W., and Rogiers, J.C., 2000, Acoustic Emission Imaging of Induced Asymmetrical Hydraulic Fractures: in Pacific Rocks 2000: Rock around the Rim. Proceedings of the Fourth North American Rock Mechanics Symposium, p. 1129-1134.

Shen, B., 1993, Mechanics of Fractures and Intervening Bridges in Hard Rocks: Engineering Geology, Royal Institute of Technology.

Shimizu, Y., Hart, R., and Cundall, R. Editors, 2004, Proceedings of 2nd International PFC Symposium: Numerical Modeling in Micromechanics via Particle Methods, Kyoto, Japan, 28-29, October.

Solberg, P., Lockner D., and Byerlee J., 1977, Shear and Tension Hydraulic Fractures in Low Permeability Rocks: Pageoph, v. 115, BirkNiuser Verlag, Basel.

Steidl, P.F., 1991, Observation of induced fractures intercepted by Mining in the Warrior Basin, Alabama: Report Topic, Gas Research Institute, Chicago, IL.

Teufel, L.W. and Clark, J.A., 1984, Hydraulic fracture propagation in layered rock: Experimental studies of fracture containment, Society of Petroleum Engineers Journal, p. 19-32.

Thallak, S.G., Rothenburg, L.R., and Dusseault, M.B., 1990, Hydraulic Fracture (Parting) Simulation in Granular Assemblies Using the Discrete Element Method, AOSTRA Journal of Research, v. 6, p. 141.

Thallak, S.G., Rothenburg, L.R., and Dusseault, M.B., 1991, Simulation of Multiple Fractures in A Discrete Element System: Proceeding of 32nd U.S. Symposium on Rock Mechanics, Norman, p. 271-280.

Thiercelin, M.J., and Makkhyu, E., 2007, Stress Field in the Vicinity of a Natural Fault Activated by the Propagation of an Induced Hydraulic Fracture: In Rock Mechanics: Meeting Society's Challenges and Demands. London: Taylor & Francis Group.

Thomas, Rex D., and Don C., 1972, Effect of Overburden Pressure and Water Saturation on Gas Permeability of Tight Sandstone Cores: Journal of Petroleum Technology. v. 24 no.2, p. 120-124.

Ting, J.M., and Corkum, B.T., 1988, Strength Behavior of Granular Materials Using Discrete Numerical Modeling, Numerical Methods in Geomechanics, v. 6, p. 205-210.

Valko, P. and Economides, M.J., 1995, Hydraulic Fracture Mechanics: John Wiley & Sons, Chichester, England.

Van Mier, J. G. M., 1984, Strain-softening of Concrete under Multiaxial Loading Conditions: PhD thesis, Eindhoven University of Technology, The Netherlands.

Veatch, R.W., Moschovidis, Z.A., and Fast, C.R., 1989, An overview of hydraulic fracturing. In: Gidley, Holditch, Nierode, Veatch, editors. Recent advances in hydraulic fracturing. Monograph, V. 12, Richardson: Society of Petroleum Engineers, p. 1-38.

Veeken, C.AM., Davies, D.R, and Walters, J.V, 1989, Limited Communication Between Hydraulic Fracture and (Deviated) Wellbore: SPE 18982, Low Permeability Reservoirs Symposium, 6-8 March, Denver, Colorado.

Vinod, P. S., Flindt, M. L., Card, R. J., and Mitchell, J. P, 1997. Dynamic fluid-loss studies in low-permeability formations with natural fractures: Paper SPE 37486 presented at the SPE production operations Symposium, Tulsa, 9–11 March.

Vonk, R.A., 1993, Micromechanical Investigation of Softening of Concrete Loaded in Compression: Heron, v. 38, p.3.

Wang, L.B., Myers, L.A., Mohammad, L.N., and Fu, Y.R., 2003, Micromechanics Study on Top-down Cracking: Transportation Research Record, Transportation Research Board Washington, D.C., p. 121–133.

Warpinski, N.R., and Teufel, L.W., 1987. Influence of Geologic Discontinuities on Hydraulic Fracture Propagation: SPE Paper No. 13224, Society of Petroleum Engineers Journal, v. 27(2), p. 209-220.

Warpinski, N.R., 1991, Hydraulic fracturing in tight, fissured media: Journal of Petroleum Technology, p. 146-209.

Warpinski, N.R., Lorenz, J.C., Branagan, P.T., Myal, F.R., and Gall, B.L., 1993, Examination of a Cored Hydraulic Fracture in a Deep Gas Well: SPE 22876.

Weijers, L., 1995, The Near-Wellbore Geometry of Hydraulic Fractures Initiated from Horizontal and Deviated Wells: PhD Dissertation, Delft University of Technology, The Netherlands, ISBN 90-407-1064-3.

Whittaker, B.N., Singh., R.N., Sun, G., 1992, Rock Fracture Mechanics: Principles, Design and Applications: Developments in Geotechnical Engineering, Elsevier, Amsterdam.

Wong, G.K., R.R. Fors, J.S. Casassa, R.H. Hite and J. Shlyapobersky, 1993, Design, Execution, and Evaluation of Frac and Pack Treatments in Unconsolidated Sand Formation in the Gulf of Mexico: SPE 26563 presented at the 68th Annual Technical Conferences and Exhibition, Houston, TX.

Wu, H., Dudley, J.W., Wong, G.K. and Chudnovsky, A., 2004. A map of fracture behavior in a vicinity of interface, in GulfRock 2004: proceedings of the 6th NARMS Symposium, eds Yale, D.P., Willson, S.M. & Abou-Sayed, A.S., Jun 6–10; Houston, Texas.

Wu, R. Kresse, O. Weng, X. Cohen C. and Gu H., 2012, SPE paper no 152052, SPE Hydraulic Fracturing Technology Conference, 6-8 February, The Woodlands, Texas, USA.

Xue, W., 2010, Numerical Investigation of Interaction between Hydraulic Fractures and Natural Fractures: Master thesis, Texas A&M University.

Yao, C., and Kim, K., 1996, Simulation of Tensile Failure in Disk using Random Lattice Network Model, Proceedings of 2nd North American Rock Mechanics Symposium: NARMS 96, 19-21, June, Montreal, PQ, Canada, p. 663-668.

Yee, K.S., 1966, Numerical Solution of Initial Boundary Value Problems Involving Maxwell's Equations in Isotropic Media: IEEE Trans. Antenn. Prop., v. 14, p. 302 - 307.

Yoon, J., 2007, Application of Experimental Design and Optimization to PFC Model Calibration in Uniaxial Compression Simulation: International Journal of Rock Mechanics & Mining Sciences v. 44, p. 871–889.

Zhang, X., Jeffrey, R., Llanos, 2004, A study of Shear Hydraulic Fracture Propagation: ARMA, Houston, June 5-9, Paper 491.

Zhang, X., Jeffrey, R., Llanos and Lecampion, 2005, Plane-strain Analysis of Post-coalescence Interaction between Fluid-driven Cracks and Natural Fractures: ARMA, Alaska, June p. 25-29, Paper 719.

Zhang, X., and Jeffrey, R., 2006, The Role of Friction and Secondary Flaws on Deflection and Re-initiation of Hydraulic Fractures at Orthogonal Pre-existing Fractures: Geop. J. Int.in-press.

Zhang X., Jeffrey R.G., and Thiercelin M., 2008, Escape of fluid-driven fractures from frictional bedding interfaces: A numerical study, Journal of Structural Geology, v 30, p. 478-490.

Zhang, Z.N., and Ghassemi, A., 2010, The Virtual Multidimensional Internal Bond Method for Simulating Fracture Propagation and Interaction in Poroelastic Rock: International Journal of Rock Mechanics & Mining Sciences.

Zhou, J., Chen, M., Jin, Y., and Zhang, G., 2008, Analysis of Fracture Propagation Behavior and Fracture Geometry Using a Tri-axial Fracturing System in Naturally Fractured Reservoirs: International Journal of rock Mechanics & Mining Science. v. 45, No. 7, p. 1143–1152.

Zhao, X.P., and Young, R.P., 2009, Numerical Simulation of Seismicity Induced by Hydraulic Fracturing in Naturally Fractured Reservoirs: SPE 124690, SPE Annual Technical Conference and Exhibition, 4-7 October, New Orleans, Louisiana, USA.

Zhou, J., Yan, J., and Chen, M., 2010, Experimental investigation of hydraulic fracturing in random naturally fractured blocks: International Journal of Rock Mechanics & Mining Sciences. 47, 1193–1199.

Zhou, J., and Xue, C., 2011, Experimental Investigation of Fracture Interaction between Natural Fractures and Hydraulic Fracture in Naturally Fractured Reservoirs: SPE EUROPEC/EAGE Annual Conference and Exhibition, 23-26 May, Vienna, Austria.